

**Université de Montréal**

**Modèles de flammelette en combustion turbulente  
avec extinction et réallumage : étude  
asymptotique et numérique, estimation d'erreur a  
posteriori et modélisation adaptative**

par

**Pascal TURBIS**

Département de mathématiques et de statistique  
Faculté des arts et des sciences

Thèse présentée à la Faculté des études supérieures  
en vue de l'obtention du grade de  
Philosophiæ Doctor (Ph.D.)  
en mathématiques

Orientation mathématiques appliquées

février 2011

**Université de Montréal**

Faculté des études supérieures

Cette thèse intitulée

**Modèles de flammelette en combustion turbulente  
avec extinction et réallumage : étude  
asymptotique et numérique, estimation d'erreur a  
posteriori et modélisation adaptative**

présentée par

**Pascal TURBIS**

a été évaluée par un jury composé des personnes suivantes :

*DELFOUR, Michel*

—————  
(président-rapporteur)

*BOURLIOUX, Anne*

—————  
(directrice de recherche)

*BÉLAIR, Jacques*

—————  
(membre du jury)

*CUENOT, Bénédicte*

—————  
(examinatrice externe)

*DELFOUR, Michel*

—————  
(représentant du doyen de la FES)

Thèse acceptée le:

*31 janvier 2011*

## SOMMAIRE

---

On s'intéresse ici aux erreurs de modélisation liées à l'usage de modèles de flammelette sous-maille en combustion turbulente non prémixée. Le but de cette thèse est de développer une stratégie d'estimation d'erreur *a posteriori* pour déterminer le meilleur modèle parmi une hiérarchie, à un coût numérique similaire à l'utilisation de ces mêmes modèles. Dans un premier temps, une stratégie faisant appel à un estimateur basé sur les résidus pondérés est développée et testée sur un système d'équations d'advection-diffusion-réaction. Dans un deuxième temps, on teste la méthodologie d'estimation d'erreur sur un autre système d'équations, où des effets d'extinction et de réallumage sont ajoutés. Lorsqu'il n'y a pas d'advection, une analyse asymptotique rigoureuse montre l'existence de plusieurs régimes de combustion déjà observés dans les simulations numériques. Nous obtenons une approximation des paramètres de réallumage et d'extinction avec la courbe en «S», un graphe de la température maximale de la flamme en fonction du nombre de Damköhler, composée de trois branches et d'une double courbure. En ajoutant des effets advectifs, on obtient également une courbe en «S» correspondant aux régimes de combustion déjà identifiés. Nous comparons les erreurs de modélisation liées aux approximations asymptotiques dans les deux régimes stables et établissons une nouvelle hiérarchie des modèles en fonction du régime de combustion. Ces erreurs sont comparées aux estimations données par la stratégie d'estimation d'erreur. Si un seul régime stable de combustion existe, l'estimateur d'erreur l'identifie correctement ; si plus d'un régime est possible, on obtient une façon systématique de choisir un régime. Pour les régimes où plus d'un modèle est approprié, la hiérarchie prédite par l'estimateur est correcte.

**Mots-clés :** Modélisation adaptative, flammelette, erreurs de modélisation, estimation d'erreur a posteriori, combustion turbulente, combustion non pré-mélangée, extinction, réallumage, analyse asymptotique.

## SUMMARY

---

We are interested here in the modeling errors of subgrid flamelet models in nonpremixed turbulent combustion. The goal of this thesis is to develop an a posteriori error estimation strategy to determine the best model within a hierarchy, with a numerical cost at most that of using the models in the first place. Firstly, we develop and test a dual-weighted residual estimator strategy on a system of advection-diffusion-reaction equations. Secondly, we test that methodology on another system of equations, where quenching and ignition effects are added. In the absence of advection, a rigorous asymptotic analysis shows the existence of many combustion regimes already observed in numerical simulations. We obtain approximations of the quenching and ignition parameters, alongside the S-shaped curve, a plot of the maximal flame temperature as a function of the Damköhler number, consisting of three branches and two bends. When advection effects are added, we still obtain a S-shaped curve corresponding to the known combustion regimes. We compare the modeling errors of the asymptotic approximations in the two stable regimes and establish new model hierarchies for each combustion regime. These errors are compared with the estimations obtained by using the error estimation strategy. When only one stable combustion regime exists, the error estimator correctly identifies that regime; when two or more regimes are possible, it gives a systematic way of choosing one regime. For regimes where more than one model is appropriate, the error estimator's predicted hierarchy is correct.

**Keywords:** Adaptive modeling, flamelet, modeling errors, a posteriori error estimation, turbulent combustion, nonpremixed combustion, quenching, ignition, asymptotic analysis.

# TABLE DES MATIÈRES

---

<b>Sommaire.....</b>	iii
<b>Summary .....</b>	v
<b>Liste des figures .....</b>	x
<b>Liste des tableaux .....</b>	xv
<b>Remerciements .....</b>	1
<b>Introduction.....</b>	2
<b>Chapitre 1. Estimation d'erreur a posteriori pour les modèles de flammelette sous-maille.....</b>	7
Résumé.....	7
1.1. Abstract .....	9
1.2. Introduction .....	10
1.3. Flamelet models .....	11
1.3.1. The asymptotic flamelet subgrid model strategy.....	13
1.3.2. The steady laminar case .....	13
1.3.3. The nonlaminar case.....	14
1.4. Modeling error estimation strategy .....	15
1.4.1. The dual-weighted residual estimator for nonlinear equations ..	16
1.4.2. A steady-state example: The mean dissipation flamelet model ..	17
1.4.3. Computing the reduced dual solution .....	18
1.4.4. Approximating the modeling error .....	20

1.5.	Application to a steady simple shear flow .....	21
1.6.	Applications to a broader class of flows.....	25
1.6.1.	Steady Childress–Soward flow.....	25
1.6.2.	Unsteady shear .....	27
1.7.	Conclusions.....	31
1.8.	References .....	32
<b>Chapitre 2. Effets de l’extinction et du réallumage dans un modèle idéalisé en combustion non prémélangée .....</b>		35
Résumé.....		35
2.1.	Abstract .....	37
2.2.	Introduction .....	37
2.3.	Governing equations .....	38
2.4.	Asymptotic analysis.....	39
2.4.1.	The lower branch and bend of the S-shaped curve.....	41
2.4.2.	The middle branch of the S-shaped curve .....	43
2.4.3.	The upper branch and bend of the S-shaped curve .....	46
2.5.	Discussion .....	49
2.6.	Conclusions.....	51
2.7.	References .....	52
<b>Chapitre 3. Un modèle élémentaire pour la validation des approximations de flammelette en combustion non prémélangée avec extinction et réallumage.....</b>		53
Résumé.....		53
3.1.	Abstract .....	55

3.2. Introduction .....	55
3.3. Governing equations .....	56
3.4. The asymptotic limit $\text{Pe} = 0$ .....	58
3.4.1. The nearly frozen regime.....	58
3.4.2. The near-equilibrium regime .....	60
3.4.3. The asymptotic flamelet subgrid model strategy.....	62
3.4.4. Construction of the flamelet approximation .....	63
3.4.5. Approximation errors .....	65
3.5. The $\text{Pe} \neq 0$ case .....	66
3.5.1. Extending the models to the $\text{Pe} \neq 0$ case.....	66
3.5.2. Modeling errors .....	71
3.6. S-shaped curves, prediction of quenching and ignition .....	72
3.7. Conclusion .....	76
3.8. References .....	77
<b>Chapitre 4. Estimation d'erreur a posteriori pour les modèles de flammelette sous-maille en présence d'extinction et de réallumage .....</b>	<b>79</b>
Résumé.....	79
4.1. Abstract .....	81
4.2. Introduction .....	81
4.3. Governing equations .....	84
4.3.1. The stable combustion regimes.....	85
4.3.2. The asymptotic flamelet subgrid model strategy.....	87
4.3.3. Flamelet models for $\text{Pe} = 0$ .....	89
4.3.4. Flamelet models for $\text{Pe} \neq 0$ .....	90

4.4.	Modeling error estimation.....	92
4.4.1.	The dual-weighted residual estimator for nonlinear equations .....	92
4.4.2.	The dual flamelet library.....	93
4.4.3.	Estimating the modeling error in the nearly frozen regime.....	96
4.5.	Application to the $\text{Pe} = 0$ case .....	98
4.6.	Application to a steady simple shear flow .....	102
4.7.	Application to the Childress–Soward flow .....	107
4.8.	Conclusion.....	109
4.9.	References .....	110
	Appendix A .....	112
	Appendix B .....	113
	<b>Conclusion.....</b>	115
	<b>Bibliographie .....</b>	117
	<b>Annexe A. Autorisations écrites des coauteurs et de l’éditeur pour la diffusion .....</b>	A-i

## LISTE DES FIGURES

---

1.1	Flamelet library—correction term $d\widehat{Y}(\widehat{Z}) = \widehat{Y} - (\widehat{Z} +  \widehat{Z} )$ .....	14
1.2	Dual flamelet library for $j(Y) = \int_{\Omega} Y(x, y) dx dy$ .....	19
1.3	Simple shear—solutions $Z$ , $Y$ , and $\omega$ for high Pe and high Da (stoichiometric level $Z = 0$ in black). .....	22
1.4	Shear flow—estimated local dissipation model errors as functions of $Da^{-1/3}$ for $Pe = 10$ (left) and $Pe = 200$ (right).....	23
1.5	Shear flow—estimated (see (1.5.6)) and exact errors as functions of $Da^{-1/3}$ for $Pe = 10$ (left) and $Pe = 200$ (right). Dots show the location of crossover points. ....	25
1.6	Childress–Soward flow—solutions $Z$ , $Y$ , and $\omega$ for high Pe, high Da, and $\delta = 0,5$ (stoichiometric level $Z = 0$ in black). .....	26
1.7	Childress–Soward flow—estimated and exact local dissipation model errors as functions of $Da^{-1/3}$ for $Pe = 10$ (left) and $Pe = 200$ (right)..	27
1.8	Childress–Soward flow—estimated and exact modeling errors as functions of a spatially constant dissipation $\chi$ .....	28
1.9	Unsteady shear—estimated (left; see (1.6.8)) and exact (right) errors as functions of $Da^{-1/3}$ . Dots show the location of crossover points: exact error curves cross at $Da = 1,6303 \times 10^2$ , estimated error curves at $Da = 3,8936 \times 10^1$ .....	30
1.10	Unsteady shear—instantaneous and mean dissipation model errors (estimated and exact) as functions of $Da^{-1/3}$ . Dots show the location of crossover points. .....	30

2.1	S-shaped curve—plot of the maximum flame temperature against Da. Critical quenching and ignition parameters $\text{Da}_E$ and $\text{Da}_I$ are also shown.....	40
2.2	Typical profiles for $T$ , $Y_1$ , and $Y_2$ in the nearly frozen regime ( $\text{Da} = 1$ ). .	41
2.3	Asymptotic solution on the lower bend of the S-shaped curve— $\theta_1(1/2)$ plotted against $\Delta_0$ . . . . .	43
2.4	Relative error between the ignition Damköhler number $\text{Da}_I$ and its approximation (2.4.7) as a function of $\varepsilon = T_\infty^2/E$ . . . . .	44
2.5	Asymptotic solution on the middle branch of the S-shaped curve— $T_b$ as a function of $\text{Da}_b$ , given by (2.4.19). . . . .	46
2.6	Typical profiles for $T$ , $Y_1$ , and $Y_2$ in the near-equilibrium regime ( $\text{Da} = 100$ ) around the flame location. Full line: exact solutions, dashed line: equilibrium solutions. . . . .	47
2.7	Asymptotic solution on the upper bend of the S-shaped curve— $\beta_1(0)$ plotted against $\delta_0^{-1/3}$ . . . . .	49
2.8	Relative error between the ignition Damköhler number $\text{Da}_E$ and its approximation (2.4.27) as a function of $\varepsilon = H^2/E$ . . . . .	51
3.1	S-shaped curve—plot of the maximum flame temperature against Da for $\text{Pe} = 0$ . Critical quenching and ignition parameters $\text{Da}_E$ and $\text{Da}_I$ are also shown. . . . .	59
3.2	Typical profiles of $T$ , $Y$ , and $Y_2$ in the nearly frozen regime ( $\text{Da} = 1$ , $\text{Pe} = 0$ ). . . . .	60
3.3	Typical profiles for $T$ , $Y$ , and $Y_2$ in the near-equilibrium regime ( $\text{Da} =$ $100$ , $\text{Pe} = 0$ ) around the flame location. Full line: exact solutions, dashed line: equilibrium solutions. . . . .	61
3.4	Flamelet library—correction term $d\widehat{Y}\left(\widehat{Z}\right) = \widehat{Y} - \left(\widehat{Z} +  \widehat{Z} \right)$ . . . . .	64

3.5	$L^2$ -norm errors between the flamelet approximation $Y_{fl}$ and the solution $Y$ of (3.4.14), plotted against $\alpha^{-1}$ .....	65
3.6	$L^2$ -norm errors between $Y$ and its approximations as functions of $Da^{-1/3}$ . Top left: approximations compared to the near-equilibrium regime solution; top right: approximations compared to the nearly frozen regime solution; bottom: lowest error curves from above plots..	67
3.7	Lowest modeling errors and S-shaped curve for $Pe = 0$ . The S-shaped curve (full line) is shown, alongside markers corresponding to the model with the lowest modeling error: frozen flow model (triangle), flamelet model (circle).....	68
3.8	Passive scalar $Z$ for various choices of $\mathbf{v}$ and $Pe$ . Stoichiometric level $Z = 0$ highlighted in black.....	69
3.9	Childress–Soward flow, $\delta = 0,5$ —data points ( $\alpha Z, \alpha (Y - (Z +  Z ))$ ) of near-equilibrium solutions for high $Da$ and various $Pe$ . The flamelet library’s data points are shown in white.....	70
3.10	Simple shear flow— $L^2$ -norm errors for $Pe = 10$ (left) and $Pe = 100$ (right) for various $Da$ .....	73
3.11	Childress–Soward flow, $\delta = 0,5$ — $L^2$ -norm errors for $Pe = 10$ (left) and $Pe = 100$ (right) for various $Da$ .....	73
3.12	Absolute values of the asymptotic slopes from Figures 3.10–3.11—simple shear flow (left), Childress–Soward flow (right).....	74
3.13	Simple shear flow—maximum temperature as a function of $Da$ for various values of $Pe$ : left, (nonnormalized) S-shaped curves; right, S-shaped curve for $Pe = 0$ (full line) and normalized points (circles) from the $Pe > 0$ data.....	74
3.14	Childress–Soward flow, $\delta = 0,5$ —maximum temperature as a function of $Da$ for various values of $Pe$ : left, (nonnormalized) S-shaped curves;	

right, S-shaped curve for $\text{Pe} = 0$ (full line) and normalized points (circles) from the $\text{Pe} > 0$ data. ....	75
3.15 Existence of solutions in the near-equilibrium and nearly frozen regimes and predictions for $\text{Da}_I$ and $\text{Da}_E$ (full lines): left, simple shear flow; right, Childress–Soward flow, $\delta = 0.5$ . A cross marker denotes the existence of a unique solution, a circle marker, the coexistence of two stable solutions. ....	76
4.1 S-shaped curve—plot of the maximum flame temperature against $\text{Da}$ for $\text{Pe} = 0$ . Critical quenching and ignition parameters $\text{Da}_E$ and $\text{Da}_I$ are also shown. ....	86
4.2 Typical profiles for $T$ , $Y$ , and $Y_2$ in the nearly frozen regime ( $\text{Da} = 1$ , $\text{Pe} = 0$ ). ....	87
4.3 Typical profiles for $T$ , $Y$ , and $Y_2$ in the near-equilibrium regime ( $\text{Da} =$ $100$ , $\text{Pe} = 0$ ) around the flame location. Full line: exact solutions, dashed line: equilibrium solutions. ....	88
4.4 Flamelet library—correction term $d\hat{Y}\left(\hat{Z}\right) = \hat{Y} - \left(\hat{Z} +  \hat{Z} \right)$ ....	90
4.5 Dual flamelet library for $j(Y) = \int_{\Omega} Y(x, y) dx dy$ ....	95
4.6 Convergence of the dual flamelet library solution $q_{fl}$ to the solution $q$ of (4.4.14) for $\text{Pe} = 0$ ....	97
4.7 $\text{Pe} = 0$ case—estimated and exact errors as functions of $\text{Da}^{-1/3}$ for the output functionals $j(Y) = L_G \int_Z Y dZ$ (left) and $j(Y, Z_0) = Y(Z_0)$ (right; $\int_Z  j(Y, Z) - j(Y_m, Z)  dZ$ is shown)....	99
4.8 $\text{Pe} = 0$ case—S-shaped curves, according to direct numerical simulation data (dashed line) and error estimator (full line)....	100
4.9 Dual flamelet library for $j(Y, x_0, y_0) = Y(x_0, y_0)$ ....	102
4.10 Simple shear— $\omega$ , $Y$ , and $Z$ for $\text{Pe} = 100$ and $\text{Da} = 10^4$ (stoichiometric level $Z = 0$ in black). ....	103

4.11 Shear flow—exact and estimated errors for $j(Y) = \int_{\Omega} Y dx dy$ , plotted against $\text{Da}^{-1/3}$ , for the local dissipation model. Left: $\text{Pe} = 10$ , right: $\text{Pe} = 100$ .....	105
4.12 Shear flow—estimated (see (4.6.6)) and exact errors as functions of $\text{Da}^{-1/3}$ for $\text{Pe} = 10$ (left) and $\text{Pe} = 100$ (right).....	106
4.13 Childress–Soward flow—solutions $\omega$ , $Y$ , and $Z$ for $\text{Pe} = 100$ , $\text{Da} = 10^4$ , and $\delta = 0,5$ (stoichiometric level $Z = 0$ in black). .....	108
4.14 Childress–Soward flow—estimated and exact $L^1$ -norm errors as functions of $\text{Da}^{-1/3}$ for $\text{Pe} = 10$ (left) and $\text{Pe} = 100$ (right).....	109

## LISTE DES TABLEAUX

---

I	Comparison between the results presented here (T) and those obtained by Liñán (L).....	50
---	---	----

## REMERCIEMENTS

---

J'aimerais remercier tous ceux avec qui j'ai partagé de bons moments pendant ces dernières années. Dans un monde idéal, je n'oublierais personne et tous accepteraient les éloges qui leur reviennent.

Les remerciements professionnels : Anne Bourlioux pour sa patience, son support et les discussions tout au long de la recherche ; Alexandre Ern et le CERMICS pour l'accueil à Paris ; les étudiants aux cycles supérieurs pour les échanges de toutes sortes ; le personnel du département pour sa présence malgré les changements, volontaires ou non, de ses effectifs ; le CRM pour ses activités, séminaires et écoles.

Les remerciements familiaux : André, Patricia, Sandra et les autres, pour leurs encouragements... et leur logement. Peu de mots pour beaucoup de travail en coulisses, c'est injuste, je sais.

Les remerciements amicaux : tous ceux qui m'ont fait oublier le travail lorsque cela s'imposait, que ce soit lors de repas, de soirées de poker ou de sorties au cinéma. Toutes les occasions sont bonnes pour que mon imagination fonctionne à plein régime.

Les remerciements financiers : le CRSNG, le FQRNT et l'INRIA pour leurs bourses respectives.

Les remerciements hors-catégorie : les personnes qui ne dévoilent pas leurs expériences personnelles lorsque j'affirme être un étudiant en mathématiques. Si une personne ne dit pas à un pâtissier que sa cuisine était un gâchis la dernière fois qu'elle a tenté de fourrer des choux à la crème, alors pourquoi suppose-t-elle que je serais intéressé de savoir qu'elle n'était pas bonne en mathématiques ?

# INTRODUCTION

---

La majorité des phénomènes naturels font intervenir des échelles de grandeur très différentes qui leur sont intrinsèques. Par exemple, les fronts atmosphériques ont des champs d'action variant de quelques centaines de mètres à des milliers de kilomètres. Le dépliage d'une protéine se fait dans un intervalle de temps variant entre  $10^{-14}$  et 1 seconde, tandis que la vibration interne des molécules qui la composent se fait dans un temps de l'ordre de la femtoseconde. D'un point de vue pratique, hormis une poignée de cas, la simulation numérique détaillée de ces phénomènes n'est pas raisonnable. Deux types d'approches sont alors envisagées pour résoudre le problème [LB] :

- effectuer un prétraitement visant à faire disparaître les petites échelles pour ne laisser à simuler que les grandes ;
- gérer conjointement, mais différemment, les petites et les grandes échelles.

La première catégorie mentionnée comprend entre autres l'homogénéisation, la mécanique statistique à l'équilibre et les méthodes de type Hartree-Fock en chimie computationnelle. Ces méthodes rendent possible le calcul numérique, mais mènent à des solutions marquées par l'absence du détail des petites échelles, bien que leur effet global sur le système soit inclus. La deuxième catégorie inclut une panoplie de méthodes, toutes spécifiques à leurs domaines d'utilisation (défauts cristallins, écoulement dans les milieux poreux ou composites, fluides non newtoniens, etc.). Pour un coût computationnel plus élevé, ces méthodes multiéchelles permettent l'utilisation de sous-méthodes de natures différentes pour chaque échelle, combinant ainsi les avantages de celles-ci [EE].

Pour notre part, le système multiéchelles qui nous intéresse est la comubustion non prémelangée. Dans cette catégorie de phénomènes, l'échelle spatiale d'intérêt est le moteur. La solution est influencée par la largeur de la zone de réaction (épaisseur de la flamme), qui elle-même est modifiée par les temps caractéristiques de réaction et de diffusion des réactifs (chimie moléculaire). La turbulence vient compliquer les choses : en plus de déformer la flamme, elle donne une nature grandement multiéchelles au phénomène en ajoutant des échelles spatio-temporelles liées au transport lagrangien des particules dans le champ. D'un point de vue numérique, le régime de réaction rapide pose un problème, car les simulations numériques doivent tenir compte de toutes les échelles associées au problème, incluant le fait que la flamme est très mince dans ce régime. La plupart des options de modélisation disponibles font partie de la première approche pour les systèmes multiéchelles :

- L'approche LES (*large eddy simulations*), soit le filtrage des petites échelles et la fermeture des équations pour ne conserver que les grandes échelles. Typiquement, cette deuxième étape se fait via les fonctions de densité de probabilité (voir [**KP2**, **WP**] pour quelques exemples et [**P2**] pour un résumé des techniques utilisées). L'approche a été validée tant pour la comparaison avec les flammes de Sandia [**KP1**] que pour des applications industrielles [**GSCP**, **PDBI**, **WS+**].
- La réduction de la chimie, consistant à ne tenir compte que des réactifs et produits des réactions importantes de la combustion [**HRP**, **PR**].
- L'approche de flammelette, où on réduit un système complexe d'équations en une équation simple menant à une librairie de flammelettes, une relation précalculable entre les scalaires réactifs et passifs [**P1**]. Cette stratégie a été utilisée auparavant pour la simulation numérique de flammes turbulentes [**CR1**, **JLRH**].

À chaque approximation de la flamme originale correspond une erreur de modélisation, utilisée pour hiérarchiser les modèles par leur performance.

L'étape de la modélisation pose un autre problème. Beaucoup de modèles mathématiques sont connus en combustion turbulente, mais aucune situation réelle

ne correspond à un seul modèle à la fois. En particulier, les phénomènes d'extinction et de réallumage peuvent changer brusquement la nature de la flamme et ainsi sortir un modèle de son cadre d'application. Les travaux précédents se sont concentrés sur la fraction de mélange et la dissipation scalaire [**CKP, ICP**], ainsi que sur le rôle joué par la dissipation de la dissipation scalaire [**PCF**] dans l'extinction et le réallumage, tant au niveau local que global.

Les travaux de cette thèse sont une suite aux travaux de Bourlioux, Majda et Volkov en combustion non pré-mélangée. Les flammes étudiées [**BM1, BM2**] sont obtenues à partir d'un système idéalisé d'équations d'advection-diffusion-réaction. La performance de modèles basés sur des flammelettes stationnaires a été étudiée dans [**BM1, V**] pour des systèmes stationnaires et instationnaires. Dans les deux cas, une hiérarchie des modèles a été obtenue, suivant l'importance de l'advection et de la réaction. L'étape suivante dans l'analyse du système d'équations et des modèles est de mettre au point une méthode permettant de choisir sur le vif le meilleur modèle à utiliser au cours des simulations numériques. Pour être viable, cette méthode devra avoir un coût numérique au plus du même ordre que celui lié à la construction de la solution de flammelette elle-même.

Lors de la résolution numérique d'équations différentielles aux dérivées partielles, il est usuel d'avoir recours à l'estimation d'erreurs de discrétisation, couplée à des stratégies d'adaptation de maillage (voir [**AO, BR, EJ**] et [**AN**] pour des exemples en éléments finis et en différences finies, respectivement). Cependant, il ne faut pas négliger les erreurs de modélisation dans la simulation numérique aux grandes échelles en combustion turbulente, puisque ces erreurs sont potentiellement aussi importantes. L'utilisation d'un estimateur d'erreurs de modélisation est plus récente [**ACS, BE1, ROV**] et fait appel à des arguments de dualité. Notre but est d'évaluer la procédure de Braack et Ern basée sur la pondération du résidu par une solution duale [**BE1**] pour l'estimation des erreurs de modélisation. Cet estimateur a également été utilisé pour l'identification de paramètres [**BBV**]. Dans le chapitre 1, nous présentons une telle stratégie et étudions sa performance pour des modèles stationnaires et instationnaires obtenus à partir de flammelettes stationnaires. Outre sa performance, le coût numérique de la procédure est évalué.

Les modèles de flammelle étudiés dans le premier chapitre sont appropriés dans un régime près de l'équilibre chimique. Pour étudier l'extinction et le ré-allumage, nous modifions le terme réactif pour obtenir jusqu'à trois régimes de combustion [L]. Deux d'entre eux sont stables : le régime près de l'équilibre, où les modèles de flammelle sont privilégiés, et le régime presque gelé, où la température de la flamme est près de celle d'une flamme en l'absence de réaction chimique. Le défi de modélisation devient double : d'abord, il faut déterminer dans quel régime se trouve la flamme, pour ensuite choisir un modèle adéquat et performant pour le régime identifié.

Les trois autres articles de cette thèse reprennent la méthodologie employée dans [BM1, V] et le chapitre 1 pour un système idéalisé avec extinction et ré-allumage. Dans le chapitre 2, en l'absence d'advection (système non physique), nous montrons que l'analyse asymptotique de Liñán [L], effectuée pour des scalaires passifs bornés sur l'axe réel, est également valide pour des scalaires passifs construits comme des perturbations d'un gradient moyen [BM1]. Dans le chapitre 3, nous analysons l'impact d'un champ de vitesse sur le comportement des flammes, en particulier sur la caractérisation des paramètres d'extinction et de ré-allumage. Nous généralisons également les modèles de flammelle pour le système idéalisé d'équations avec advection. Finalement, dans le chapitre 4, nous validons la performance de l'estimateur d'erreur de modélisation dans ce contexte. Encore une fois, le coût numérique d'une telle procédure est crucial pour son utilisation.

**Contributions à la recherche :** Pour tous les articles de cette thèse, j'ai effectué la totalité des travaux de recherche, des simulations numériques et des graphiques, sous la supervision des professeurs Anne Bourlioux et Alexandre Ern (pendant mon séjour au CERMICS à l'École des Ponts Paris-Tech à l'automne 2006). Des rencontres hebdomadaires permettaient de générer de nouveaux points de vue et axes de recherche. L'article du premier chapitre a été soumis en juillet 2008 au *Multiscale Modeling and Simulation*, accepté pour publication en octobre 2009 et publié électroniquement en janvier 2010. Pour les simulations numériques de la section 1.6.2, j'ai modifié le code appartenant à Oleg Volkov pour y ajouter

le calcul des erreurs de modélisation dans la norme désirée. Quant à la rédaction des articles, le travail du premier chapitre a été partagé principalement entre Anne Bourlioux et moi-même, avec des corrections et des changements proposés par Alexandre Ern à chaque stade de l'écriture. Pour les deux derniers chapitres, j'ai produit le premier jet et les modifications ultérieures ont été partagées entre les auteurs.

Voici la référence complète de l'article du premier chapitre, reproduit ici avec la permission de la Society for Industrial and Applied Mathematics : A. BOURLIOUX, A. ERN, P. TURBIS, *A posteriori error estimation for subgrid flamelet models*, Mult. Mod. Simul., 8 (2010), pp. 481–497.

# Chapitre 1

---

## ESTIMATION D'ERREUR A POSTERIORI POUR LES MODÈLES DE FLAMMELETTE SOUS-MAILLE

### RÉSUMÉ

Une stratégie d'estimation des erreurs, basée sur les résidus pondérés, est évaluée dans le contexte des erreurs de modélisation liées à une classe de modèles sous-maille fréquemment utilisée en combustion turbulente. L'approche est mise en œuvre et validée sur un problème test idéalisé, composé d'un système d'équations multiéchelles d'advection-diffusion-réaction. Le régime de combustion ciblé est obtenu dans la limite d'une réaction rapide. Une simulation numérique détaillée, avec une résolution numérique adéquate pour les petites échelles réactives, serait trop coûteuse. Un modèle sous-maille est alors utilisé pour compenser l'effet des termes réactifs à plus grande échelle. La classe de modèles sous-maille considérée ici est basée sur l'approximation asymptotique de flammelette, menant aux librairies de flammelettes, des relations précalculables entre les scalaires réactifs et les scalaires passifs appropriés. Nous montrons qu'une librairie similaire peut être construite pour les solutions duales. La performance d'une telle stratégie d'estimation d'erreurs est validée par comparaison avec les erreurs exactes pour des cas tests stationnaires et instationnaires. L'estimateur nous donne les mêmes ordres asymptotiques que les simulations numériques détaillées ; cela mène à un

nouveau point de vue sur la mise en œuvre de modèles de flammelette pour les cas tests instationnaires.

## A posteriori error estimation for subgrid flamelet models

ANNE BOURLIOUX<sup>1</sup>, ALEXANDRE ERN<sup>2</sup>, PASCAL TURBIS<sup>1</sup>

### 1.1. ABSTRACT

A dual-weighted residual error estimation strategy is applied to the modeling error associated with a class of subgrid scale models widely used in turbulent combustion. The approach is implemented and validated for an idealized test problem consisting of a system of multiscale advection-reaction-diffusion equations. The regime of interest corresponds to the limit of fast reaction. A fully resolved numerical simulation of the resulting very fine reaction scale would be excessively demanding, so typically a subgrid model is used instead to account for its impact at large scales. The class of subgrid models investigated here is based on the asymptotic flamelet approximation, which leads to the so-called flamelet libraries, i.e., precomputed tables expressing the reactive scalars in terms of the appropriate passive scalar. We show that a similar library can be constructed for the dual-based estimator. The performance of the estimation strategy is validated by comparison with exact results for steady and unsteady test cases. Asymptotic scalings are recovered, and new light is shed on some specific implementations of the flamelet models for unsteady test cases.

**Key words.** numerical combustion, model selection, a posteriori error estimate, flamelet, nonpremixed flames

**AMS subject classifications.** 65J15, 65M15, 65N15, 76F10, 76F65

**DOI.** 10.1137/080726562

---

1. Département de mathématiques et de statistique, Université de Montréal, CP 6128 succ. Centre-ville, Montréal (Québec) H3C 3J7, Canada. The work of these authors was funded by NSERC and FQRNT-INRIA.

2. Université Paris-Est, CERMICS, École des Ponts, 6 et 8 av. Blaise Pascal, 77455 Marne la Vallée CEDEX 2, FRANCE.

Copyright ©2010 Society for Industrial and Applied Mathematics. Reprinted with permission. All rights reserved.

## 1.2. INTRODUCTION

Turbulent combustion simulations in the fast reaction regime are challenging multiscale problems because one needs to account for a very wide range of scales, from scales associated with turbulence down to the very small scales associated with thin flames. A direct numerical simulation approach, where one attempts to resolve all of these scales, would be prohibitively expensive for most realistic simulations. Instead, in large eddy simulations, only large scales are resolved and the effect of small scales is modeled. For the type of nonpremixed flames considered here, a widespread model is based on the so-called flamelet approach. The procedure is described in more detail in section 1.3.1; only an outline is given here. The governing equations for the chemical species mass fractions are unsteady, multidimensional, advection-diffusion-reaction equations. In the asymptotic limit of thin flames (fast reaction), it is possible to reduce those equations to a steady, one-dimensional equation, where the solution is expressed in terms of an appropriate reaction progress variable. After proper nondimensionalization, the reduced equation can be made parameter-free, and its solution can be compiled once and for all as a *flamelet library*, i.e., a precomputed table of the nondimensionalized solution for the reactive scalars in terms of the reaction progress variable [P1]. This approach has been extensively used in the simulation of turbulent flames [CR1, JLRH], including their large eddy simulations [CR2]. There are several strategies to implement the asymptotic reduction of the original equations, and this leads to a hierarchy of models. To each model corresponds a modeling error, because the reactive scalars satisfy the flamelet equations instead of the original equations. Good estimates of the modeling errors are needed to select the best model in any given situation.

In this paper, we investigate a strategy to estimate this modeling error a posteriori, similarly to the approach that is often used to estimate discretization errors in mesh-adaptive algorithms. With a good modeling error estimator, one could

design an effective strategy to select the appropriate model within a hierarchy of models so as to satisfy some error tolerance. Taken a step further, one could then combine this control with a discretization error control, so as to balance both sources of errors (see [BE1] for an example and [BE2] for an application to combustion simulations). A requirement for a viable strategy is that this a posteriori error analysis must be performed at a computational cost at most of the same order as the cost of using the flamelet model in the first place.

The strategy is evaluated in the context of an idealized model for turbulent nonpremixed flames consisting of a system of advection-reaction-diffusion equations, as described in section 1.3, where we also give details on the asymptotic flamelet model. The dual-weighted residual approach to modeling error estimation introduced in [BE1] is summarized and developed for our model in section 1.4. This idealized model is sufficiently simple that systematic parametric studies are feasible and numerical errors can be completely controlled. Section 1.5 describes the implementation of the strategy in the case of a steady shear flow. We validate our strategy to identify the best flamelet approximation with several numerical experiments. The good performance of the model selection strategy is confirmed when applied to a wider class of flows in section 1.6, including unsteady test cases.

### 1.3. FLAMELET MODELS

The idealized turbulent nonpremixed combustion model considered herein consists of a coupled system of advection-reaction-diffusion partial differential equations (PDEs) for the reactive scalars  $Y_1$  and  $Y_2$ , representing the mass fractions of fuel and oxidizer, respectively:

$$\frac{\partial Y_1}{\partial t} + \text{Pe } \mathbf{v} \cdot \nabla Y_1 = \Delta Y_1 - \text{Da } Y_1 Y_2, \quad (1.3.1)$$

$$\frac{\partial Y_2}{\partial t} + \text{Pe } \mathbf{v} \cdot \nabla Y_2 = \Delta Y_2 - \text{Da } Y_1 Y_2. \quad (1.3.2)$$

The flow field  $\mathbf{v}$  is chosen to be bidimensional, incompressible, and biperiodic of period  $P$ . The Péclet number  $\text{Pe}$  characterizes the importance of advection compared to diffusion, and the Damköhler number  $\text{Da}$  the importance of reaction

compared to diffusion. Turbulent combustion in the flamelet regime corresponds to the limit of large Pe and large Da.

A convenient strategy for solving (1.3.1)–(1.3.2) stems from the observation that the scalar  $Z = (Y_1 - Y_2)/2$  obeys the much simpler advection-diffusion equation

$$\frac{\partial Z}{\partial t} + \text{Pe } \mathbf{v} \cdot \nabla Z = \Delta Z. \quad (1.3.3)$$

The resulting equation no longer contains the nonlinear reaction term; therefore analysis and numerical simulations are much simpler for the passive scalar  $Z$  than for the reactive scalars. One can substitute this to (1.3.2), with (1.3.1) for the reactive scalar (now labeled  $Y$ ) written as

$$\frac{\partial Y}{\partial t} + \text{Pe } \mathbf{v} \cdot \nabla Y = \Delta Y - \text{Da } Y (Y - 2Z). \quad (1.3.4)$$

We look for a solution for the passive scalar  $Z$  as a perturbation of a mean gradient in the  $x$ -direction, i.e.,  $Z(x, y, t) = x/L_G + Z_p(x, y, t)$ , where  $L_G$  is the length scale associated with the imposed mean gradient and  $Z_p(x, y, t)$  is a periodic, zero-mean perturbation induced by the velocity field  $\mathbf{v}$ . The solution of (1.3.4) is computed on  $\Omega \times [0, T]$ , with  $\Omega = [-L, L] \times [0, P]$  and  $L$  large enough so that chemical equilibrium, given by  $Y = Z + |Z|$ , is satisfied at  $x = \pm L$ . The test cases are set up so that three distinct scales exist in the problem: the large scale  $L_G$ , the intermediate scale  $P$  due to the flow field, and the very thin flame thickness. The presence of this last very small scale in the solution for the reactive scalar is a computational challenge. Flamelet models are an approximation to the solution of (1.3.4) so that the impact of the fine-scale features of the solution can be accounted for without being fully resolved. Equation (1.3.3) has been studied exhaustively to analyze the performance of a very wide class of turbulence models [**BM2, MK**]. The particular setup for the passive scalar allows for a direct link with homogenization theory predictions. The analysis was extended to the reactive case [**BM1, V**] to study the performance of a hierarchy of flamelet models for both steady and unsteady cases.

### 1.3.1. The asymptotic flamelet subgrid model strategy

The flamelet subgrid modeling strategy can be outlined as follows. The objective is to predict the solution  $\bar{Y}$  of the equation for the reactive scalar defined as

$$\bar{Y} = \int Y(x, y) dx dy, \quad (1.3.5)$$

with the integration performed over elements of the large-scale mesh. For nonreactive variables, the filtered solution can be obtained as the solution of the filtered governing equation. If the equation is nonlinear to begin with, filtering leads to terms which can no longer be expressed solely as functions of the filtered variables and subgrid models are needed to express those unclosed terms as functions of the large-scale variables only. In the case of nonlinear reaction terms, there is no known strategy to formulate such a closure model at the level of the governing equation. Instead, in the flamelet regime,  $\bar{Y}$  is approximated by

$$\bar{Y} = \int Y(Z) \text{PDF}(Z) dZ. \quad (1.3.6)$$

This approximation is based on the following assumptions:

- (1) The resolved reactive scalar  $Y$  can be expressed as a function of the passive scalar  $Z$  (and other statistics of  $Z$ , depending on the model).
- (2) The probability distribution function of  $Z$ ,  $\text{PDF}(Z)$ , is known or can be modeled.

Assumption 2 is plausible because  $Z$  satisfies a much simpler equation (with no reaction term). Assumption 1 is the source of the modeling error that is investigated in this paper.

### 1.3.2. The steady laminar case

In the steady case with  $\text{Pe} = 0$ , it is easy to express  $Y$  as a function of  $Z$ . Indeed,  $Z_p = 0$  since  $Z = x/L_G$  solves (1.3.3). With a change of variables from  $x$  to  $Z$ , one can rewrite (1.3.4) as the ordinary differential equation (ODE)

$$\frac{d^2Y}{dZ^2} = \text{Da} L_G^2 Y (Y - 2Z). \quad (1.3.7)$$

Let  $\alpha \stackrel{\text{def}}{=} \text{Da} L_G^2$  (Damköhler group). Substitution of the normalized variables  $\hat{Z} = \alpha^{1/3} Z$  and  $\hat{Y} = \alpha^{1/3} Y$  in (1.3.7) leads to the parameter-free equation

$$\frac{d^2\hat{Y}}{d\hat{Z}^2} = \hat{Y} (\hat{Y} - 2\hat{Z}). \quad (1.3.8)$$

The solution of this equation can be computed once and for all and stored in a *flamelet library*. Figure 1.1 displays the flamelet solution in terms of the normalized correction to equilibrium  $d\hat{Y}(\hat{Z}) = \hat{Y} - (\hat{Z} + |\hat{Z}|)$ .

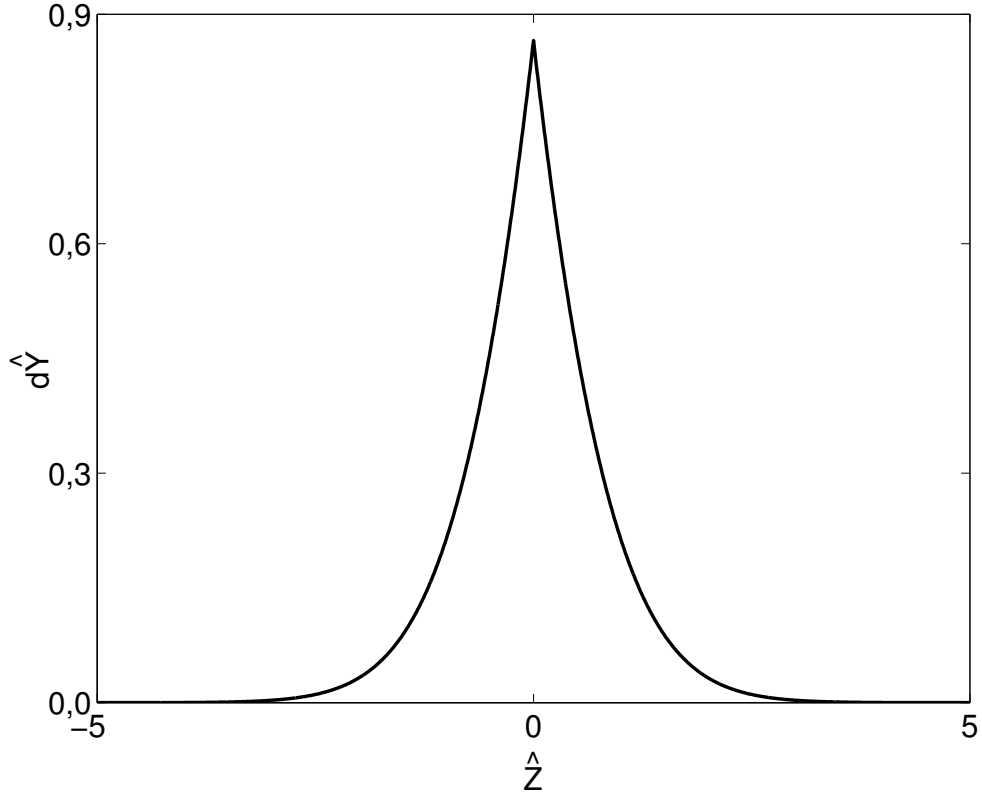


FIGURE 1.1. Flamelet library—correction term  $d\hat{Y}(\hat{Z}) = \hat{Y} - (\hat{Z} + |\hat{Z}|)$ .

### 1.3.3. The nonlaminar case

For  $\text{Pe} \neq 0$ , one would also like to express  $Y$  as a function of  $Z$  using the flamelet library previously defined. This would therefore reduce the computational cost of the problem from that of solving a bidimensional PDE (eq. (1.3.4)) down to computing—once—the solution of an ODE (eq. (1.3.8)) in terms of  $\hat{Z}$  and interpolating.

Let  $\chi_{ld} \stackrel{\text{def}}{=} |\nabla Z|^2$  be the local dissipation. In the steady laminar case,  $\chi_{ld} = 1/L_G^2$  and one can rewrite the Damköhler group as  $\alpha = \text{Da}/\chi_{ld}$ . In practical applications, the exact value of the local dissipation is not always available. Instead, one might have access only to its mean value  $\langle |\nabla Z|^2 \rangle$ , where  $\langle \cdot \rangle$  denotes averaging. In general, a flamelet model is obtained by selecting a parameter  $\chi$  called the dissipation (possibly time- and/or spatially varying), and the model can be written as

$$Y_{fl} = \alpha^{-1/3} \hat{Y}(\alpha^{1/3} Z), \quad (1.3.9)$$

with  $\alpha$  the Damköhler group corresponding to the specific choice of  $\chi$ . The simplest choices for the parameter  $\chi$  are either the mean or the local dissipation, but other choices will be discussed in section 1.6.

The flamelet approach just described can be summarized as follows:

- (1) Compute, once and for all, the flamelet library using (1.3.8). This yields the function  $\hat{Y}$ , that is, a way of modeling the reactive scalar  $Y$  as a function of the passive scalar  $Z$ .
- (2) Compute the passive scalar  $Z$  using (1.3.3). This equation is independent of Da and can be solved on a grid as coarse as the flow field allows.
- (3) Compute the dissipation. For more complex flamelet models, all required statistics of  $Z$  are computed in this step.
- (4) Use (1.3.9) to get an approximate solution  $Y_{fl}$  to the solution  $Y$  of (1.3.4).

At the end of the process, one obtains a coarse-grid solution taking small-scale features into account. For all choices of  $\chi$ , this approximation is asymptotically valid for large Da [BM1]. Out of this validity zone, modeling errors can become significant and model selection becomes crucial. One can accomplish this using a modeling error estimator and choosing the model giving the smallest error. This approach will be investigated in the following sections of the paper.

#### 1.4. MODELING ERROR ESTIMATION STRATEGY

Duality arguments have been used extensively to estimate a posteriori discretization errors in numerical solutions of PDEs, for example, for finite elements

[AO, BR, EJ] and finite differences [AN]. Another application is parameter identification; see [BBV] for an example in the context of combustion models. A more recent application is the estimation of modeling errors [ACS, BE1, ROV], where the objective now is to efficiently assess the errors that result from the approximation of the solution of a complex equation by the solution of a simpler model equation, which can be solved at a much lesser cost. We now summarize the approach introduced in [BE1] and give an example using the mean dissipation flamelet model to discuss its implementation.

#### 1.4.1. The dual-weighted residual estimator for nonlinear equations

The objective is to solve the following PDE, from now on referred to as the primal equation, written in weak form as

$$\text{Find } Y \in V \text{ such that } a(Y)(\varphi) + d(Y)(\varphi) = (f, \varphi) \quad \forall \varphi \in V. \quad (1.4.1)$$

The forms  $a, d : V \times V \rightarrow \mathbb{R}$  are linear in their second argument;  $V$  is an appropriate Hilbert space. Suppose that for computational efficiency reasons, one instead solves the reduced primal equation obtained by neglecting the form  $d$  in (1.4.1):

$$\text{Find } Y_{fl} \in V \text{ such that } a(Y_{fl})(\varphi) = (f, \varphi) \quad \forall \varphi \in V. \quad (1.4.2)$$

In the following, the subscript  $\cdot_{fl}$  will be used for solutions of reduced equations. The impact of using the reduced primal solution  $Y_{fl}$  in place of the primal solution  $Y$  is evaluated in terms of a given linear output functional  $j : V \rightarrow \mathbb{R}$ . The modeling error to be estimated is  $j(Y) - j(Y_{fl})$ . The first step in the estimation strategy is to consider the dual equation corresponding to  $j$ :

$$\text{Find } q \in V \text{ such that } a'(Y)(\psi, q) + d'(Y)(\psi, q) = j'(Y)(\psi) \quad \forall \psi \in V, \quad (1.4.3)$$

where  $a'(Y)(v, \varphi) \stackrel{\text{def}}{=} \lim_{\varepsilon \rightarrow 0} \frac{a(Y + \varepsilon v)(\varphi) - a(Y)(\varphi)}{\varepsilon}$  is the directional derivative of  $a$  at  $Y$  in the  $v$ -direction ( $d'(Y)(v, \varphi)$  and  $j'(Y)(v)$  are defined similarly). A reduced dual equation approximating (1.4.3) is obtained by ignoring the form  $d'$  and replacing  $Y$  by its approximation  $Y_{fl}$ :

$$\text{Find } q_{fl} \in V \text{ such that } a'(Y_{fl})(\psi, q_{fl}) = j'(Y_{fl})(\psi) \quad \forall \psi \in V. \quad (1.4.4)$$

Braack and Ern [BE1] have shown that if  $a(Y)(\cdot)$ ,  $d(Y)(\cdot)$ , and  $j(Y)$  are sufficiently differentiable,

$$j(Y) - j(Y_{fl}) = -d(Y_{fl})(q_{fl}) - \frac{1}{2} \{ d(Y_{fl})(q - q_{fl}) + d'(Y_{fl})(Y - Y_{fl}, q_{fl}) - R \}, \quad (1.4.5)$$

where

$$R = \int_0^1 L'''((Y_{fl}, q_{fl}) + \lambda e)(e, e, e) \cdot \lambda (1 - \lambda) d\lambda \quad (1.4.6)$$

is cubic in the error  $e \stackrel{\text{def}}{=} (Y - Y_{fl}, q - q_{fl})$  and  $L$  is defined on  $V \times V$  by

$$L(Y, q) = j(Y) + (f, q) - a(Y)(q) - d(Y)(q). \quad (1.4.7)$$

The modeling error is given by  $j(Y) - j(Y_{fl}) \approx -d(Y_{fl})(q_{fl})$  to first order in  $\|d\|$  [BE1]. We will show in section 1.4.4 using asymptotics in the Damköhler number that  $-d(Y_{fl})(q_{fl})$  is indeed the dominating term for our setup.

#### 1.4.2. A steady-state example: The mean dissipation flamelet model

To illustrate this modeling error estimation methodology when applied to our steady-state setup, the mean dissipation flamelet approximation will be detailed further. This example will also lead us to some interesting observations regarding practical implementations of this method.

The primal equation consists of solving (1.3.4) for  $Y$ , which we rewrite as

$$\text{Pe} \mathbf{v} \cdot \nabla Y - \Delta Y + \text{Da} Y (Y - 2Z) \frac{|\nabla Z|^2}{\chi} = \text{Da} Y (Y - 2Z) \left( \frac{|\nabla Z|^2}{\chi} - 1 \right), \quad (1.4.8)$$

with the dissipation  $\chi$  given by  $\chi = \langle |\nabla Z|^2 \rangle$ . The reduced primal equation is obtained by differentiating (1.3.9) to obtain a PDE for the approximate solution  $Y_{fl}$ :

$$\text{Pe} \mathbf{v} \cdot \nabla Y_{fl} - \Delta Y_{fl} + \text{Da} Y_{fl} (Y_{fl} - 2Z) \frac{|\nabla Z|^2}{\chi} = 0. \quad (1.4.9)$$

Thus, we obtain the forms

$$a(Y)(\varphi) = \int_{\Omega} \left\{ (-\text{Pe} \mathbf{v} \cdot \nabla \varphi) Y + \nabla Y \cdot \nabla \varphi + \text{Da} Y (Y - 2Z) \frac{|\nabla Z|^2}{\chi} \varphi \right\} dx dy, \quad (1.4.10)$$

$$d(Y)(\varphi) = \int_{\Omega} \text{Da} Y (Y - 2Z) \left( 1 - \frac{|\nabla Z|^2}{\chi} \right) \varphi dx dy, \quad (1.4.11)$$

with the space  $V = \{f \in H^1(\Omega) \mid f(x, 0) = f(x, P) \ \forall x \in [-L, L], f(\pm L, y) = 0 \ \forall y \in [0, P]\}$ . Note that  $Y \notin V$ , but one can write  $Y = Y_0 + Z + |Z|$ , where  $Y_0 \in V$ ; this also applies to  $Y_{fl}$ .

Consider the output functional

$$j(Y) = \int_{\Omega} Y(x, y) dx dy. \quad (1.4.12)$$

This leads to the following expressions to be plugged into the dual and reduced dual equations (1.4.3)–(1.4.4):

$$a'(Y)(\psi, q) = \int_{\Omega} \left\{ (-Pe \mathbf{v} \cdot \nabla q) \psi + \nabla \psi \cdot \nabla q + 2Da(Y - Z) \frac{|\nabla Z|^2}{\chi} q \psi \right\} dx dy, \quad (1.4.13)$$

$$d'(Y)(\psi, q) = \int_{\Omega} 2Da(Y - Z) \left( 1 - \frac{|\nabla Z|^2}{\chi} \right) q \psi dx dy, \quad (1.4.14)$$

$$j'(Y)(\psi) = \int_{\Omega} \psi dx dy. \quad (1.4.15)$$

The modeling error can be approximated using

$$\int_{\Omega} (Y - Y_{fl}) dx dy \approx - \int_{\Omega} Da Y_{fl} (Y_{fl} - 2Z) \left( 1 - \frac{|\nabla Z|^2}{\chi} \right) q_{fl} dx dy. \quad (1.4.16)$$

### 1.4.3. Computing the reduced dual solution

For the previous example, if we assume  $q$  and  $q_{fl}$  are sufficiently differentiable, then they solve

$$-Pe \mathbf{v} \cdot \nabla q - \Delta q + 2Da(Y - Z) q = 1 \quad (1.4.17)$$

and

$$-Pe \mathbf{v} \cdot \nabla q_{fl} - \Delta q_{fl} + 2Da(Y_{fl} - Z) \frac{|\nabla Z|^2}{\chi} q_{fl} = 1, \quad (1.4.18)$$

respectively, in  $\Omega$ . It is not desirable to solve (1.4.18) numerically, since the equation is a multiscale problem; for large  $Da$ , the solution has fine-scale features, and a very fine mesh is required for accuracy, making the estimation strategy an order of magnitude more expensive than the modeling strategy to which it is applied. For the modeling error estimation strategy to be useful, one must find a way to solve (1.4.18) at a cost at most that of the flamelet approximation. To approximate its solution, one goes back to the steady laminar flamelet. For  $Pe = 0$ ,

(1.4.17)–(1.4.18) reduce to

$$-\frac{1}{L_G^2} \frac{d^2 q}{dZ^2} + 2 \text{Da} (Y - Z) q = 1. \quad (1.4.19)$$

Let  $\hat{q} = \text{Da}^{2/3} L_G^{-2/3} q$ . Using the previous normalizations for  $Y$  and  $Z$ , one obtains

$$-\frac{d^2 \hat{q}}{d\hat{Z}^2} + 2 (\hat{Y} - \hat{Z}) \hat{q} = 1. \quad (1.4.20)$$

As for the flamelet approximation, one can compute the solution of (1.4.20) once and for all and store it into a *dual flamelet library*; see Figure 1.2. One can also expand this to turbulent cases by defining  $\hat{q} = \text{Da}^{2/3} \chi^{1/3} q$ . This dual flamelet library provides a good approximation to the solutions of (1.4.17)–(1.4.18) at least if the Damköhler number is large enough, while controlling the computational cost of the error estimator.

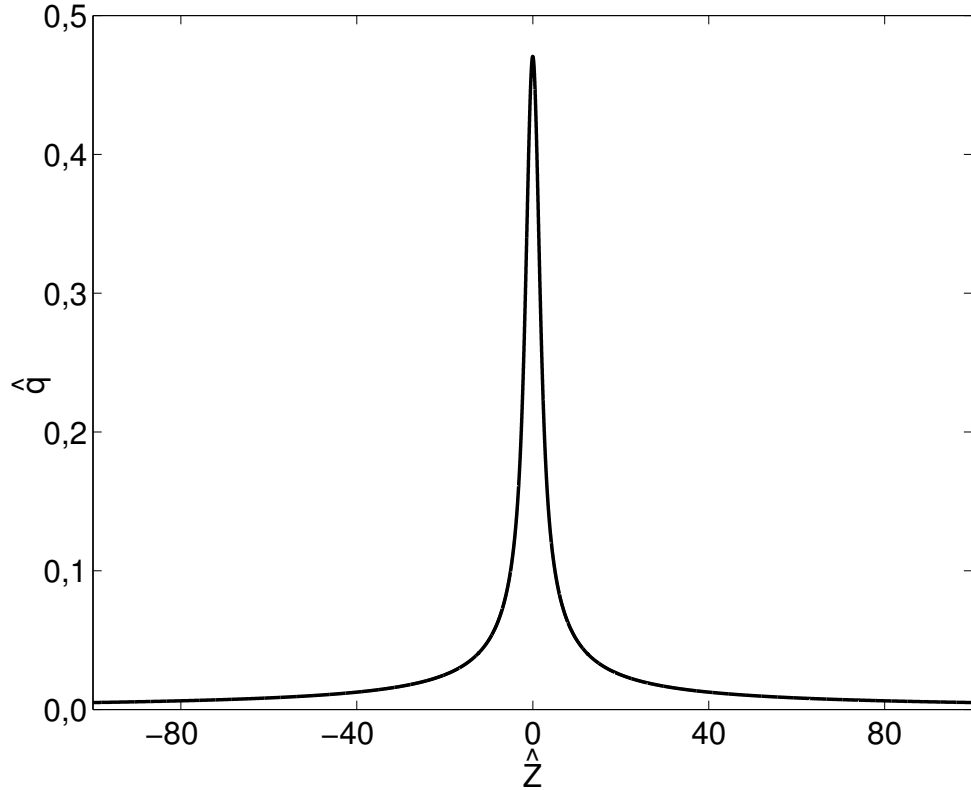


FIGURE 1.2. Dual flamelet library for  $j(Y) = \int_{\Omega} Y(x, y) dx dy$ .

Two estimation strategies are used in this paper:

- (1) Strategy 1: Solving (1.4.17) directly and estimating the modeling error using  $-d(Y_{fl})(q)$ . As shown in the next section, this strategy leads to excellent performance of the estimators (they are exact for linear equations). This is a purely theoretical exercise, since it is too expensive computationally for practical purposes.
- (2) Strategy 2: Estimating the modeling error using  $-d(Y_{fl})(q_{fl})$ , where

$$q_{fl} = \text{Da}^{-2/3} \chi^{-1/3} \hat{q} \left( \text{Da}^{1/3} \chi^{-1/3} Z \right) \quad (1.4.21)$$

and  $\hat{q}(\hat{Z})$  is the dual flamelet library. This strategy will be shown to be very cost effective and reliable.

#### 1.4.4. Approximating the modeling error

In [BE1], it is supposed that  $\|d\|$  is small enough to lead to a single-term modeling error estimation. Even in the mean dissipation example (section 1.4.2), one cannot compute  $\|d\|$  easily. In this subsection, further analysis will show that  $-d(Y_{fl})(q_{fl})$  is larger in the flamelet regime than the neglected terms.

First, note that  $|Y - Y_{fl}| = O(\text{Da}^{-1/3})$  [BM1],  $|q - q_{fl}| = O(\text{Da}^{-2/3})$  (this can be deduced using the  $\hat{q}$  normalization), and the reaction zone is of size  $O(\text{Da}^{-1/3})$  (based on the  $\hat{Z}$  normalization). By checking the order of the various terms in (1.4.2) with respect to  $\text{Da}$ , one obtains

$$\begin{aligned} |d(Y_{fl})(q_{fl})| &= \left| \int_{\Omega} \text{Da} Y_{fl} (Y_{fl} - 2Z) \left( 1 - \frac{|\nabla Z|^2}{\chi} \right) q_{fl} dx dy \right| \\ &\leq \text{Da}^{-1/3} \left\| \hat{Y} (\hat{Y} - 2\hat{Z}) \hat{q} \right\|_{L^{\infty}(\Omega)} \left\| 1 - \frac{|\nabla Z|^2}{\chi} \right\|_{L^{\infty}(\Omega)} |\Omega| \\ &= O(\text{Da}^{-1/3}), \end{aligned} \quad (1.4.22)$$

$$\begin{aligned} |d(Y_{fl})(q - q_{fl})| &= \left| \int_{\Omega} \text{Da} Y_{fl} (Y_{fl} - 2Z) \left( 1 - \frac{|\nabla Z|^2}{\chi} \right) (q - q_{fl}) dx dy \right| \\ &\leq \text{Da}^{1/3} \left\| \hat{Y} (\hat{Y} - 2\hat{Z}) \hat{q} \right\|_{L^{\infty}} \left\| 1 - \frac{|\nabla Z|^2}{\chi} \right\|_{L^{\infty}} \int_{\Omega} |q - q_{fl}| dx dy \\ &= O(\text{Da}^{-2/3}), \end{aligned} \quad (1.4.23)$$

(taking into account the size of the reaction zone)

$$\begin{aligned}
|d'(Y_{fl})(Y - Y_{fl}, q_{fl})| &= \left| \int_{\Omega} 2 \text{Da} (Y_{fl} - Z) \left( 1 - \frac{|\nabla Z|^2}{\chi} \right) (Y - Y_{fl}) q_{fl} dx dy \right| \\
&\leq 2 \left\| (\widehat{Y} - \widehat{Z}) \widehat{q} \right\|_{L^\infty} \left\| 1 - \frac{|\nabla Z|^2}{\chi} \right\|_{L^\infty} \int_{\Omega} |Y - Y_{fl}| dx dy \\
&= O(\text{Da}^{-2/3}),
\end{aligned} \tag{1.4.24}$$

$$\begin{aligned}
|R| &= 6 \text{Da} \left| \int_0^1 \lambda (1 - \lambda) d\lambda \int_{\Omega} (Y - Y_{fl})^2 (q - q_{fl}) dx dy \right| \\
&\leq \text{Da} \int_{\Omega} |Y - Y_{fl}|^2 |q - q_{fl}| dx dy \\
&= O(\text{Da}^{-2/3}).
\end{aligned} \tag{1.4.25}$$

Hence  $-d(Y_{fl})(q_{fl})$  is the largest term for sufficiently large Da.

## 1.5. APPLICATION TO A STEADY SIMPLE SHEAR FLOW

We investigate next some numerical results of the application of this strategy to the estimation of the modeling error associated with the flamelet subgrid approximation. As a first example, we consider a steady simple shear flow,  $\mathbf{v} = (\sin(K_J y), 0)$ , with periodicity  $P = 2\pi/K_J$ . The steady solution of (1.3.3) is given by

$$Z(x, y) = \frac{1}{L_G} \left\{ x - \frac{\text{Pe}}{K_J^2} \sin(K_J y) \right\}. \tag{1.5.1}$$

There is no explicit solution for the reactive scalar  $Y$ . In the limit of infinite Da,  $Y$  converges to the equilibrium solution  $Y_{eq} \stackrel{\text{def}}{=} Z + |Z|$ , obtained as the solution for which the reaction rate  $\omega = \text{Da} Y (Y - 2Z)$  is a delta function centered around  $Z = 0$ ; at large but finite Da, the departure from  $Y_{eq}$  is expected to be small. It is fairly straightforward to compute it numerically with arbitrary accuracy [BM1]. Figure 1.3 shows the solutions  $Z$ ,  $Y$ , and  $\omega$  corresponding to  $\text{Pe} = 200$ ,  $\text{Da} = 10^4$ ,  $K_J = 2\pi$ , and  $L_G = 10$ . The contour corresponding to the stoichiometric level  $Z = 0$  is also shown. As seen from the figure, for this large Da example, the reaction zone is a narrow band closely aligned with the  $Z = 0$  level. The flamelet approximation  $Y = Y(Z)$  is therefore very good in this case.

In this section, two flamelet models are studied:

- (1) the *local dissipation model*, with  $\chi = |\nabla Z|^2$ ;

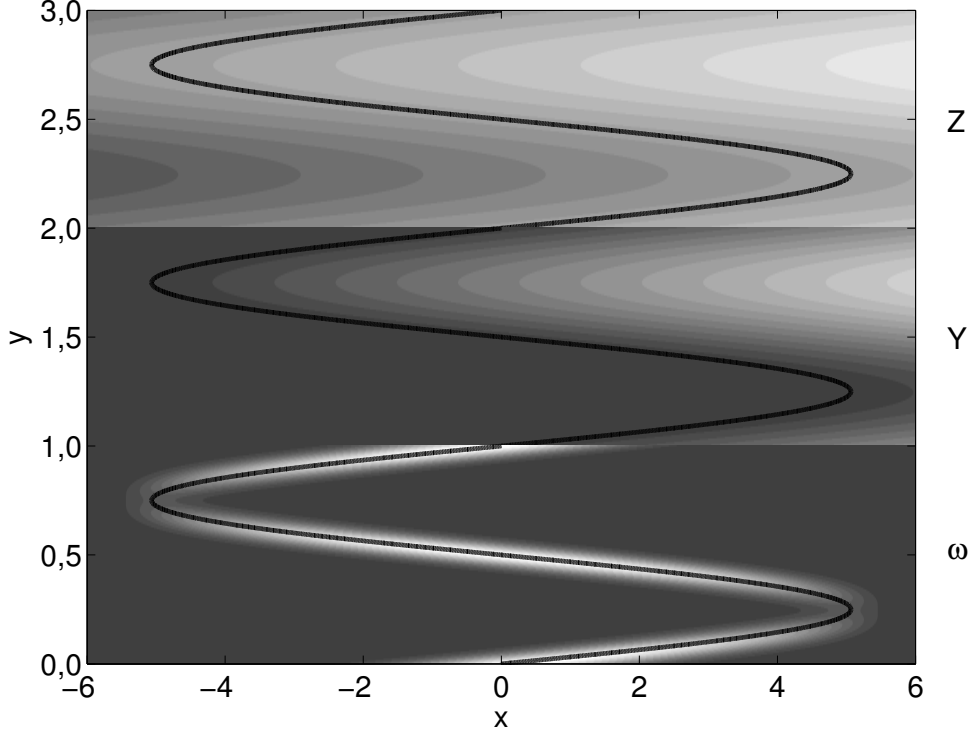


FIGURE 1.3. Simple shear—solutions  $Z$ ,  $Y$ , and  $\omega$  for high Pe and high Da (stoichiometric level  $Z = 0$  in black).

(2) the *mean dissipation model*, with  $\chi = \langle |\nabla Z|^2 \rangle$ .

Plugging these values of  $\chi$  into (1.3.9) gives two solutions, whose respective performances in the Pe-Da parameter space have been analyzed previously [BM1].

We validate the error estimator by comparing the predictions with exact values for the modeling errors. The exact solution  $Y$  is obtained numerically by using Newton's method and centered finite differences to solve (1.3.4). Convergence is very fast if one uses the flamelet solution as an initial guess [BM1]. A very fine mesh is used so that discretization errors are very small compared to modeling errors. Throughout the rest of this paper,  $L_G = L = 10$  and  $K_J = 2\pi$  [BM1].

Figure 1.4 shows the errors on  $j(Y)$  for the local dissipation model for Péclet numbers 10 and 200. Three curves are shown: exact errors, estimations using  $q$  (strategy 1, dual equation), and estimations using  $q_{fl}$  (strategy 2, dual flamelet library). For both values of Pe, the curves for the first strategy follow the exact error curves very closely. This indicates that the dual flamelet library approximation is not a concern. The difference between the estimation using  $q_{fl}$  and the

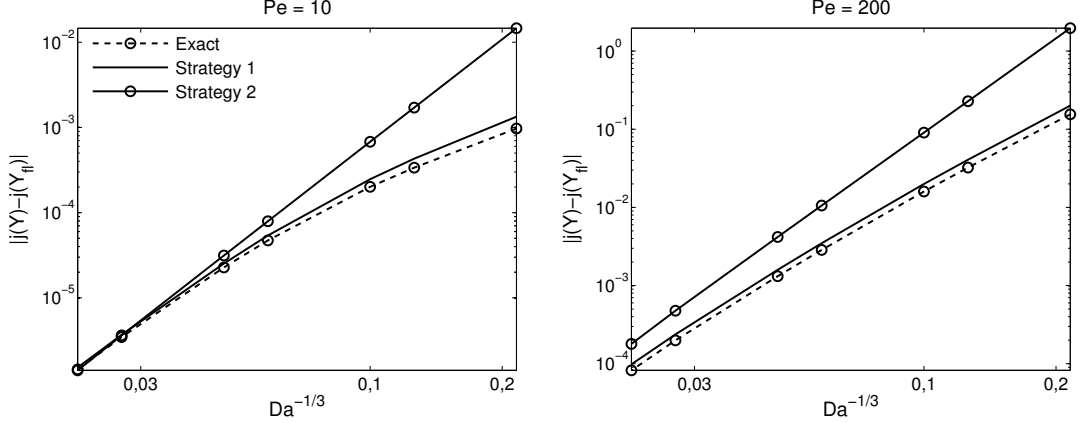


FIGURE 1.4. Shear flow—estimated local dissipation model errors as functions of  $\text{Da}^{-1/3}$  for  $\text{Pe} = 10$  (left) and  $\text{Pe} = 200$  (right).

exact values is therefore the result of the flamelet-type approximation. In the flamelet regime, the agreement between the estimated and exact errors is very good. Out of this zone, errors are overestimated by about one order of magnitude by the estimator. The asymptotic trend of the error is also recovered by the estimator; the modeling error is of order  $\text{Da}^{-4/3}$  for large  $\text{Da}$ .

For this choice of output functional, one cannot compare both flamelet models, as the modeling error estimator is identically 0 for  $\chi = \langle |\nabla Z|^2 \rangle$ . To see why this is true, note that (1.5.1) guarantees that the  $(x, y) \mapsto (\hat{Z}, y)$  coordinate system transformation is bijective. One can rewrite the mean dissipation model error estimator  $-d(Y_{fl})(q_{fl})$  into the  $(\hat{Z}, y)$  coordinate system

$$\begin{aligned} -d(Y_{fl})(q_{fl}) &= - \int_{\Omega} \text{Da} Y_{fl} (Y_{fl} - 2Z) \left( 1 - \frac{|\nabla Z|^2}{\chi} \right) q_{fl} dx dy \\ &= -L_G \text{Da}^{-1/3} \chi^{-2/3} \int_{\hat{Z}} \hat{Y} (\hat{Y} - 2\hat{Z}) \hat{q} d\hat{Z} \int_y (\chi - |\nabla Z|^2) dy. \end{aligned} \quad (1.5.2)$$

Hence the error estimator will be identically zero for  $\chi = \langle |\nabla Z|^2 \rangle$ . This is a direct consequence of using the dual flamelet library. By looking at the estimated errors, one would guess that the mean dissipation flamelet model gives a smaller error than the local dissipation flamelet model. This is a false assumption [BM1].

To compare both flamelet models effectively, one must use a different output functional. Here, we use

$$j(Y, y_0) = \int_{\Omega} Y(x, y_0) dx = L_G \int_{\Omega} Y(Z, y_0) dZ \quad (1.5.3)$$

as the output functional. With this new choice of  $j$ , the primal dual equation (1.4.17) becomes

$$-\text{Pe} \mathbf{v} \cdot \nabla q - \Delta q + 2\text{Da}(Y - Z) q = \delta(y - y_0). \quad (1.5.4)$$

Using the same approximations for  $q$  made in section 1.4.3, one gets

$$-\frac{d^2 \hat{q}}{d \hat{Z}^2} + 2(\hat{Y} - \hat{Z}) \hat{q} = \delta(y - y_0). \quad (1.5.5)$$

Since the mean and local dissipations are constant for a given value of  $y$  and  $(x, y) \mapsto (\hat{Z}, y)$  is a valid coordinate system, the solution of (1.5.5) can be written as the solution of the dual flamelet library (eq. (1.4.20)) times  $\delta(y - y_0)$ . Thus the previous primal and dual flamelet libraries are used to estimate

$$\int_{y_0} |j(Y, y_0) - j(Y_{fl}, y_0)| dy_0 = L_G \int_y \left| \int_Z (Y(Z, y) - Y_{fl}(Z, y)) dZ \right| dy. \quad (1.5.6)$$

This new choice of  $j$  ensures that no analytical cancellations appear in the process.

Figure 1.5 shows the estimated and exact errors for this choice of output functional. Again, the error estimator is very good in the flamelet regime while overestimating the exact error by one or two orders of magnitude away from that regime. One also recognizes the same asymptotic trends observed in Figure 1.4 for the error estimator. By using a variable change similar to the one used in (1.5.2), one shows that the mean dissipation flamelet modeling error is of order  $\text{Da}^{-2/3}$ , while the local dissipation flamelet modeling error is of order  $\text{Da}^{-4/3}$ ; both asymptotic behaviors are recovered by the error estimator. The modeling error estimator predicts which flamelet model is better with good accuracy. For  $\text{Pe} = 10$ , there is qualitative agreement between exact and estimated crossover values of  $\text{Da}$ ; for  $\text{Pe} = 200$ , the crossover value is slightly overestimated. In conclusion, one could use the estimator to efficiently predict which model is better for a given set of parameters.

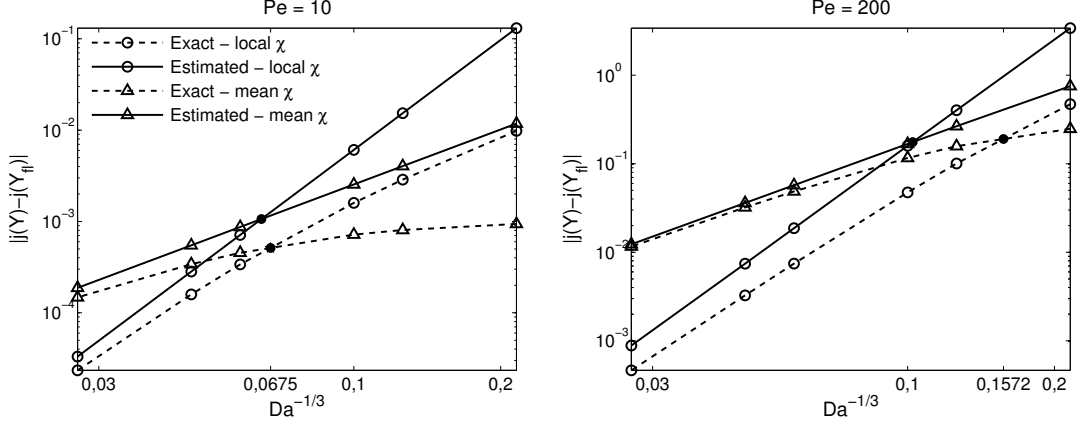


FIGURE 1.5. Shear flow—estimated (see (1.5.6)) and exact errors as functions of  $\text{Da}^{-1/3}$  for  $\text{Pe} = 10$  (left) and  $\text{Pe} = 200$  (right). Dots show the location of crossover points.

## 1.6. APPLICATIONS TO A BROADER CLASS OF FLOWS

In this section, we generalize the approach to a wider class of flow fields, including unsteady flows. For most flows, the change of variables from  $(x, y)$  to  $(Z, y)$  is no longer bijective, as was the case for the simple shear, and the dissipation is no longer a function of  $y$  only.

### 1.6.1. Steady Childress–Soward flow

First, we investigate the flow given by

$$\mathbf{v} = \left( -\frac{\partial F}{\partial y}, \frac{\partial F}{\partial x} \right), \quad (1.6.1)$$

where

$$F(x, y) = K (\sin(K_J x) \sin(K_J y) + \delta \cos(K_J x) \cos(K_J y)). \quad (1.6.2)$$

For this Childress–Soward flow, the constant  $K$  is chosen so that the mean kinetic energy is 1. The behavior of the flow changes drastically with  $\delta$ ;  $\delta = 0$  corresponds to a tilted shear flow, while  $\delta = 1$  is a small-scale array of eddies. The case  $\delta = 0.5$  is of particular interest to complex flows, as it is a mix of shear and eddies [BM1]. Numerical results for the passive scalar  $Z$ , the reactive scalar  $Y$ , and the reaction rate  $\omega$  are shown in Figure 1.6 for  $\delta = 0.5$ , alongside the stoichiometric level

$Z = 0$ . Other parameters used in the numerical simulation are  $\text{Pe} = 200$  and  $\text{Da} = 10^4$ .

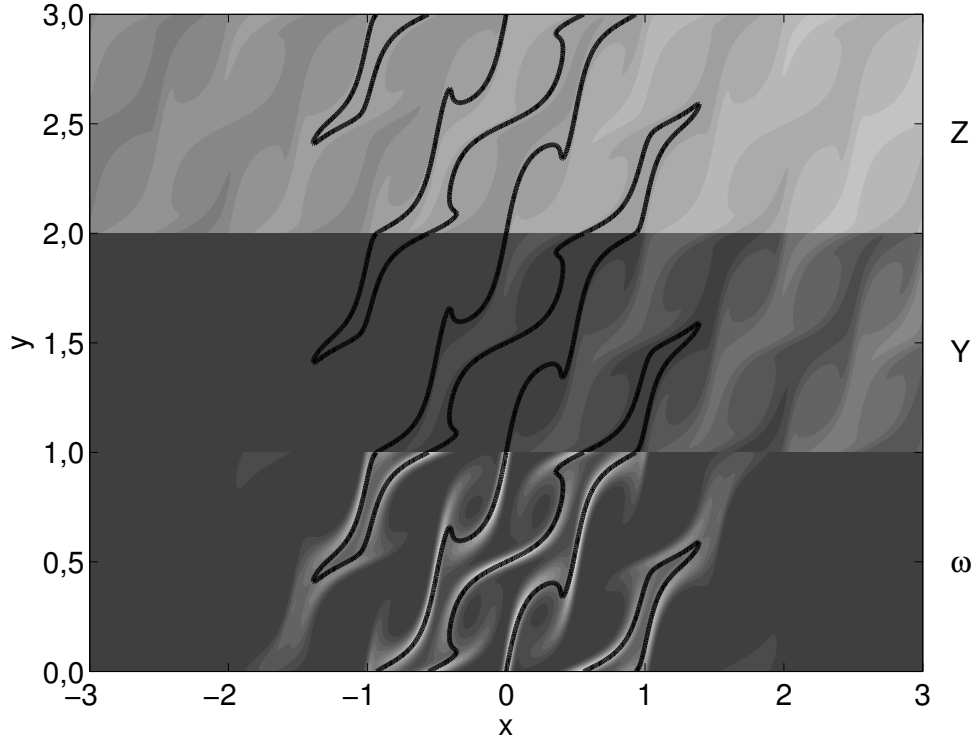


FIGURE 1.6. Childress–Soward flow—solutions  $Z$ ,  $Y$ , and  $\omega$  for high  $\text{Pe}$ , high  $\text{Da}$ , and  $\delta = 0,5$  (stoichiometric level  $Z = 0$  in black).

The first experiment consists of estimating the modeling error corresponding to the local dissipation model as a function of  $\text{Da}^{-1/3}$  for Péclet numbers 10 and 200. The estimated and exact errors on  $j(Y)$  for the Childress–Soward flow (with  $\delta = 0,5$ ) are shown in Figure 1.7. Similarly to the simple shear flow case, the error estimator is very good in the flamelet regime, performs quite well away from that regime, and has correct asymptotic convergence of the estimator at high  $\text{Da}$  values ( $O(\text{Da}^{-4/3})$ ).

In the next experiment, we investigate a generalized version of the mean dissipation model, in which the dissipation is spatially constant but not necessarily equal to the mean dissipation. In Figure 1.8, the exact and estimated errors on  $j(Y)$  (expectation of  $Y$ ) are plotted against the constant dissipation  $\chi$  for  $\delta = 0,5$ ,  $\text{Pe} = 10$ , and  $\text{Da} = 100$ . One can see that the exact value of the modeling error has a nonzero minimum value near  $\chi = \langle |\nabla Z|^2 \rangle = 2,0860 \times 10^{-2}$ . As was the

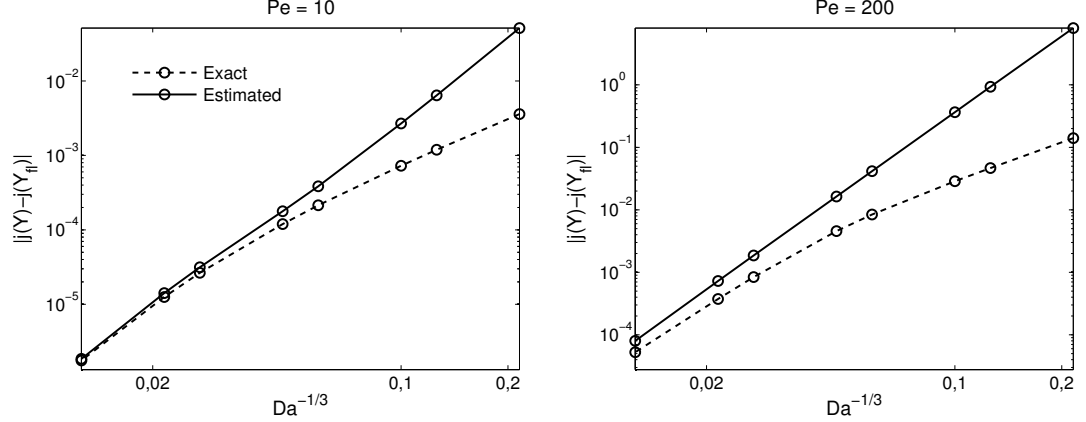


FIGURE 1.7. Childress–Soward flow—estimated and exact local dissipation model errors as functions of  $\text{Da}^{-1/3}$  for  $\text{Pe} = 10$  (left) and  $\text{Pe} = 200$  (right).

case for the steady simple shear flow, the mean dissipation model leads to an identically zero estimation for the modeling error. Overall, the error estimator captures very well the qualitative trends of the exact modeling error.

### 1.6.2. Unsteady shear

We now study the performance of the modeling error estimator for a class of unsteady flamelet models. The velocity field is given by  $\mathbf{v} = (\sin(K_J y), \cos(\omega t))$ . We seek a solution of the form

$$Z(x, y, t) = \frac{x}{L_G} + Z_p(y, t), \quad (1.6.3)$$

where  $Z_p(y, t) = A(t) \cos(K_J y - \phi(t))$ . There is no analytical solution for this setup, but the numerical solution for  $Z$  is obtained very easily by solving a system of two ODEs, with the initial conditions specified to obtain the unique time-periodic solution. For this type of problem, one chooses

$$j(Y) = \frac{\omega}{2\pi} \int_{t=0}^{2\pi/\omega} \int_{\Omega} Y(x, y, t) \, dx \, dy \, dt \quad (1.6.4)$$

as the output functional.

Even for this unsteady problem, one seeks a steady flamelet approximation to the solution. The modeling challenge is to specify at each time the appropriate value for the dissipation parameter in the flamelet model. We consider here only

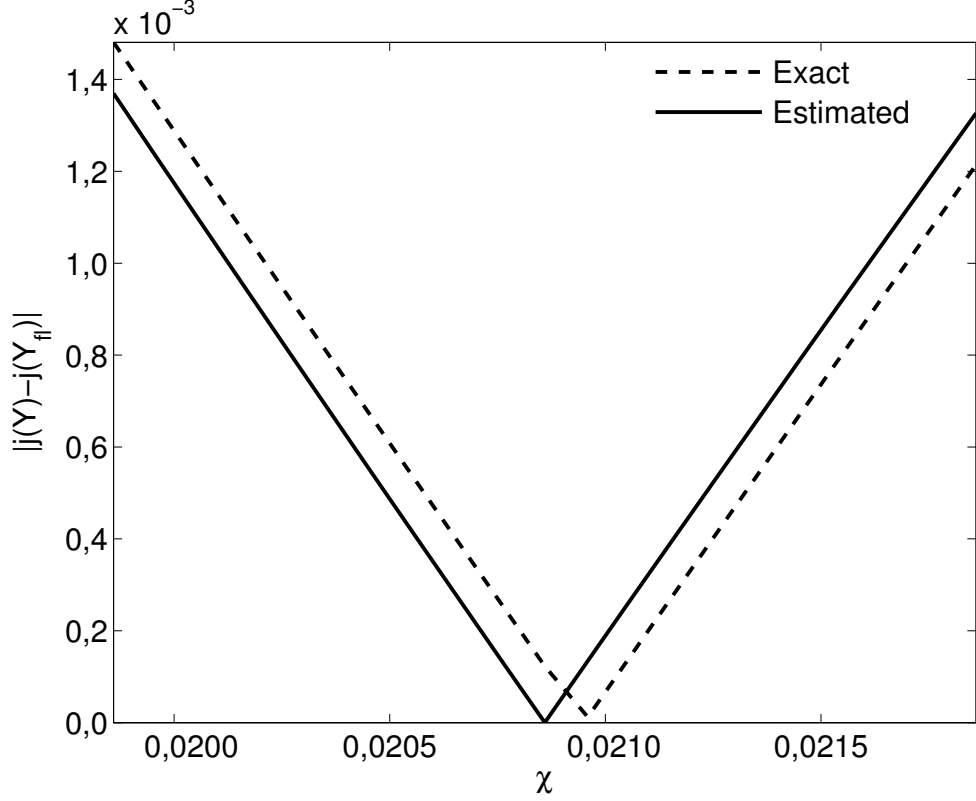


FIGURE 1.8. Childress–Soward flow—estimated and exact modeling errors as functions of a spatially constant dissipation  $\chi$ .

dissipations of the form  $\chi = \chi(t)$  (no spatial dependence). Here are three flamelet models, first proposed in [CEP] and studied for the present setup in [V]:

- (1) Instantaneous dissipation model:  $\chi_{inst}(t) = \langle |\nabla Z|^2(y, t) \rangle_y$  (spatial mean only).
- (2) Mean dissipation model:  $\chi_{mean}(t) = \langle \chi_{inst}(t) \rangle_t$  (spatiotemporal mean).
- (3) One-dimensional full unsteady laminar flamelet assumption (1-D FULFA [CEP, V]) model:  $\chi_F(t)$ , which solves

$$\frac{d\chi_F}{dt} = 3\widehat{Y} \left( \widehat{Z} = 0 \right) (\chi_{inst} - \chi_F) (Da^2 |\chi_F|)^{1/3}. \quad (1.6.5)$$

One expects that the instantaneous dissipation model performs best if the chemistry is very fast (large Da), whereas the mean dissipation model is better for slow chemistry. This was indeed confirmed in [V]. Moreover, it was also shown that the 1-D FULFA model, which links the two other models at intermediate

values of Da, is the optimal model for all flamelet models using a dissipation of the form  $\chi = \chi(t)$ , but this performance comes at a higher computational cost.

In the  $(\hat{Z}, y, t)$  coordinate system, the modeling error estimator for any dissipation  $\chi = \chi(t)$  is expressed as

$$\begin{aligned} -\frac{2\pi}{\omega L_G} (j(Y) - j(Y_{fl})) &\approx \text{Da}^{-4/3} \int_t \frac{d}{dt} (\chi^{1/3}) \int_{(\hat{Z}, y)} (\hat{Y} - \hat{Y}' \hat{Z}) \hat{q} d\hat{Z} dy dt \\ &+ \text{Da}^{-2/3} \int_t \chi^{2/3} \int_y \left(1 - \frac{|\nabla Z|^2}{\chi}\right) \int_{\hat{Z}} \hat{Y} (\hat{Y} - 2\hat{Z}) \hat{q} d\hat{Z} dy dt. \end{aligned} \quad (1.6.6)$$

The first term is equal to 0 since  $\chi$  is time-periodic. From the previous expression, one sees that the various dissipation models lead to different residual control strategies:

- (1) The instantaneous dissipation model controls the second term of the residual, whose contribution vanishes after integration with respect to  $y$ .
- (2) The mean dissipation model controls the first term of the residual, which is identically zero before integration. Incidentally, as was the case for the steady shear, the contribution of the second term of the residual also vanishes after integration with respect to  $y$  and  $t$ .
- (3) The 1-D FULFA model simultaneously controls both terms of the residual, which is identically zero along the stoichiometric level  $Z = 0$ —this is how the model is constructed in the first place.

To compare the performance of the flamelet models, we choose a slightly different output functional to avoid the numerical cancellation associated with the mean dissipation model for the present setup. Similarly to the steady simple shear case, one chooses

$$j(Y, y_0) = \frac{\omega}{2\pi} \int_{(x,t)} Y(x, y_0, t) dx dt = \frac{\omega L_G}{2\pi} \int_{(Z,t)} Y(Z, y_0, t) dZ dt \quad (1.6.7)$$

as the output functional to estimate

$$\int_{y_0} |j(Y, y_0) - j(Y_{fl}, y_0)| dy_0. \quad (1.6.8)$$

Figure 1.9 shows the computed errors for this functional as a function of  $\text{Da}^{-1/3}$  for  $\text{Pe} = 200$ . The exact error computations show that

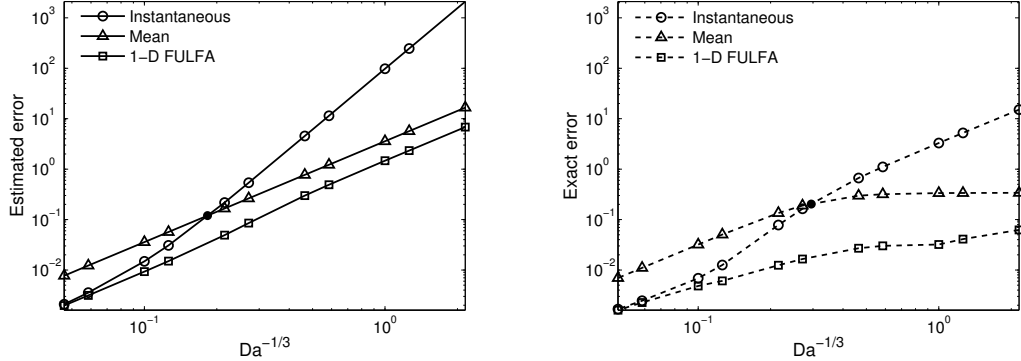


FIGURE 1.9. Unsteady shear—estimated (left; see (1.6.8)) and exact (right) errors as functions of  $\text{Da}^{-1/3}$ . Dots show the location of crossover points: exact error curves cross at  $\text{Da} = 1,6303 \times 10^2$ , estimated error curves at  $\text{Da} = 3,8936 \times 10^1$ .

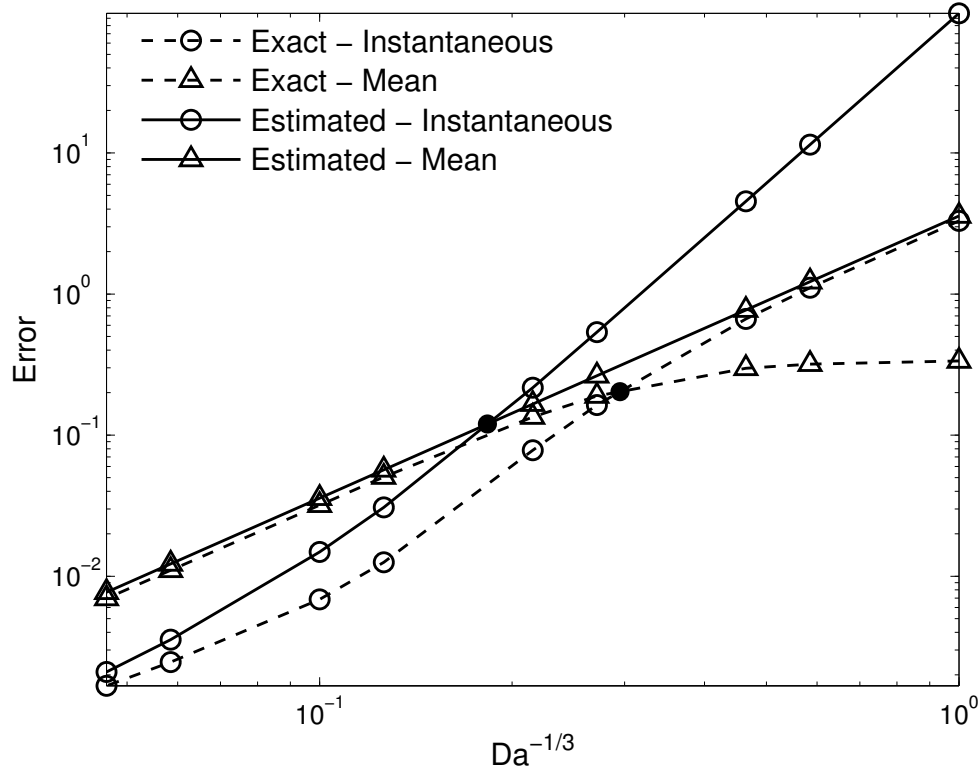


FIGURE 1.10. Unsteady shear—instantaneous and mean dissipation model errors (estimated and exact) as functions of  $\text{Da}^{-1/3}$ . Dots show the location of crossover points.

- (1) the 1-D FULFA model is the best model across the range of values for Da;
- (2) the mean dissipation model is a better choice than the instantaneous dissipation for small Da values;
- (3) the instantaneous dissipation model is better than the mean dissipation model at large Da values and eventually coincides with the 1-D FULFA model for  $\text{Da} \rightarrow \infty$ .

These qualitative features are all recovered by the error estimator. Figure 1.10 shows a close-up of Figure 1.9 for the instantaneous and mean dissipation models. All exact error curves are matched at high Da by their error estimator counterparts. The asymptotic behavior of the error estimation curve of the mean dissipation model recovers the exact error curves of the instantaneous dissipation model at low Da and of the mean dissipation model at high Da values. Those observations are in agreement with the above discussion on the residual control strategy of the different models. Quantitatively, the error estimator overshoots the crossover point of the mean and instantaneous dissipation models by less than one order of magnitude. Therefore, one could use the estimator to choose a model within the three-model hierarchy presented here:

- (1) Choose the best model (1-D FULFA) if computational cost is not an issue, simply because it is the model with the lowest modeling error (estimated and exact).
- (2) Choose the model corresponding to the lowest error estimation between the instantaneous and mean dissipation models if computational cost is an issue. For this case, the estimator's prediction is qualitatively accurate and easy to compute.

## 1.7. CONCLUSIONS

A dual-weighted residual strategy has been successfully implemented to assess the performance of several dissipation-based flamelet models which are frequently used for large-scale simulations in nonpremixed combustion. The estimations are asymptotically correct for high Damköhler numbers. The error estimator also

correctly identifies a posteriori the best model within a hierarchy, or the best model parameter for a given simulation. The estimation strategy can be made as computationally efficient as the modeling strategy itself because, in both cases, precomputed libraries for the solutions can be used. A natural extension of the work presented here is to combine the flamelet modeling error estimation with estimations of other sources of errors in a typical large-scale simulation in turbulent combustion, such as other modeling errors (reduced chemistry, simplified diffusion models, other subgrid models for the passive scalar and the velocity field, etc.) as well as discretization errors. In particular, a slightly more complex test case is being investigated where the chemical reaction term is of Arrhenius kinetics type, allowing for extinction and reignition to occur. An interesting question is whether the estimator described here will be able to detect such events so that the appropriate strategy for the reactive scalars can be automatically adjusted as the simulation runs.

## 1.8. REFERENCES

- [ACS] R. L. ACTIS, B. A. SZABO, C. SCHWAB, *Hierarchic models for laminated plates and shells*, Comput. Meth. Appl. Mech. Eng., 172 (1999), pp. 79–107.
- [AN] A. K. ALEKSEEV, I. M. NAVON, *On a posteriori pointwise error estimation using adjoint temperature and Lagrange remainder*, Comput. Methods Appl. Mech. Eng., 194 (2000), pp. 2211–2228.
- [AO] M. AINSWORTH, J. T. ODEN, *A posteriori error estimation in finite element analysis*, First ed., John Wiley & Sons, New York, 2001.
- [BBV] R. BECKER, M. BRAACK, B. VEXLER, *Parameter identification for chemical models in combustion problems*, Appl. Numer. Math., 54 (2005), pp. 519–536.
- [BE1] M. BRAACK AND A. ERN, *A posteriori control of modeling errors and discretization errors*, SIAM J. Mult. Mod. Simul., 1 (2003), pp. 221–238.

- [BE2] M. BRAACK, A. ERN, *Coupling multimodeling with local mesh refinement for the numerical computation of laminar flames*, Comb. Theory Mod., 8 (2004), pp. 771–788.
- [BM1] A. BOURLIOUX AND A. J. MAJDA, *An elementary model for the validation of flamelet approximation in nonpremixed turbulent combustion*, Comb. Theory Mod., 4 (2000), pp. 189–210.
- [BM2] A. BOURLIOUX AND A. J. MAJDA, *Elementary models with PDF intermittency for passive scalars with a mean gradient*, Phys. Fluids, 14 (2002), pp. 881–897.
- [BR] R. BECKER, R. RANNACHER, *An optimal control approach to a posteriori error estimation in finite element methods*, Acta Numer., 10 (2001), pp. 1–102.
- [CEP] B. CUENOT, F. N. EGOLFOPOULOS AND T. POINSOT, *An unsteady laminar flamelet model for non-premixed combustion*, Comb. Theory Mod., 4 (2000), pp. 77–97.
- [CR1] A. W. COOK AND J. J. RILEY, *A subgrid model for equilibrium chemistry in turbulent flows*, Phys. Fluids, 6 (1994), pp. 2868–2870.
- [CR2] A. W. COOK AND J. J. RILEY, *Subgrid-scale modeling for turbulent reacting flows*, Combust. Flame, 112 (1998), pp. 593–606.
- [EJ] K. ERIKSSON, C. JOHNSON, *An adaptive finite element method for linear elliptic problems*, Math. Comp., 50 (1988), pp. 361–383.
- [JLRH] J. JIMENEZ, A. LIÑÁN, M. ROGERS, F. HIGUERA, *A priori testing of sub-grid models for chemically reacting nonpremixed turbulent shear flows*, J. Fluid Mech., 349 (1998), pp. 149–171.
- [MK] A. J. MAJDA AND P. R. KRAMER, *Simplified models for turbulent diffusion: theory, numerical modelling, and physical phenomena*, Phys. Rep., 314 (1999), pp. 237–574.
- [P] N. PETERS, *Laminar diffusion flamelet models in non-premixed models in turbulent combustion*, Prog. Energy Combust. Sci., 10 (1984), pp. 319–339.

- [ROV] A. ROMKES, J. T. ODEN, K. VEMAGANTI, *Multi-scale goal-oriented adaptive modeling of random heterogeneous materials*, Mechanics of Materials, 38 (2006), pp. 859–872.
- [V] O. VOLKOV, *Validation des modèles de flammelettes instationnaires en combustion turbulente non-prémélangée*, thèse de doctorat, Université de Montréal (2005).

# Chapitre 2

---

## EFFETS DE L'EXTINCTION ET DU RÉALLUMAGE DANS UN MODÈLE IDÉALISÉ EN COMBUSTION NON PRÉMÉLANGÉE

### RÉSUMÉ

Un problème test idéalisé, formé d'un système d'équations de diffusion-réaction, est modifié pour inclure la possibilité d'un réallumage ou d'une extinction de la flamme. À l'instar du problème original, le scalaire passif est un gradient moyen. Le taux de réaction inclut maintenant un terme de type Arrhenius ; nous introduisons alors un scalaire passif additionnel. Pour de grandes énergies d'activation, une analyse asymptotique mène à la courbe en «S» classique, un graphe de la température maximale de la flamme en fonction du nombre de Damköhler. Ce graphe, formé de trois branches et d'une double courbure, correspond aux trois régimes de combustion suivants :

- (1) Un régime près de l'équilibre, où deux régions à l'équilibre chimique sont séparées par une zone de réaction très mince. Ce régime correspond à la branche et la courbure supérieures de la courbe en «S».
- (2) Un régime en combustion partielle, où les réactifs fuient partiellement au travers d'une zone de réaction mince, pour atteindre des régions chimiquement gelées. Ce régime instable correspond à la branche centrale de la courbe en «S».

(3) Un régime presque gelé, où les écarts de température par rapport à une flamme chimiquement gelée sont faibles. Le réallumage est possible lorsque la réaction devient plus intense. Ce régime correspond à la branche et la courbure inférieures de la courbe en «S».

Nous obtenons également les paramètres critiques d'extinction et de réallumage. Les résultats présentés ici sont similaires à ceux obtenus par Liñán [L] pour un scalaire passif borné.

# Quenching and ignition effects in an idealized nonpremixed combustion model

PASCAL TURBIS

## 2.1. ABSTRACT

We extend an idealized test problem consisting of a system of diffusion-reaction equations to include ignition and quenching scenarios. As in the original model, the passive scalar is a mean gradient. The reaction rate is changed to one of Arrhenius kinetics type; an additional passive scalar is introduced. For high activation energies, an asymptotic analysis leads to the classic S-shaped curve, a plot of the maximum flame temperature against the Damköhler number. It consists of three branches and two bends, corresponding to the following three combustion regimes:

- (1) A near-equilibrium regime, where two equilibrium flow regions are separated by a thin reaction zone. This regime covers the upper branch and bend of the S-shaped curve.
- (2) A partial burning regime, where both reactants leak through a thin reaction zone to reach regions of frozen flow. This unstable regime covers the middle branch of the S-shaped curve.
- (3) A nearly frozen regime, where temperature deviations from the frozen flow values are very small. As the reaction increases, ignition can happen. This regime covers the bottom branch and bend of the S-shaped curve.

We also obtain critical ignition and extinction parameters. The results obtained herein are similar to the ones obtained by Liñán [L] for counterflow diffusion flames using a bounded passive scalar.

## 2.2. INTRODUCTION

To study the effects of turbulence on nonpremixed combustion, Bourlioux and Madja introduced an elementary system of advection-diffusion-reaction equations, featuring a passive scalar with a mean gradient [**BM1**, **BM2**]. They also compared the performance of flamelet approximations based on the so-called flamelet

library, a precomputed table of the nondimensionalized solution for the reactive scalars in terms of the reaction progress variable [P1]. These approximations are valid for near-equilibrium combustion. For most practical combustion simulations, one has to deal with the coexistence of more stable combustion regimes.

This paper features the preliminary work required to extend the Bourlioux and Madja results to cases where ignition and quenching are possible. We present here the results when the chemistry is modified and no advection effects are present. As it turns out, the asymptotic analysis of Liñán [L], done for a passive scalar limited to an unit length interval, can be extended to a passive scalar with a mean gradient. In section 2.3, the idealized system of ordinary differential equations (ODEs) is introduced. Multiplicity of solutions leads to three distinct combustion regimes. Asymptotic analysis for each of these regimes is done in section 2.4, leading to analytical formulae for the critical ignition and extinction parameters. Finally, in section 2.5, we compare this setup and its corresponding results to the counterflow diffusion flames setup studied by Liñán.

### 2.3. GOVERNING EQUATIONS

The model consists of the following system of diffusion-reaction equations for the reactive scalars  $Y_1$  (fuel mass fraction),  $Y_2$  (oxidizer mass fraction), and  $T$  (temperature):

$$\frac{d^2Y_1}{dx^2} = \text{Da}Y_1Y_2 \exp(-E/T), \quad (2.3.1)$$

$$\frac{d^2Y_2}{dx^2} = \text{Da}Y_1Y_2 \exp(-E/T), \quad (2.3.2)$$

$$\frac{d^2T}{dx^2} = -\text{Da}Y_1Y_2 \exp(-E/T). \quad (2.3.3)$$

The Damköhler number Da measures the importance of reaction compared to diffusion. In the limit of large values of the activation energy  $E$  and Da, the reaction zone is very thin. Both  $T$  and  $E$  are made nondimensional using the values of the heat release per unit mass of fuel ( $Q$ ) and specific heat ( $c_p$ ).

A convenient strategy for solving (2.3.1)–(2.3.3) stems from the observation that the passive scalars  $Z = \frac{Y_1 - Y_2}{2}$  and  $H = T + \frac{Y_1 + Y_2}{2}$  obey the much simpler

diffusion equations

$$\frac{d^2Z}{dx^2} = \frac{d^2H}{dx^2} = 0. \quad (2.3.4)$$

The resulting equations no longer contain nonlinear reaction terms and their solutions are easily obtained. The enthalpy  $H$  is the maximum flame temperature in the limit  $\text{Da} \rightarrow +\infty$ , where instantaneous combustion happens on the stoichiometric level  $Z = 0$ . Solutions of (2.3.1)–(2.3.3) are computed on  $\Omega = [-L, L]$ , with boundary conditions

$$Y_1(\pm L) = |Z(\pm L)| + Z(\pm L), \quad (2.3.5)$$

$$Y_2(\pm L) = |Z(\pm L)| - Z(\pm L), \quad (2.3.6)$$

$$T(\pm L) = T_\infty. \quad (2.3.7)$$

Equations (2.3.5)–(2.3.6) correspond to chemical equilibrium for the reactive scalars ( $Y_1(-L) = 0 = Y_2(L)$ ). Boundary conditions on the passive scalars are imposed so that  $Z$  corresponds to a mean gradient, i.e.,  $Z(x) = x/L_G$  ( $L_G \in \mathbb{R}$ ), and  $H$  as a constant, a direct result of the definition of  $H$  and equations (2.3.5)–(2.3.7). Unless otherwise mentioned, the values  $L_G = 10$ ,  $T_\infty = 1$ ,  $L = 40$  and  $E = 15$  are used throughout the next sections. The test cases are set up so that two distinct scales exist in the problem: the large scale  $L_G$  associated with the imposed gradient and the very thin flame thickness (at least in the so-called near-equilibrium regime, see below).

This system of equations is presented in its full form in [MS]. The system presented here features no advection effects and a linear passive scalar  $Z$  on a bounded domain, unlike the model presented in [L], which features the passive scalar  $Z$  written as a centered error function (erfc)—see Table I for a complete comparison of both setups. In all cases, the passive scalar  $Z$  is linear near the stoichiometric level; we will show in the next section that the behavior of  $Z$  outside the reaction zone does not critically affect the asymptotic results.

## 2.4. ASYMPTOTIC ANALYSIS

In this section, asymptotic analysis for high activation energies is performed. The goal is to recover the so-called S-shaped curve, a plot of the maximum

flame temperature as a function of the Damköhler number, consisting of three branches and two bends, as shown in Figure 2.1. The lower branch and bend correspond to the nearly frozen regime and ignition, the middle branch, to an unstable partial burning regime, and the upper branch and bend are related to the near-equilibrium regime and quenching of the flame. The unstable middle branch cannot be computed and is crudely approximated to link the upper and lower branches. The asymptotics presented here are similar to the analysis in [L], a consequence of the similarity of the profile of the passive scalar  $Z$  in the reaction zone for both setups. Three regimes, two stable and one unstable, exist for the symmetrical setup presented here. A fourth premixed flame regime would be possible if the temperatures at the boundaries were not equal [L], but this is not considered here.

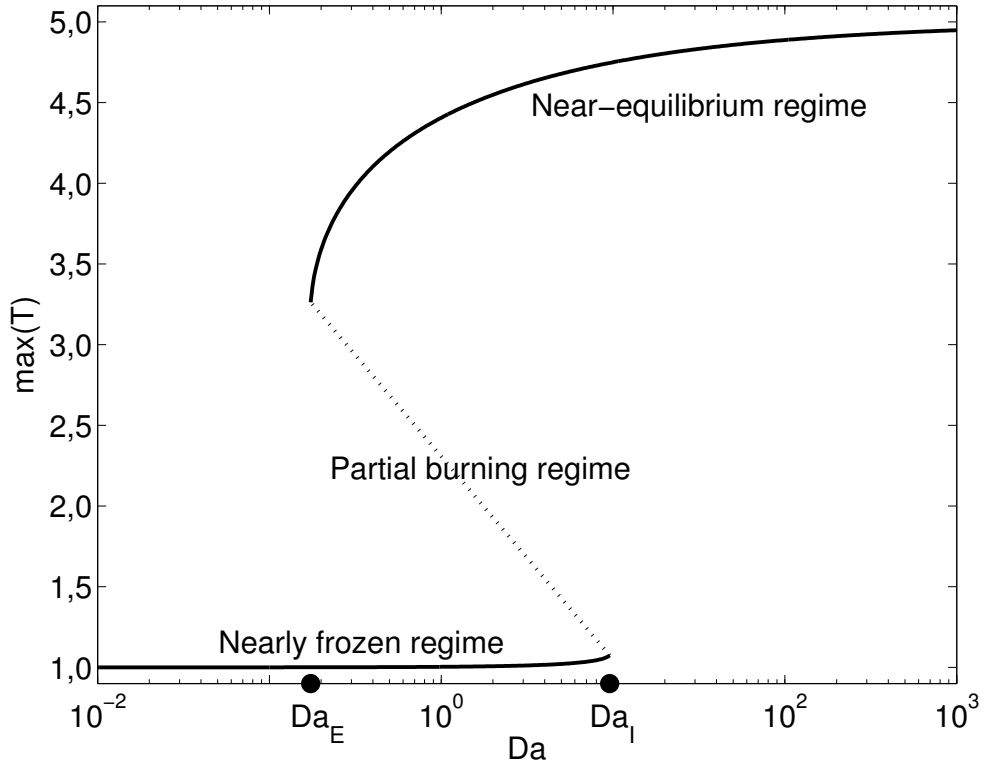


FIGURE 2.1. S-shaped curve—plot of the maximum flame temperature against  $Da$ . Critical quenching and ignition parameters  $Da_E$  and  $Da_I$  are also shown.

The passive scalars  $Z$  and  $H$  are given by

$$Z = \frac{x}{L_G}, \quad (2.4.1)$$

$$H = T_\infty + \frac{L}{L_G}. \quad (2.4.2)$$

Throughout this section, we will study the following ODE, obtained by expressing (2.3.3) using both passive scalars:

$$\frac{d^2T}{dx^2} + Da [(H - T)^2 - Z^2] \exp\left(-\frac{E}{T}\right) = 0. \quad (2.4.3)$$

#### 2.4.1. The lower branch and bend of the S-shaped curve

In the nearly frozen regime, the temperature is first approximated by  $T_\infty$ , corresponding to a frozen chemical reaction. To account for chemical effects, small departures from this temperature value happen at higher orders in the asymptotic expansion [L]. Typical solutions for the reactive scalars in this regime are presented in Figure 2.2.

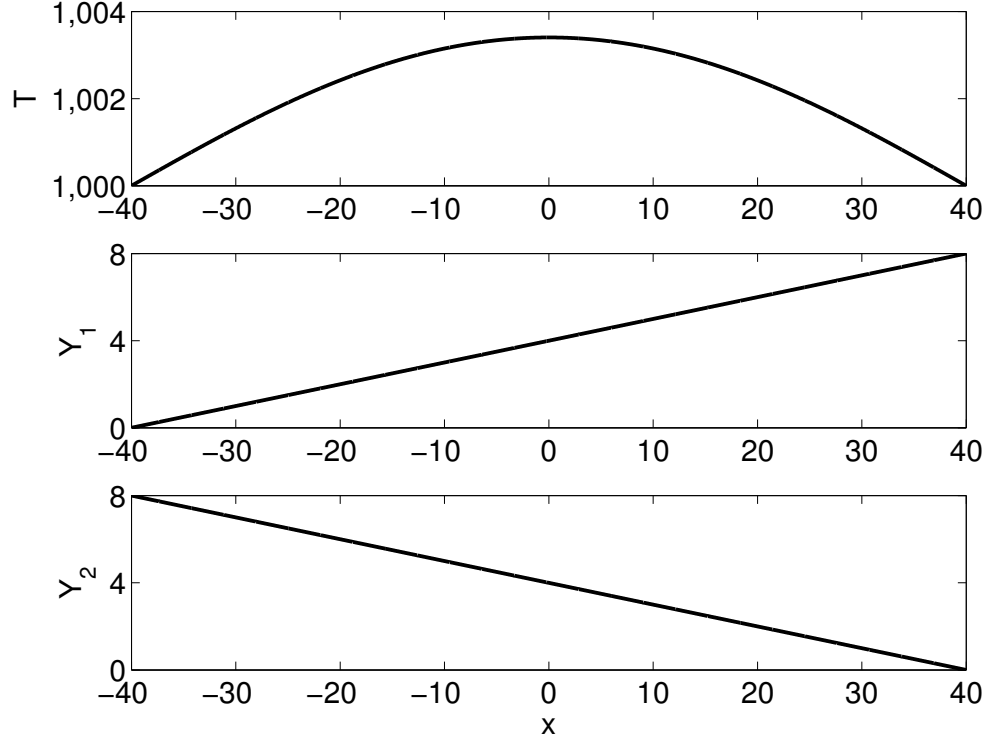


FIGURE 2.2. Typical profiles for  $T$ ,  $Y_1$ , and  $Y_2$  in the nearly frozen regime ( $Da = 1$ ).

The asymptotic expansions are done with respect to the small parameter  $\varepsilon = T_\infty^2/E$ . We want to determine the value(s) of Da for which the temperature departure from  $T_\infty$  at  $x = 0$  (flame location) is of order  $\varepsilon$ . To do so, the following expansions are plugged into (2.4.3):

(1) Temperature:

$$T = T_\infty + \varepsilon \theta_1(x) + \varepsilon^2 \theta_2(x) + O(\varepsilon^3), \quad (2.4.4)$$

(2) Reduced Damköhler number:

$$\frac{Da}{L_G^2} \exp\left(-\frac{E}{T_\infty}\right) \frac{E}{T_\infty^2} = \widetilde{\Delta}_0 + \varepsilon \widetilde{\Delta}_1 + O(\varepsilon^2). \quad (2.4.5)$$

Using the relation  $\frac{1}{x+a} = \frac{1}{a} - \frac{x}{a^2} + O(x^2)$ , we obtain an ODE for  $\theta_1$  at  $O(\varepsilon)$ , which we rewrite in terms of  $y = (x+L)/2L$  and  $\Delta_0 = 16\widetilde{\Delta}_0 L^4$  as

$$\frac{d^2\theta_1}{dy^2} + \Delta_0 y(1-y) \exp(\theta_1) = 0, \quad (2.4.6)$$

with boundary conditions  $\theta_1(0) = \theta_1(1) = 0$ . We refer the reader to [L] for a discussion about the order at which chemical effects must be retained. To solve this ODE numerically for each value of  $\Delta_0$ , we use centered finite differences and Newton's method with initial guess  $\theta_1(y) = C(1 - 2|y - \frac{1}{2}|)$  for  $C \geq 0$ ; we choose multiple values of  $C$  to capture the multiplicity of solutions for a given value of  $\Delta_0$ . Figure 2.3 shows the maximum value of  $\theta_1$  (at  $y = 1/2$ ) as a function of  $\Delta_0$ .

There is a critical value of  $\Delta_0$  (16,3037) for which two solutions exist for smaller values of  $\Delta_0$  and none for larger values of  $\Delta_0$ . This characterizes the lower branch and bend of the S-shaped curve. Assuming the reduced Damköhler number is approximately equal to  $\widetilde{\Delta}_0$ , we obtain an approximation of  $Da_I$ , the ignition Damköhler number:

$$Da_I \approx 1,019 \frac{L_G^2}{L^4} \exp\left(\frac{E}{T_\infty}\right) \frac{T_\infty^2}{E}. \quad (2.4.7)$$

Figure 2.4 shows the relative error of the approximation given by (2.4.7) to the exact computed value of  $Da_I$  for  $E \in [15, 100]$ . For small values of  $\varepsilon$ , we obtain a very good approximation. Due to the symmetry of the setup, we always obtain clearly defined ignition conditions as long as  $E$  is large enough [L].

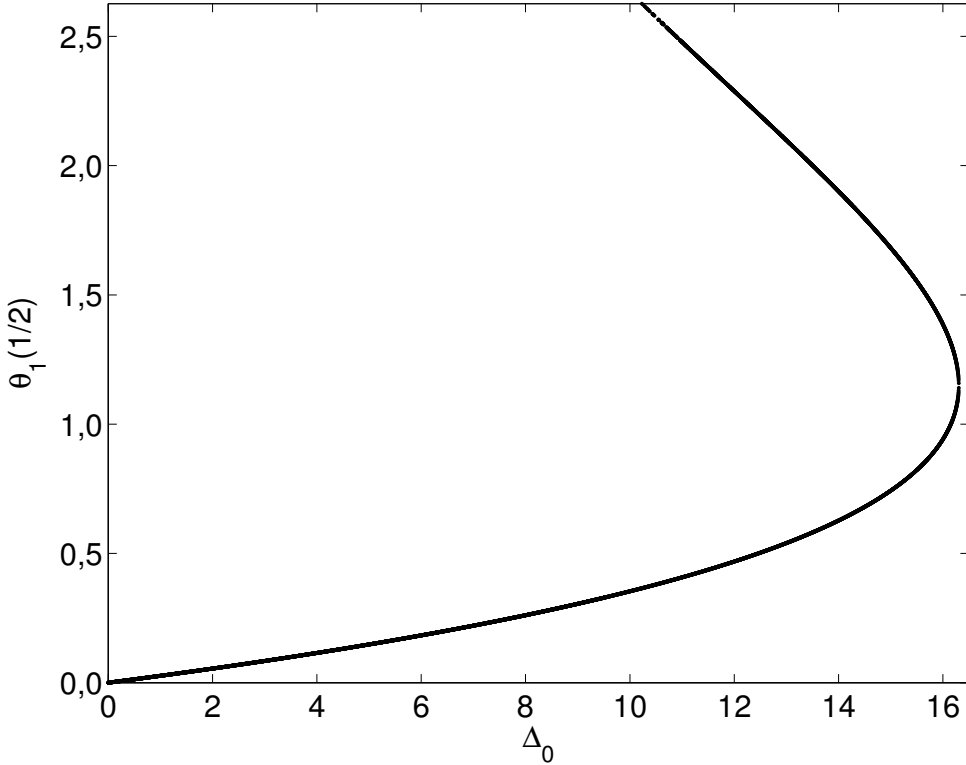


FIGURE 2.3. Asymptotic solution on the lower bend of the S-shaped curve— $\theta_1(1/2)$  plotted against  $\Delta_0$ .

#### 2.4.2. The middle branch of the S-shaped curve

In this partial burning regime, two frozen flow zones are separated by a thin reaction zone. If  $E$  is large compared to the maximum temperature, a small change in temperature will freeze the chemical reaction. The Damköhler number is large enough so that the diffusion and reaction terms are of the same order at the flame location  $[L]$ . The temperature is first approximated by a piecewise linear function from the boundary conditions  $T = T_\infty$  to an unknown maximum temperature  $T_b$  at  $x = 0$ . Small departures from this approximation in the reaction zone are functions of the small parameter  $\varepsilon = T_b^2/E$ . Outside the reaction zone, the flow is frozen to all algebraic orders of  $\varepsilon$ . Asymptotic expansions (2.4.8) through (2.4.10) are used in (2.4.3):

- (1) Outer solution ( $|x| \gg \varepsilon$ ):

$$T = T_b + \frac{T_\infty - T_b}{L} |x|; \quad (2.4.8)$$

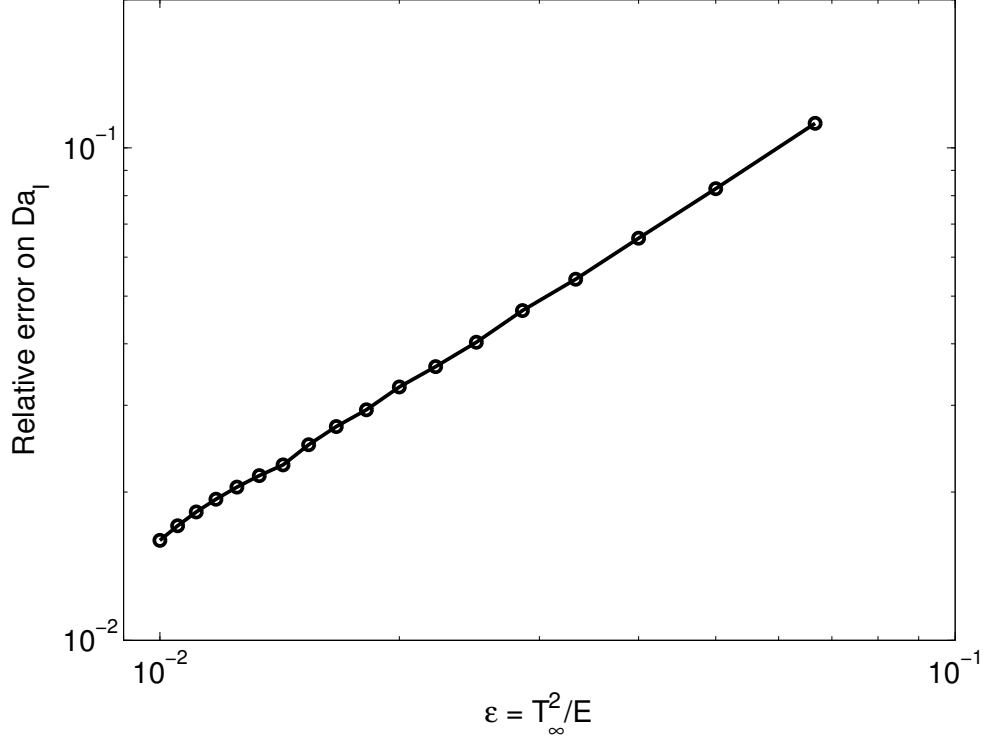


FIGURE 2.4. Relative error between the ignition Damköhler number  $Da_I$  and its approximation (2.4.7) as a function of  $\varepsilon = T_\infty^2/E$ .

(2) Inner solution ( $\zeta = x/\varepsilon$ ):

$$T = T_b + \varepsilon \Phi_1(\zeta) + \varepsilon^2 \Phi_2(\zeta) + O(\varepsilon^3); \quad (2.4.9)$$

(3) Damköhler number:

$$Da = Da_b(1 + b_1\varepsilon + b_2\varepsilon^2 + O(\varepsilon^3)). \quad (2.4.10)$$

We want to find  $Da_b$  as a function of  $T_b$  by matching the inner and outer solutions. Rewriting (2.4.3) in terms of  $\zeta$  and inserting expansions (2.4.9)–(2.4.10) in it, we get

$$0 = \varepsilon^{-1} \left( \frac{d^2 \Phi_1}{d\zeta^2} + \Lambda_0 \exp(\Phi_1) \right) + O(1), \quad (2.4.11)$$

where  $\Lambda_0 = Da_b (H - T_b)^2 \exp\left(-\frac{E}{T_b}\right) \frac{T_b^2}{E}$ . Denote by  $\Phi_m$  and  $\zeta_m$  the maximum of  $\Phi_1$  and the value of  $\zeta$  at which it is attained, respectively. (We expect  $\zeta_m$  to be equal to 0 due to the symmetry of the setup.) Multiple integrations from  $\zeta$  to

$\zeta_m$  yield

$$\Phi_1 = \Phi_m - 2 \ln \left\{ \cosh \left[ \left( \frac{\Lambda_0}{2} \exp \Phi_m \right)^{1/2} (\zeta - \zeta_m) \right] \right\}. \quad (2.4.12)$$

We also have, in the  $\zeta \rightarrow \pm\infty$  limits,

$$\Phi_1 \approx \Phi_m + \ln 4 \mp (\zeta - \zeta_m) (2\Lambda_0 \exp \Phi_m)^{1/2}. \quad (2.4.13)$$

The inner and outer expansions match on an intermediate scale  $y$  such that  $x = \varepsilon^\gamma y$  and  $\zeta = \varepsilon^{\gamma-1} y$  for some  $\gamma \in (0, 1)$ . By inserting the last expressions in the original inner and outer expansions, now written in terms of  $y$ , we obtain the following:

(1) Outer solutions (for  $\pm x \gg \varepsilon$ ):

$$T = T_b \mp \varepsilon^\gamma y \frac{T_b - T_\infty}{L} \quad (2.4.14)$$

(2) Inner solution (in the limit  $\zeta \rightarrow \pm\infty$ ):

$$T = T_b \mp \varepsilon^\gamma y (2\Lambda_0 \exp \Phi_m)^{1/2} + \varepsilon \left[ \Phi_m + \ln 4 \pm \zeta_m (2\Lambda_0 \exp \Phi_m)^{1/2} \right] + \text{h.o.t.} \quad (2.4.15)$$

Higher order terms are denoted by the abbreviation h.o.t.. Matching (2.4.14) and (2.4.15), we conclude that

- at order  $O(1)$ , the matching is already done, since we assumed that the temperature was  $T_b$  at the flame location ;
- at order  $O(\varepsilon^\gamma)$ , temperature slopes are identical, leading to

$$\frac{T_b - T_\infty}{L} = (2\Lambda_0 \exp \Phi_m)^{1/2}; \quad (2.4.16)$$

- at order  $O(\varepsilon)$ ,

$$0 = \Phi_m + \ln 4 \mp \zeta_m (2\Lambda_0 \exp \Phi_m)^{1/2}. \quad (2.4.17)$$

Hence  $\zeta_m = 0$ ,  $\exp \Phi_m = 1/4$  and

$$\Lambda_0 = \frac{2}{L^2} (T_b - T_\infty)^2. \quad (2.4.18)$$

From the definition of  $\Lambda_0$  and (2.4.18), we find a relation between  $\text{Da}_b$  and  $T_b$ :

$$\text{Da}_b (H - T_b)^2 \exp \left( -\frac{E}{T_b} \right) \frac{T_b^2}{E} = \frac{2}{L^2} (T_b - T_\infty)^2. \quad (2.4.19)$$

Numerical solutions  $(\text{Da}_b, T_b)$  of (2.4.19) are shown in Figure 2.5. The curve is very similar to a typical S-shaped curve; however, the previous expansions only hold for the middle branch. On the lower branch, values of  $T_b - T_\infty$  are not large compared to  $T_\infty^2/E$ , which lead to larger reaction zones than those considered here. On the upper branch,  $\text{Da}_b$  goes to infinity when  $Y_1$  or  $Y_2$  goes to 0 at the flame location, so the expansion for the reaction zone fails [L].

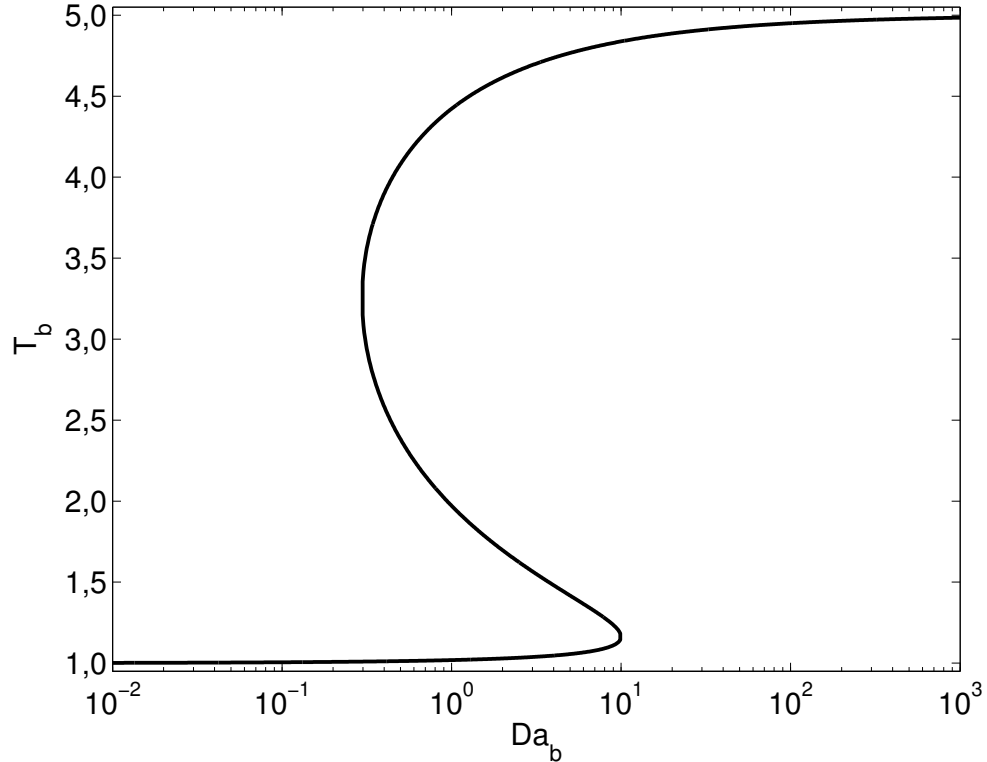


FIGURE 2.5. Asymptotic solution on the middle branch of the S-shaped curve— $T_b$  as a function of  $\text{Da}_b$ , given by (2.4.19).

#### 2.4.3. The upper branch and bend of the S-shaped curve

This part of the S-shaped curve is a near-equilibrium regime controlled by diffusion. Two equilibrium zones are separated by a very thin near-equilibrium reaction zone. For the next set of asymptotic expansions, we use  $\varepsilon = H^2/E$  as the small parameter. We want to find the value(s) of  $\text{Da}$  for which the temperature departure from  $H$  at  $x = 0$  (equilibrium temperature at the flame location) is of order  $\varepsilon$ . Typical profiles of the reactive scalars in this regime are presented in Figure 2.6.

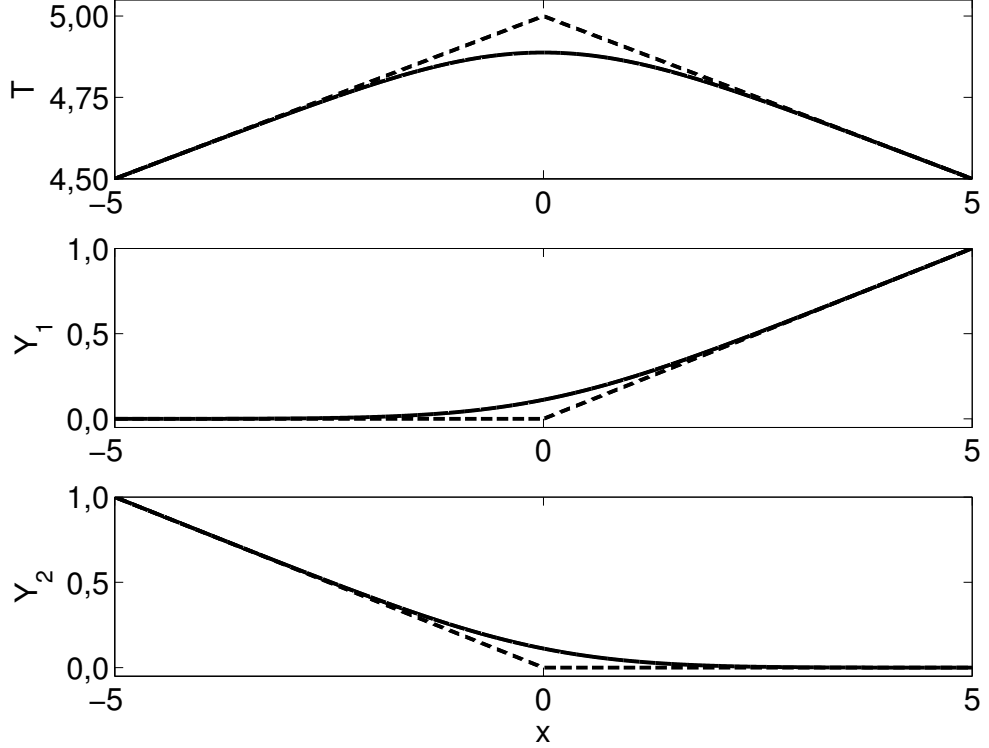


FIGURE 2.6. Typical profiles for  $T$ ,  $Y_1$ , and  $Y_2$  in the near-equilibrium regime ( $\text{Da} = 100$ ) around the flame location. Full line: exact solutions, dashed line: equilibrium solutions.

For the asymptotic analysis, we introduce the following expansions:

(1) Outer solution, for  $|x| \gg \varepsilon$ :

$$T = H - (H - T_\infty) \frac{|x|}{L}; \quad (2.4.20)$$

(2) Inner solution, with  $\zeta = \frac{\delta_0^{1/3} x}{\varepsilon L_G}$ :

$$T = H - \delta_0^{-1/3} (\varepsilon \beta_1(\zeta) + O(\varepsilon^2)); \quad (2.4.21)$$

(3) Reduced Damköhler number  $\delta$ :

$$\delta = L_G^2 \text{Da} \left( \frac{H^2}{E} \right)^3 \exp \left( -\frac{E}{H} \right) = \delta_0 + \varepsilon \delta_1 + O(\varepsilon^2). \quad (2.4.22)$$

By rewriting (2.4.3) in terms of  $\zeta$  and inserting expressions (2.4.21)–(2.4.22) in the new equation, we get

$$0 = \varepsilon^{-1} \frac{\delta_0^{1/3}}{L_G^2} \left[ -\frac{d^2 \beta_1}{d \zeta^2} + (\beta_1^2 - \zeta^2) \exp \left( -\delta_0^{-1/3} \beta_1 \right) \right] + O(1). \quad (2.4.23)$$

The matching is done on an intermediate scale  $y$  such that  $x = \varepsilon^\gamma y$  for some  $\gamma \in (0, 1)$ ; this provides boundary conditions on  $\beta_1$ . Since  $\frac{H - T_\infty}{L} = \frac{1}{L_G}$ , we write

(1) the outer solution (for  $\pm x \gg \varepsilon$ ) as

$$T = H \mp \varepsilon^\gamma \frac{y}{L_G}; \quad (2.4.24)$$

(2) the inner solution as

$$T = H - \delta_0^{-1/3} \varepsilon \beta_1 \left( \frac{\delta_0^{1/3} \varepsilon^{\gamma-1} y}{L_G} \right) + \text{h.o.t..} \quad (2.4.25)$$

Differentiation of (2.4.24)–(2.4.25) with respect to  $y$  and matching yields

$$\lim_{\zeta \rightarrow \pm\infty} \frac{d\beta_1}{d\zeta} = \pm 1. \quad (2.4.26)$$

Equation (2.4.23) for  $\beta_1$  is solved numerically for each value of  $\delta_0^{-1/3}$ ; again, we use centered finite differences and Newton's method. Multiple initial guesses help capture the multiplicity of solutions for a given value of  $\delta_0^{-1/3}$ . The maximal value of  $\beta_1$  (attained at  $\zeta = 0$ ) is plotted against  $\delta_0^{-1/3}$  in Figure 2.7. As shown in this figure, there exists two solutions for  $\delta_0^{-1/3} < 1,0934$  and none for  $\delta_0^{-1/3} > 1,0934$ . This behavior characterizes the upper branch and bend of the S-shaped curve, and therefore a reduced extinction Damköhler number exists. One can approximate  $\text{Da}_E$ , the extinction Damköhler number, by assuming that  $\delta \approx \delta_0$ :

$$\text{Da}_E \approx 0,765 \frac{E^3}{H^6 L_G^2} \exp \left( \frac{E}{H} \right). \quad (2.4.27)$$

Figure 2.8 shows the relative error of the approximation given by (2.4.27) to the exact computed value for  $E \in [15, 250]$ . To obtain a relative error below 10% for the tested values of  $\varepsilon$ , one would need to include the term  $\delta_1$  in the reduced Damköhler number expression. For this preliminary work, equation (2.4.27) will be sufficient.

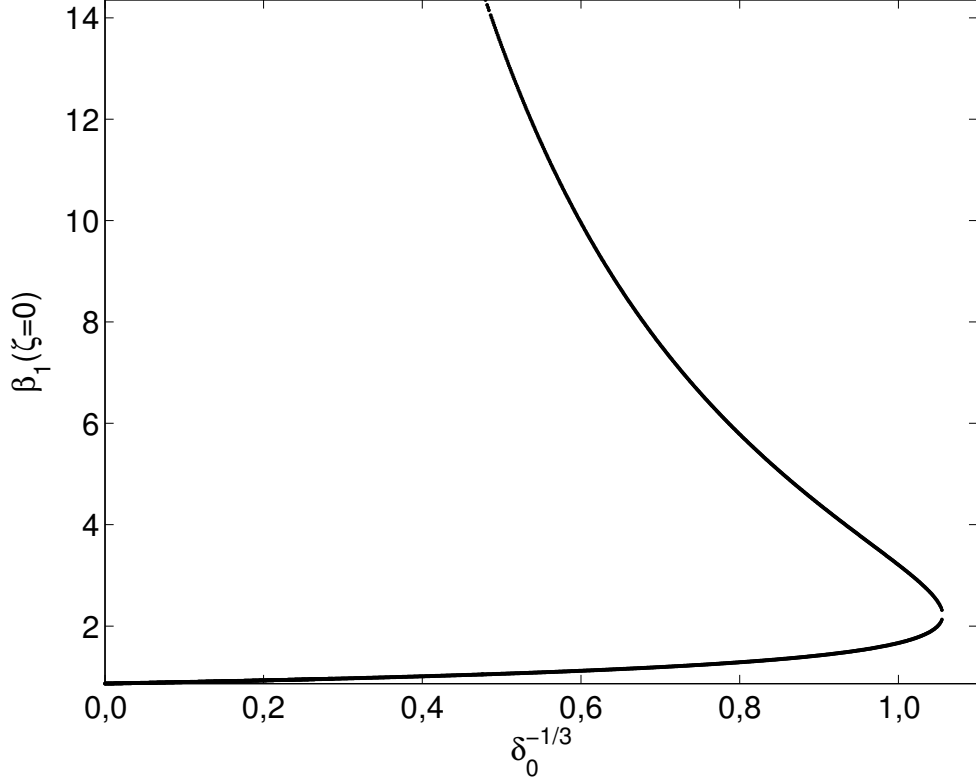


FIGURE 2.7. Asymptotic solution on the upper bend of the S-shaped curve— $\beta_1(0)$  plotted against  $\delta_0^{-1/3}$ .

## 2.5. DISCUSSION

In this section, we compare the results presented in the last section with similar results from Liñán for a slightly different setup. We assumed that the temperature difference between both boundaries is zero and the fuel and oxidizer concentrations are the same at each jet. These assumptions are equivalent to the use of the values  $\beta = 0$  and  $\alpha = 1$  in [L]. Table I summarizes the characteristics of each model. As mentioned before, the presence of advection effects, a bounded passive scalar  $Z$ , and an unbounded domain in Liñán's work contrast with the proposed model in this paper. In the end, the main relations for each combustion regime are the same, as shown from the last three items of the table. We expect that some results depend on the slope of  $Z$  at  $x = 0$ , which is why the parameter  $L_G$  appears some of our results.

Item	Description	
ODE to solve	(T)	$\frac{d^2T}{dx^2} + \text{Da}Y_1Y_2 \exp(-E/T) = 0$
	(L)	$\frac{d^2T}{dx^2} + x \frac{dT}{dx} + \text{Da}Y_1Y_2 \exp(-E/T) = 0$
Domain $\Omega$	(T)	$[-L, L]$
	(L)	$\mathbb{R}$
Boundary conditions on $T$	(T)	$T(\pm L) = T_\infty$
	(L)	$\lim_{x \rightarrow \pm\infty} T(x) = T_\infty$
Boundary conditions on $Y_1$	(T)	$Y_1(\pm L) =  Z(\pm L)  + Z(\pm L)$
	(L)	$\lim_{x \rightarrow -\infty} Y_1(x) = 1 = 1 - \lim_{x \rightarrow +\infty} Y_1(x)$
Boundary conditions on $Y_2$	(T)	$Y_2(\pm L) =  Z(\pm L)  - Z(\pm L)$
	(L)	$\lim_{x \rightarrow +\infty} Y_2(x) = 1 = 1 - \lim_{x \rightarrow -\infty} Y_2(x)$
Passive scalar $Z$	(T)	$\frac{x}{L_G}$
	(L)	$\frac{1}{2} \left[ \text{erfc} \left( \frac{x}{\sqrt{2}} \right) - 1 \right]$
Passive scalar $H$	(T)	$\frac{L}{L_G} + T_\infty$
	(L)	$\frac{1}{2} + T_\infty$
Approximation of $\text{Da}_I$	(T)	$\frac{1,019 L_G^2}{L^4} \exp \left( \frac{E}{T_\infty} \right) \frac{T_\infty^2}{E}$
	(L)	$2,5925 \exp \left( \frac{E}{T_\infty} \right) \frac{T_\infty^2}{E}$
Relation between $T_b$ and $\text{Da}_b$	(T)	$\text{Da}_b (H - T_b)^2 \exp \left( -\frac{E}{T_b} \right) \frac{T_b^2}{E} = \frac{2}{L^2} (T_b - T_\infty)^2$
	(L)	$\text{Da}_b (H - T_b)^2 \exp \left( -\frac{E}{T_b} \right) \frac{T_b^2}{E} = \frac{1}{\pi} (T_b - T_\infty)^2$
Approximation of $\text{Da}_E$	(T)	$\frac{0,765}{L_G^2} \frac{E^3}{H^6} \exp \left( \frac{E}{H} \right)$
	(L)	$0,136 \frac{E^3}{H^6} \exp \left( \frac{E}{H} \right)$

TABLE I. Comparison between the results presented here (T) and those obtained by Liñán (L)

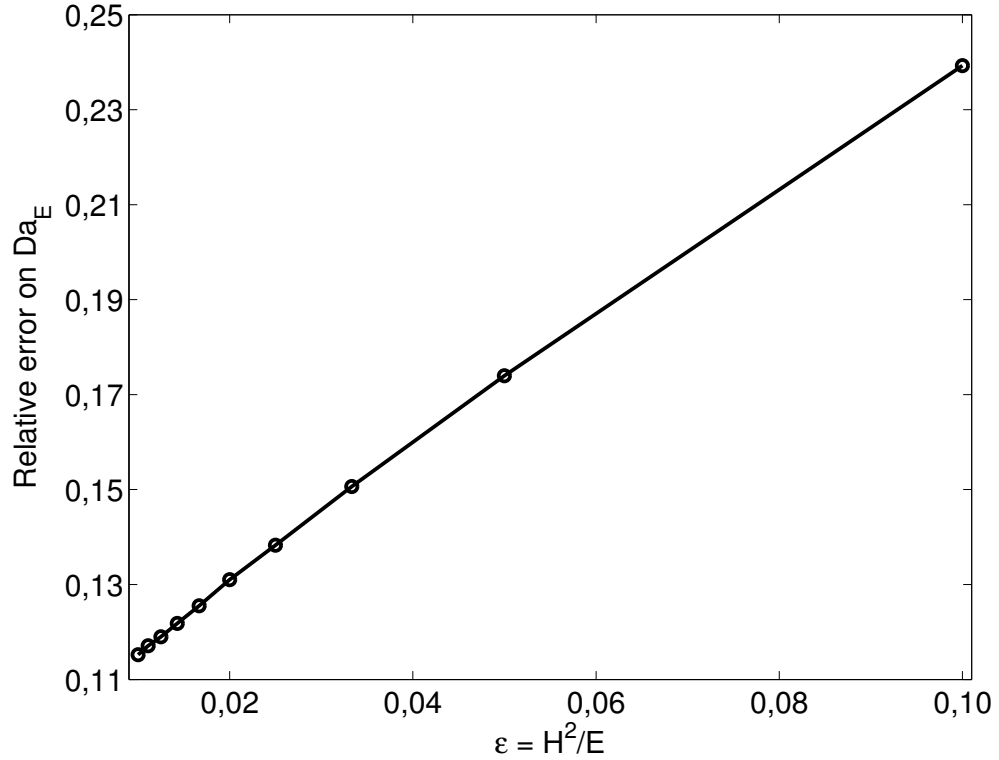


FIGURE 2.8. Relative error between the ignition Damköhler number  $Da_E$  and its approximation (2.4.27) as a function of  $\varepsilon = H^2/E$ .

## 2.6. CONCLUSIONS

The so-called S-shaped curve, a plot of the maximum flame temperature as a function of the Damköhler number, has been recovered for a model featuring a passive scalar with a mean gradient. Using large activation energy asymptotic analysis, we have identified three distinct combustion regimes: a nearly frozen regime, describing the lower branch and bend of the S-shaped curve, a near-equilibrium regime, explaining the upper branch and bend, and a theoretical partial burning regime, covering the middle branch. We have obtained analytical expressions for asymptotic approximations of the critical ignition and quenching Damköhler numbers. Despite numerous differences of our model with the one presented in [L] (absence of advection, linear passive scalar  $Z$ , bounded domain), we have come to the same conclusions as Liñán, since both profiles for  $Z$  are linear near the flame location. Using a mean gradient setup is mathematically convenient. Moreover, the results above confirm that it is relevant to practical

applications, because it behaves qualitatively like the classical model. The preliminary work presented here is a step towards investigating a more complex test case (presented in [BM1] for  $E = 0$ ), where advection effects are added to mimic turbulence. One key issue is to analyze how advection influences the S-shaped curves, and in particular the quenching and ignition of the flame.

## 2.7. REFERENCES

- [BM1] A. BOURLIOUX AND A. J. MAJDA, *An elementary model for the validation of flamelet approximation in nonpremixed turbulent combustion*, Comb. Theory Mod., 4 (2000), pp. 189–210.
- [BM2] A. BOURLIOUX AND A. J. MAJDA, *Elementary models with PDF intermittency for passive scalars with a mean gradient*, Phys. Fluids, 14 (2002), pp. 881–897.
- [L] A. LIÑÁN, *The asymptotic structure of counterflow diffusion flames for large activation energies*, Acta Astronautica, 1 (1974), pp. 1007–1039.
- [MS] A. J. MADJA AND P. SOUGADINIS, *The effect of turbulence on mixing in prototype reaction diffusion systems*, Comm. Pure Appl. Math., 53 (2000), pp. 1284–1304.
- [P] N. PETERS, *Laminar diffusion flamelet models in non-premixed models in turbulent combustion*, Prog. Energy Combust. Sci., 10 (1984), pp. 319–339.

# Chapitre 3

---

## UN MODÈLE ÉLÉMENTAIRE POUR LA VALIDATION DES APPROXIMATIONS DE FLAMMELETTE EN COMBUSTION NON PRÉMÉLANGÉE AVEC EXTINCTION ET RÉALLUMAGE

### RÉSUMÉ

Dans cet article, nous étudions un système idéalisé d'équations d'advection-diffusion-réaction pour la combustion non prémélangée avec extinction et réallumage. La performance de modèles sous-maille est évaluée pour des équations avec un scalaire passif dominé par un gradient moyen. En l'absence d'advection, une analyse asymptotique rigoureuse est disponible afin de caractériser la courbe en «S» composée de trois branches et d'une double courbure, un graphe de la température maximale en fonction du nombre de Damköhler. Aucune analyse similaire n'est disponible lorsque l'advection devient importante. Cependant, les simulations numériques nous permettent de reconstruire toutes les courbes en «S» à partir de la courbe en «S» sans advection. Nous obtenons ainsi de très bonnes approximations des paramètres globaux d'extinction et de réallumage. Nous découvrons un lien entre les solutions près de l'équilibre pour des énergies d'activation nulles et non nulles via la librairie de flammelettes, une relation précalculable entre les scalaires réactifs et les scalaires passifs appropriés. Nous

comparons également les erreurs de modélisation liées à l'utilisation de modèles sous-maille dans les régimes près de l'équilibre et presque gelé.

# An elementary model for the validation of flamelet approximations in nonpremixed combustion with quenching and ignition

ANNE BOURLIOUX, PASCAL TURBIS

## 3.1. ABSTRACT

In this paper, we study a set of advection-diffusion-reaction equations which constitutes an idealized model for nonpremixed combustion including quenching and ignition effects. The performance of asymptotic flamelet-type subgrid models is investigated for setups where the passive scalar is driven by a mean gradient. In the absence of advection, rigorous asymptotic analysis is available to characterize the S-shaped curve, a plot of the maximum flame temperature as a function of the Damköhler number, consisting of three branches and two bends. While no such analysis is available in the presence of advection, numerical simulations allow us to recover S-shaped curves based on the curve from the advection-free setup. We show that this leads to very good approximations for the global quenching and ignition parameters. We find a link between the near-equilibrium solutions for zero and nonzero activation energies through the flamelet library, a precomputed table expressing the reactive scalars in terms of the appropriate passive scalars. We also compare modeling errors for subgrid near-equilibrium and frozen flow models.

## 3.2. INTRODUCTION

Modeling quenching and ignition phenomena has always been a big part of combustion research. Not only is it a key problem for practical applications, but the nonuniqueness of solutions is also a good mathematical challenge. Liñán analyzed a one-dimensional system for counterflow diffusion flames [L]. His asymptotic analysis using a bounded passive scalar lead to the identification and characterization of all combustion regimes, described by the well-known S-shaped curve, a plot of the maximum flame temperature as a function of the Damköhler number. Using this setup as a guide and the preliminary work in [T], the two-dimensional idealized system of equations for nonpremixed combustion proposed by Bourlioux

and Majda [**BM1**, **BM2**] will be extended to include the possibility of quenching and ignition, while retaining fundamental aspects of the original model, such as the use of a passive scalar written as a perturbation of a mean gradient.

In section 3.3, the system of partial differential equations (PDEs) used here will be stated. Section 3.4 summarizes the results in the absence of advection presented in [T]. Most importantly, we characterize the two stable combustion regimes and assess the performance of subgrid models in those regimes. In section 3.5, we add advection effects to the system to mimic turbulence, and compare the results with this setup with those obtained using an idealized model without quenching and ignition. Finally, in section 3.6, we discuss how to relate the S-shaped curves in the presence of advection to the advection-free case.

### 3.3. GOVERNING EQUATIONS

The idealized nonpremixed combustion model considered herein consists of a coupled system of advection-reaction-diffusion partial differential equations (PDEs) in two spatial dimensions for the reactive scalars  $Y$  (fuel mass fraction),  $Y_2$  (oxidizer mass fraction), and  $T$  (nondimensional temperature):

$$\frac{\partial Y}{\partial t} + \text{Pe } \mathbf{v} \cdot \nabla Y = \Delta Y - \text{Da } YY_2 \exp(-E/T), \quad (3.3.1)$$

$$\frac{\partial Y_2}{\partial t} + \text{Pe } \mathbf{v} \cdot \nabla Y_2 = \Delta Y_2 - \text{Da } YY_2 \exp(-E/T), \quad (3.3.2)$$

$$\frac{\partial T}{\partial t} + \text{Pe } \mathbf{v} \cdot \nabla T = \Delta T + \text{Da } YY_2 \exp(-E/T). \quad (3.3.3)$$

The flow field  $\mathbf{v}(x, y)$  is chosen to be bidimensional, incompressible, and biperiodic of period  $P$ . The Péclet number  $\text{Pe}$  characterizes the importance of advection compared to diffusion, and the Damköhler number  $\text{Da}$  the importance of reaction compared to diffusion. In the limit of large values of the activation energy  $E$  and  $\text{Da}$ , the reaction zone is very thin. Both  $T$  and  $E$  are made nondimensional using the values of the heat release per unit mass of fuel ( $Q$ ) and specific heat ( $c_p$ ). As long as  $E$  is large enough, multiple combustion regimes are possible in some areas of the Pe-Da parameter space [T].

A convenient strategy for solving (3.3.1)–(3.3.3) stems from the observation that the passive scalars  $Z = (Y - Y_2)/2$  and  $H = T + (Y + Y_2)/2$  obey the much

simpler advection-diffusion equations

$$\frac{\partial Z}{\partial t} + \text{Pe } \mathbf{v} \cdot \nabla Z = \Delta Z, \quad (3.3.4)$$

$$\frac{\partial H}{\partial t} + \text{Pe } \mathbf{v} \cdot \nabla H = \Delta H. \quad (3.3.5)$$

The resulting equations no longer contains the nonlinear reaction term, therefore analysis and numerical simulations are much simpler for the passive scalars than for the reactive scalars. We substitute these to (3.3.2)–(3.3.3), and (3.3.1) for the reactive scalar is now written as

$$\frac{\partial Y}{\partial t} + \text{Pe } \mathbf{v} \cdot \nabla Y = \Delta Y - \text{Da } Y (Y - 2Z) \exp\left(\frac{-E}{H - Y + Z}\right). \quad (3.3.6)$$

We look for a solution for the passive scalar  $Z$  as a perturbation of a mean gradient in the  $x$ -direction, i.e.,  $Z(x, y, t) = x/L_G + Z_p(x, y, t)$ , where  $L_G$  is the length scale associated with the imposed mean gradient and  $Z_p$  is a periodic, zero-mean perturbation induced by the velocity field  $\mathbf{v}$ . We compute the steady-state solutions of (3.3.6) on  $\Omega = [-L, L] \times [0, P]$ , with boundary conditions  $Y = |Z| + Z$ ,  $Y_2 = |Z| - Z$  (chemical equilibrium), and  $T = T_\infty$  on  $\{-L, L\} \times [0, P]$ ; we also enforce periodicity of all scalars in the  $y$ -direction. The boundary conditions on the passive scalar  $H$  are obtained by using its definition and the boundary conditions on the reactive scalars.

Unless otherwise mentioned, the values  $P = 1$ ,  $L_G = 10$ ,  $T_\infty = 1$ ,  $L = 40$ , and  $E = 15$  will be used throughout the next sections. The test cases are set up so that three distinct scales exist in the problem: the large scale  $L_G$ , the intermediate scale  $P$  due to the flow field, and the very thin flame thickness. The presence of this last very small scale in the solution for the reactive scalar is a computational challenge. Equation (3.3.4) has been studied exhaustively to analyze the performance of a very wide class of turbulence models [**BM2**, **MK**]. The particular setup for the passive scalar allows for a direct link with homogenization theory predictions. For  $E = 0$ , the analysis was extended to the reactive case to study the performance of a hierarchy of flamelet models for both steady and unsteady cases [**BM1**, **V**]. For a nonzero activation energy, a rigorous asymptotic analysis was done in [**T**] for

$\text{Pe} = 0$ . For  $\text{Pe} \neq 0$ , some homogenization results on (3.3.1)–(3.3.3) were obtained in [MS].

### 3.4. THE ASYMPTOTIC LIMIT $\text{Pe} = 0$

If the activation energy is large enough, multiple combustion regimes exist, leading to the well-known S-shaped curve, a plot of the maximum flame temperature as a function of  $\text{Da}$ , shown in Figure 3.1. The ignition and extinction Damköhler numbers  $\text{Da}_I$  and  $\text{Da}_E$ , two critical values of  $\text{Da}$  described later, are also shown. We will review the asymptotic behavior for large activation energies  $[\mathbf{T}]$  of the reactive scalars in the two stable regimes: the nearly frozen regime, which covers the lower branch and bend of the S-shaped curve, and the near-equilibrium regime, which covers the upper branch and bend of the S-shaped curve. The unstable middle branch cannot be computed and is crudely approximated in the figure to link the upper and lower branches. We will also discuss different approximations of these stable solutions and compare their corresponding modeling errors.

For  $\text{Pe} = 0$ , the passive scalars are given by

$$Z = \frac{x}{L_G}, \quad (3.4.1)$$

$$H = T_\infty + \frac{L}{L_G}. \quad (3.4.2)$$

Thus, the system of three PDEs (3.3.1)–(3.3.3) can be reduced to the single ordinary differential equation (ODE)

$$\frac{d^2T}{dx^2} + \text{Da} [(H - T)^2 - Z^2] \exp\left(-\frac{E}{T}\right) = 0. \quad (3.4.3)$$

#### 3.4.1. The nearly frozen regime

In the nearly frozen regime, the temperature is first approximated by  $T_\infty$  everywhere in  $\Omega$ , corresponding to a frozen chemical reaction. To account for chemical effects, small departures of order  $O(\varepsilon)$  from this temperature value, where  $\varepsilon = T_\infty^2/E$ , are related to the nonlinearity of the Arrhenius exponent in the reaction term. This term is also responsible for ignition effects. Typical profiles

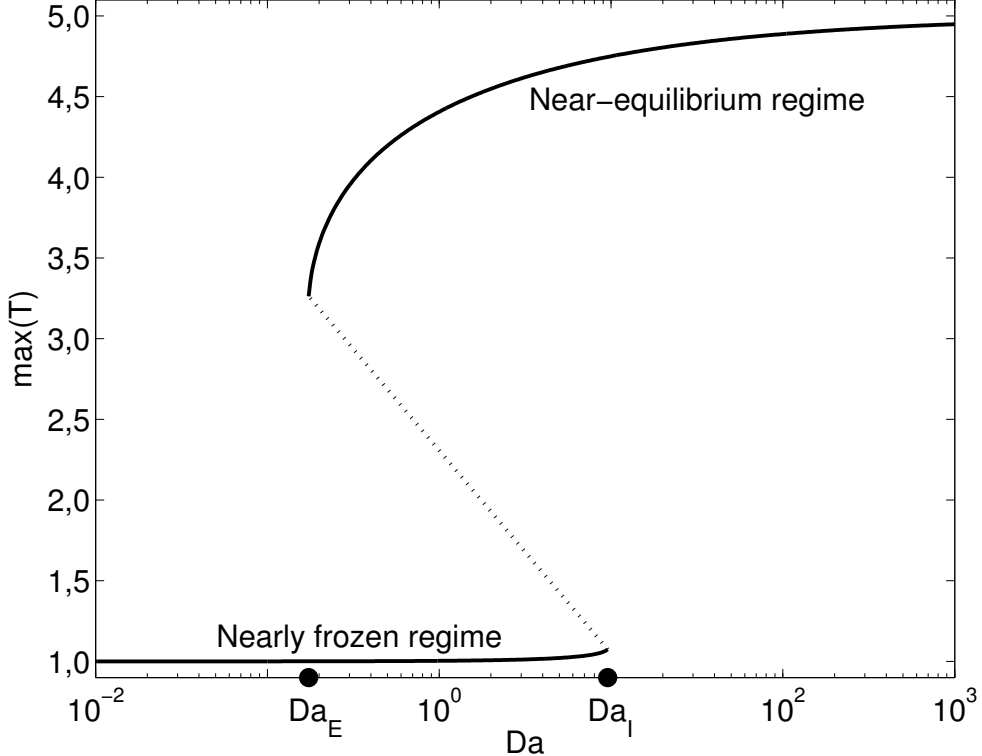


FIGURE 3.1. S-shaped curve—plot of the maximum flame temperature against  $Da$  for  $Pe = 0$ . Critical quenching and ignition parameters  $Da_E$  and  $Da_I$  are also shown.

for the reactive scalars in this regime are presented in Figure 3.2 for  $Pe = 0$  and  $Da = 1$ .

To obtain the value(s) of  $Da$  for which the departure from  $T_\infty$  at  $x = 0$  (flame position) is of order  $O(\varepsilon)$ , we plug the expansions

$$T = T_\infty + \varepsilon \theta_1(x) + O(\varepsilon^2), \quad (3.4.4)$$

$$\frac{Da}{L_G^2} \exp\left(-\frac{E}{T_\infty}\right) \frac{E}{T_\infty^2} = \Delta_0 + \varepsilon \Delta_1 + O(\varepsilon^2). \quad (3.4.5)$$

into (3.4.3), leading to an ODE for  $\theta_1(x)$  involving  $\Delta_0$ . There exists a critical value of  $\Delta_0$  for which this ODE has 2 solutions for smaller values of  $\Delta_0$ , and none for larger values of  $\Delta_0$  [T]. The number of possible solutions characterizes the lower branch and bend of the S-shaped curve, and leads to the existence of the ignition Damköhler number  $Da_I$  (see Figure 3.1). For  $Da < Da_I$ , two stable solutions exist, for  $Da > Da_I$ , only a near-equilibrium solution exists, which we

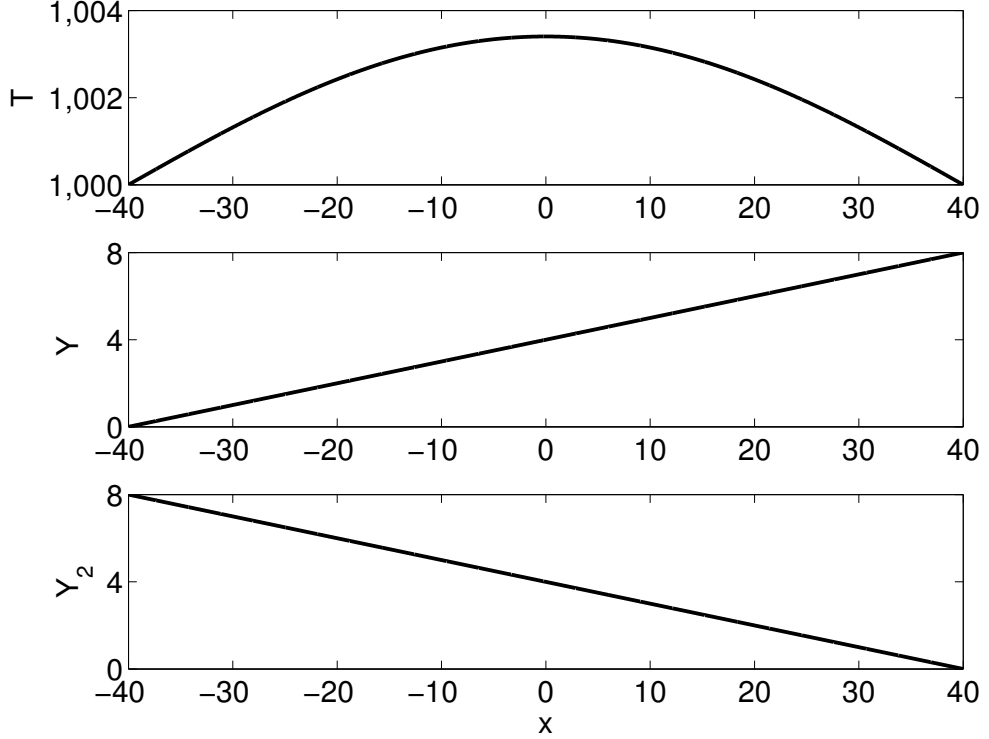


FIGURE 3.2. Typical profiles of  $T$ ,  $Y$ , and  $Y_2$  in the nearly frozen regime ( $\text{Da} = 1$ ,  $\text{Pe} = 0$ ).

will describe in section 3.4.2. Due to the symmetry of the setup, we always obtain clearly defined ignition conditions as long as  $E$  is large enough [L].

Throughout this paper, we will use the frozen flow approximation  $T = T_\infty$  on  $\Omega$  as our model in the nearly frozen regime. Using the passive scalar definitions, this corresponds to  $Y = Y_{ff} = H - T_\infty + Z$ .

### 3.4.2. The near-equilibrium regime

Flames in the near-equilibrium regime are made of a thin diffusion-controlled burning region separating two equilibrium regions. The temperature inside the reaction zone is close to the equilibrium value  $H$ , and small deviations of order  $O(\varepsilon)$ , where  $\varepsilon = H^2/E$ , are expected. Typical profiles for  $T$ ,  $Y$ , and  $Y_2$  in this regime are shown in Figure 3.3 for the values  $\text{Pe} = 0$  and  $\text{Da} = 100$ . The non-linearity of the reaction term is responsible for the existence of quenching. This regime covers the upper branch and bend of the S-shaped curve (see Figure 3.1).

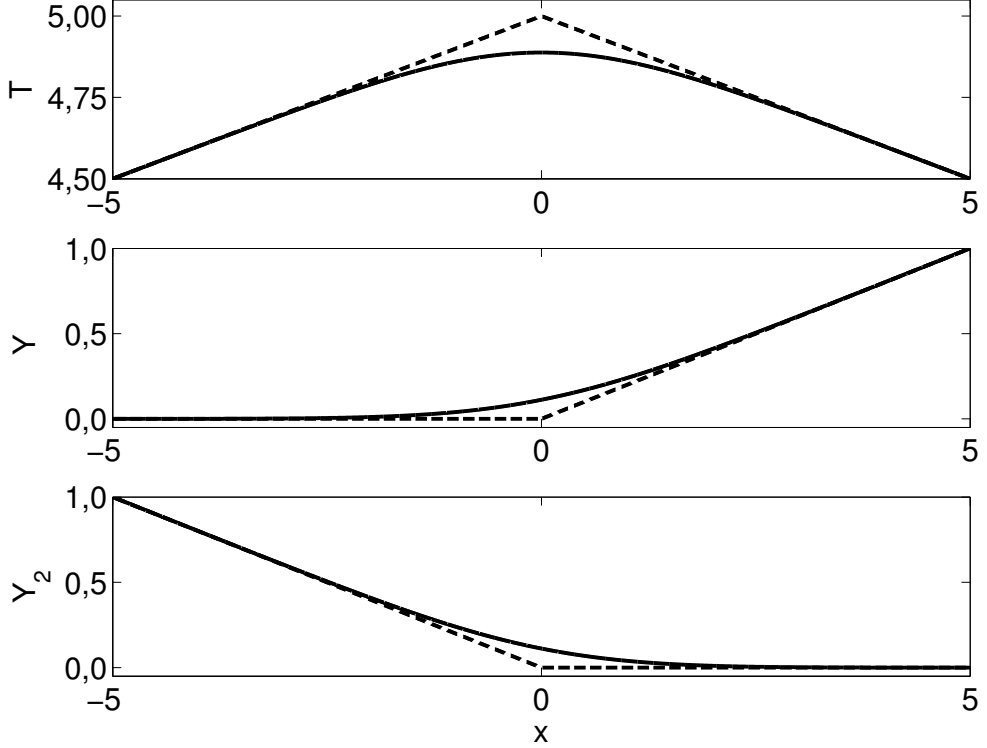


FIGURE 3.3. Typical profiles for  $T$ ,  $Y$ , and  $Y_2$  in the near-equilibrium regime ( $\text{Da} = 100$ ,  $\text{Pe} = 0$ ) around the flame location.  
 Full line: exact solutions, dashed line: equilibrium solutions.

We want to find the value(s) of  $\text{Da}$  for which the temperature departure from  $H$  at  $x = 0$  is of order  $O(\varepsilon)$ . Equilibrium is assumed outside of the reaction zone (outer solution), while the reaction zone temperature is determined by the following expansions:

- Inner solution, with  $\zeta = \frac{\delta_0^{1/3} x}{\varepsilon L_G}$ ,

$$T = H - \delta_0^{-1/3} (\varepsilon \beta_1(\zeta) + O(\varepsilon^2)); \quad (3.4.6)$$

- Reduced Damköhler number  $\delta$ ,

$$\delta = L_G^2 \text{Da} \left( \frac{H^2}{E} \right)^3 \exp \left( -\frac{E}{H} \right) = \delta_0 + \varepsilon \delta_1 + O(\varepsilon^2). \quad (3.4.7)$$

By inserting these expansions into (3.4.3) and matching the inner and outer solutions on an intermediate scale, we obtain an ODE for  $\beta_1(\zeta)$  in terms of  $\delta_0$ . There exists a critical value of  $\delta_0$  for which the ODE has two solutions for higher values of  $\delta_0$ , and none for lower values [T]. The switch from the existence of two

stable solutions to a single nearly frozen solution is characterized by the extinction Damköhler number  $\text{Da}_E$ . Flamelet models are used to approximate  $Y$  in the near-equilibrium regime, and are described in the next sections.

Note that if  $\varepsilon$  is small, then  $\delta \approx \delta_0$  and we have

$$\zeta \approx \left( L_G^2 \text{Da} \exp\left(\frac{-E}{H}\right) \right)^{1/3} \frac{x}{L_G}, \quad (3.4.8)$$

$$\begin{aligned} Y = H + T - Z &= \delta_0^{-1/3} \varepsilon \beta_1 + O(\varepsilon^2) \\ &\approx \left( L_G^2 \text{Da} \exp\left(\frac{-E}{H}\right) \right)^{-1/3} \beta_1. \end{aligned} \quad (3.4.9)$$

### 3.4.3. The asymptotic flamelet subgrid model strategy

The flamelet subgrid modeling strategy used in the near-equilibrium regime is reviewed here. The objective is to predict the solution  $\bar{Y}$  of the equation for the reactive scalar defined as

$$\bar{Y} = \int Y(x, y) dx dy, \quad (3.4.10)$$

with the integration performed over elements of the large-scale mesh. For nonreactive variables, the filtered solution can be obtained as the solution of the filtered governing equation. If the equation is nonlinear to begin with, filtering leads to terms which can no longer be expressed solely as functions of the filtered variables and subgrid models are needed to express those unclosed terms as functions of the large-scale variables only. In the case of nonlinear reaction terms, there is no known strategy to formulate such a closure model at the level of the governing equation. Instead, in the flamelet regime,  $\bar{Y}$  is approximated by

$$\bar{Y} = \int Y(Z, H) \text{PDF}(Z, H) dZ dH. \quad (3.4.11)$$

This approximation is based on the following assumptions:

- (1) The resolved reactive scalar  $Y$  can be expressed as a function of the passive scalars  $Z$  and  $H$  (and other statistics, depending on the model).
- (2) The joint probability distribution function of  $Z$  and  $H$ ,  $\text{PDF}(Z, H)$ , is known or can be modeled.

Assumption 2 is plausible because the passive scalars satisfy much simpler equations (with no reaction term). Assumption 1 is the source of the modeling error.

### 3.4.4. Construction of the flamelet approximation

For  $\text{Pe} = 0$  and  $E = 0$ , it is easy to express  $Y$  as function of  $Z$  solely. Indeed,  $Z_p = 0$  since  $Z = x/L_G$  solves (3.3.4). With a change of variables from  $x$  to  $Z$ , we rewrite (3.3.6) as the ODE

$$\frac{d^2Y}{dZ^2} = \text{Da} L_G^2 Y (Y - 2Z). \quad (3.4.12)$$

Let  $\alpha = (\text{Da} L_G^2)^{1/3}$  (Damköhler group). Substitution of the normalized variables  $\hat{Z} = \alpha Z$  and  $\hat{Y} = \alpha Y$  in (3.4.12) leads to the parameter-free equation

$$\frac{d^2\hat{Y}}{d\hat{Z}^2} = \hat{Y} (\hat{Y} - 2\hat{Z}). \quad (3.4.13)$$

The solution of this equation can be computed once and for all and stored in a *flamelet library*. Figure 3.4 displays the flamelet solution in terms of the normalized departure from equilibrium  $d\hat{Y}(\hat{Z}) = \hat{Y} - (\hat{Z} + |\hat{Z}|)$ . By using normalizations and table lookups, we find a flamelet approximation of the form  $Y = Y(Z)$ .

For  $E \neq 0$ ,  $Y$  solves

$$\frac{d^2Y}{dZ^2} = \text{Da} L_G^2 Y (Y - 2Z) \exp\left(\frac{-E}{H - Y + Z}\right). \quad (3.4.14)$$

It is impossible to reduce the previous four-parameter equation (for  $L_G$ ,  $\text{Da}$ ,  $H$ , and  $E$ ) to an equation with less than three parameters. However, we can approximate (3.4.14) by a normalized parameter-free equation using an unique normalization parameter. To do so, the results obtained for a simpler chemistry ( $E = 0$ ) will be extended to the  $E \neq 0$  case using the asymptotic relations in the near-equilibrium regime.

For a nonzero activation energy, we use (3.4.1), (3.4.8), and (3.4.9) to define a new Damköhler group  $\alpha$ , given by

$$\alpha = \left( L_G^2 \text{Da} \exp\left(\frac{-E}{H}\right) \right)^{1/3}. \quad (3.4.15)$$

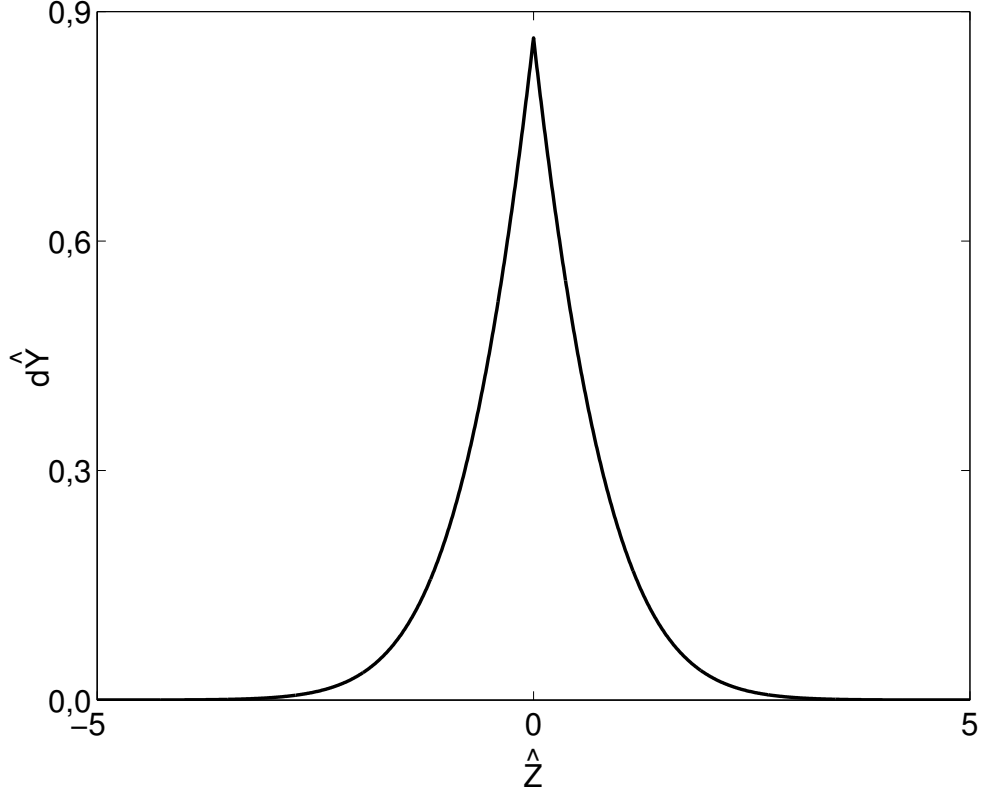


FIGURE 3.4. Flamelet library—correction term  $d\hat{Y}(\hat{Z}) = \hat{Y} - (\hat{Z} + |\hat{Z}|)$ .

The new normalized variables  $(\hat{Z}, \hat{Y})$  lead to a variety of flamelet libraries. To construct them, we compute the solution of (3.4.14) using centered finite differences and Newton's method, then normalize  $Z$  and  $Y$  using the Damköhler group. Many values of  $\alpha$  were tested out by varying  $E$  and Da. As  $\alpha$  grows, the new flamelet libraries converge to the solution of (3.4.12). Figure 3.5 shows that, in the  $\alpha \rightarrow +\infty$  limit, the flamelet approximation

$$Y_{fl} = [\alpha(Z, H)]^{-1} \hat{Y}(\alpha(Z, H) Z), \quad (3.4.16)$$

with  $\alpha$  given by (3.4.15) and  $\hat{Y}$  the solution of (3.4.13), converges in  $L^2$ -norm to the solution  $Y$  of (3.4.14). The local error  $|Y - Y_{fl}|$  is of order  $O(\alpha^{-2})$  [BM1] and we integrate its square on a reaction zone of order  $O(\alpha^{-1})$ , therefore

$$\|Y - Y_{fl}\|_{L^2} = O(\alpha^{-5/2}), \quad (3.4.17)$$

a scaling recovered in the numerical simulations. Unlike the  $E = 0$  case, where the flamelet solution solves (3.4.14), modeling errors on  $Y_{fl}$  are not equal to zero

when  $E \neq 0$ . In the next subsection, we will compare the errors on  $Y_{fl}$  and on the frozen flow model  $Y_{ff}$ .

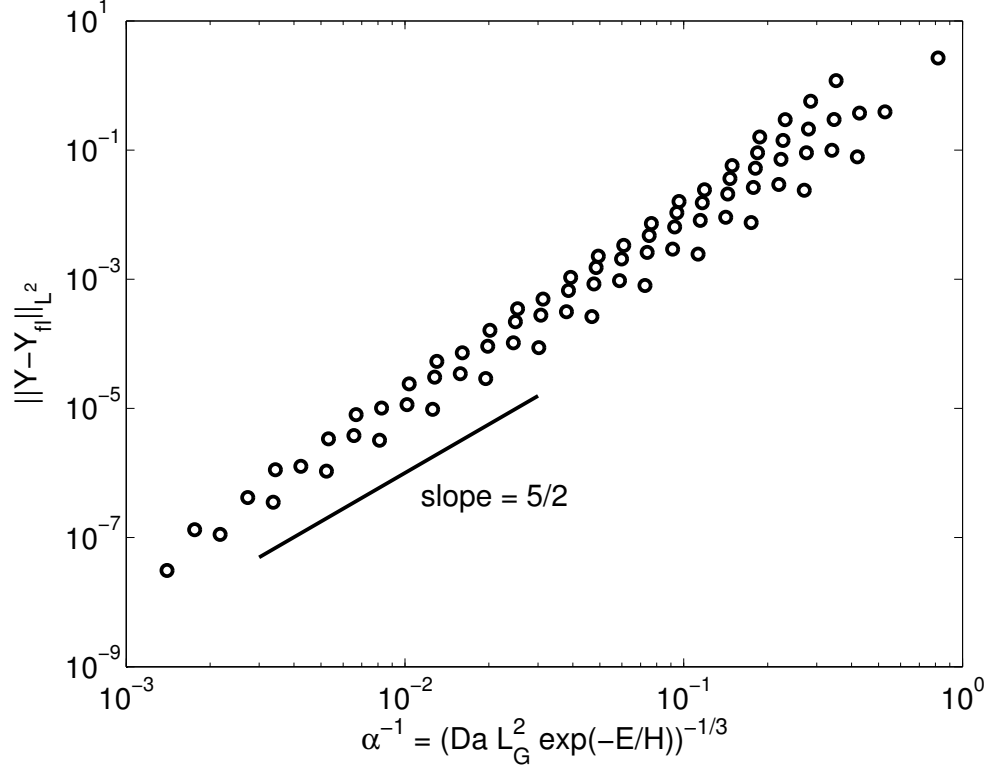


FIGURE 3.5.  $L^2$ -norm errors between the flamelet approximation  $Y_{fl}$  and the solution  $Y$  of (3.4.14), plotted against  $\alpha^{-1}$ .

### 3.4.5. Approximation errors

In Figure 3.6, we compare the modeling errors for the frozen flow and flamelet models on each stable branch of the S-shaped curve. We plot the  $L^2$ -norm modeling errors on  $Y_{ff}$  and  $Y_{fl}$  against  $\text{Da}^{-1/3}$ . As expected, the flamelet solution  $Y_{fl}$  is a better choice for near-equilibrium flames and the frozen flow approximation  $Y_{ff}$  performs best for nearly frozen combustion. This model hierarchy remains the same throughout a particular branch. As  $\text{Da} \rightarrow 0$ , the modeling error  $\|Y - Y_{ff}\|_{L^2}$  is of order  $O(\text{Da}^1)$ , a scaling recovered from the asymptotic expansions in [T]; as  $\text{Da} \rightarrow +\infty$ ,  $\|Y - Y_{fl}\|_{L^2}$  is of order  $O(\alpha^{-5/2}) = O(\text{Da}^{-5/6})$ .

The lowest error curves for each stable branch of the S-shaped curve intersect at the Damköhler number value  $\text{Da}^* = 3.76 \times 10^0$ , located between

$\text{Da}_I = 1,74 \times 10^{-1}$  and  $\text{Da}_E = 9,55 \times 10^0$ , an interval where both stable combustion regimes exist. In Figure 3.7, the S-shaped curve is shown, alongside markers corresponding to the model with the lowest modeling error. For values of Da where only one stable regime exists, modeling errors are lower for the asymptotically correct model. The modeling error also gives a way of systematically choosing between stable regimes if they both exist. In this case, we would choose the near-equilibrium regime for  $\text{Da} > \text{Da}^*$ , and the nearly frozen regime for  $\text{Da} < \text{Da}^*$ , leading to a degenerate S-shaped curve.

### 3.5. THE $\text{Pe} \neq 0$ CASE

In this section, we study the behavior of solutions when advection effects are included. We show that some results found here can be linked to the results for  $\text{Pe} = 0$ . Comparisons are made between the various flame models, and links with the zero activation energy results are found.

Following [BM1], the following flows are studied:

- the simple shear flow,  $\mathbf{v} = (\sin(2\pi y), 0)$ ;
- the Childress–Soward flow,  $\mathbf{v} = (-\partial F/\partial y, \partial F/\partial x)$ , where the stream function is given by  $F(x, y) = K (\sin(2\pi x) \sin(2\pi y) + \delta \cos(2\pi x) \cos(2\pi y))$ , and  $K$  is normalized so the kinetic energy is unity.

Figure 3.8 shows the passive scalar  $Z$  for these two flows and for two values of  $\text{Pe}$ . In Figure 3.8 and throughout this paper, the value  $\delta = 0,5$  will be used for the Childress–Soward flow, because this choice is the most interesting one, as it leads to a mix of shear and eddies.

#### 3.5.1. Extending the models to the $\text{Pe} \neq 0$ case

The frozen flow approximation  $T = T_\infty$  is equivalent to  $Y_{ff} = H - T_\infty + Z$ , therefore it is rather trivial to extend and compute this approximation when  $\text{Pe} \neq 0$ . In the near-equilibrium regime, we would also like to express  $Y$  as a function of  $Z$  and  $H$  using the flamelet library previously defined. This would therefore reduce the computational cost of the problem from that of solving the bidimensional PDE (3.3.6) down to computing—once—the solution of the ODE

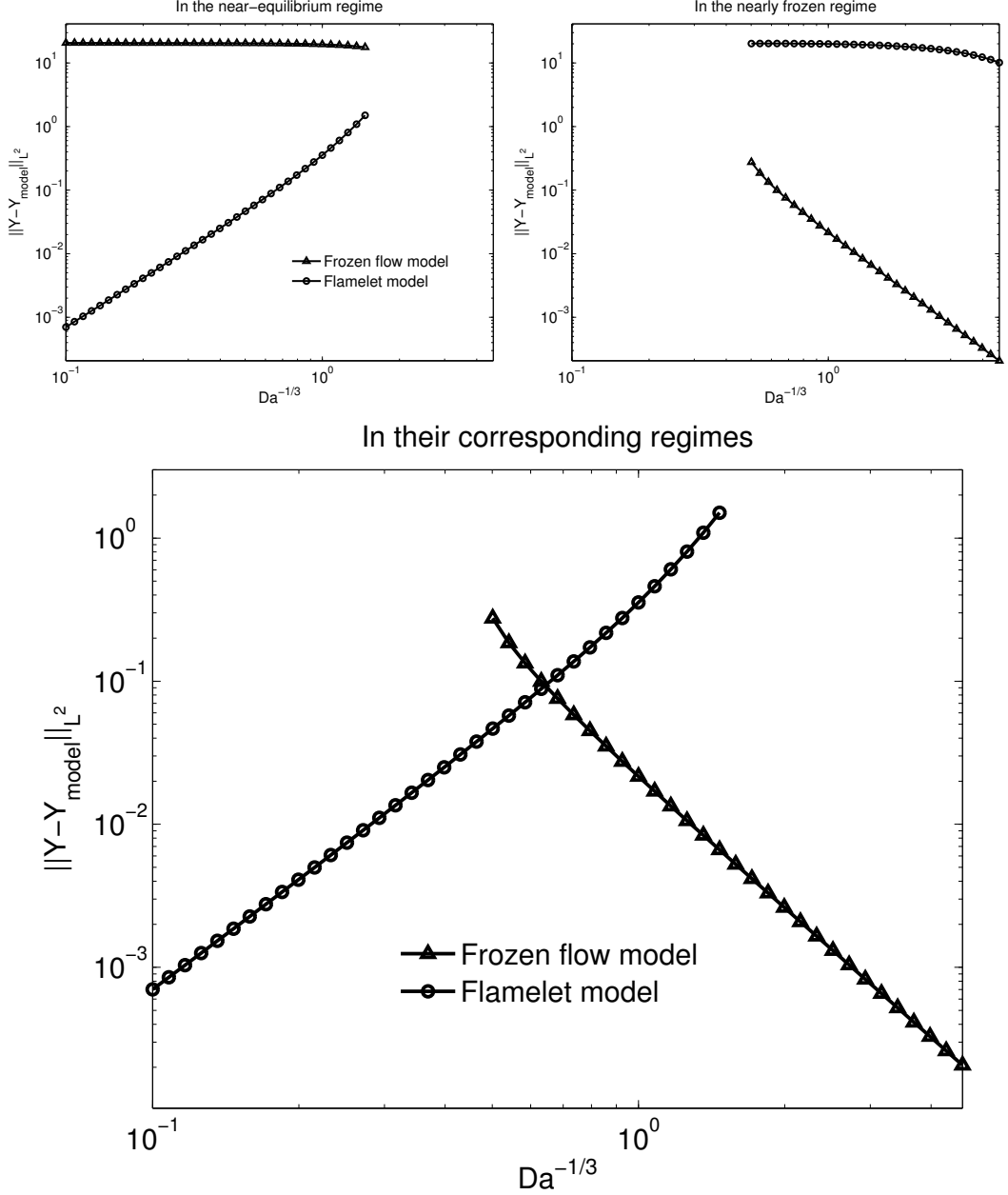


FIGURE 3.6.  $L^2$ -norm errors between  $Y$  and its approximations as functions of  $\text{Da}^{-1/3}$ . Top left: approximations compared to the near-equilibrium regime solution; top right: approximations compared to the nearly frozen regime solution; bottom: lowest error curves from above plots.

(3.4.13) in terms of  $\widehat{Z}$  and solving the much simpler passive scalar PDEs (3.3.4)–(3.3.5). Two levels of approximations are used to obtain the solution  $Y$  for  $\text{Pe} \neq 0$ .

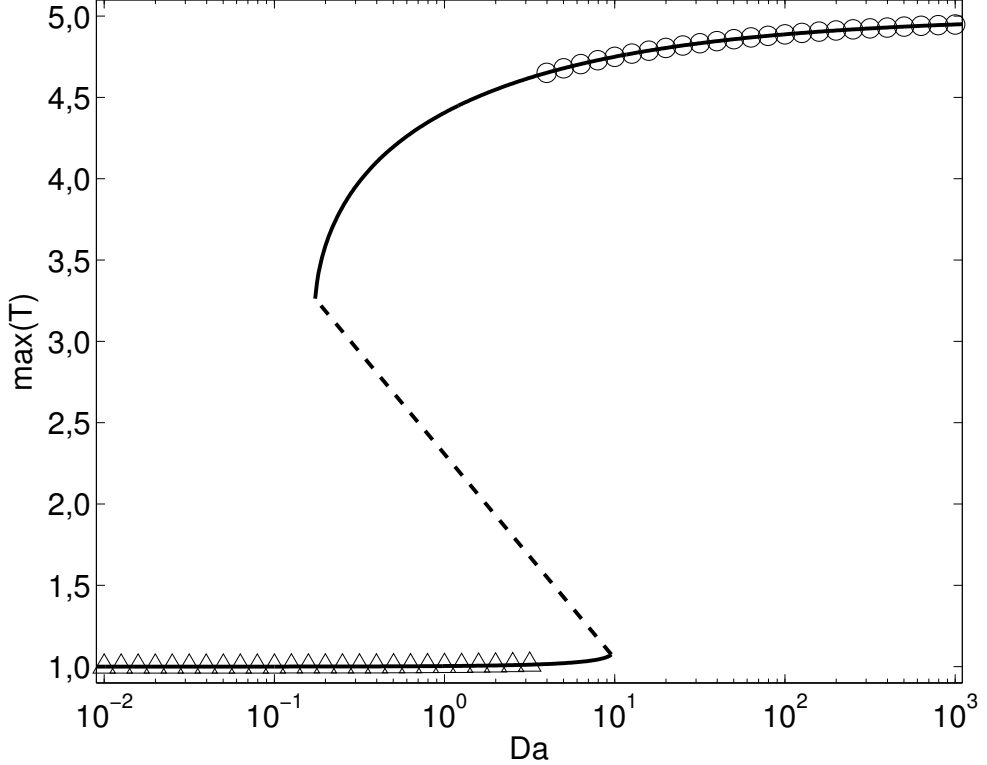


FIGURE 3.7. Lowest modeling errors and S-shaped curve for  $\text{Pe} = 0$ . The S-shaped curve (full line) is shown, alongside markers corresponding to the model with the lowest modeling error: frozen flow model (triangle), flamelet model (circle).

The first level of approximation consists of assuming that  $Y$  can be expressed as a flamelet from a library, obtained as the solution for  $\text{Pe} = 0$ . The second level of approximation is that this  $\text{Pe} = 0$  solution is obtained from a flamelet solution with  $E = 0$ .

Let  $\chi_{ld} = |\nabla Z|^2$  be the local dissipation. For  $\text{Pe} = 0$ ,  $\chi_{ld} = 1/L_G^2$  and we rewrite the Damköhler group as

$$\alpha = [\text{Da}/\chi_{ld} \exp(-E/H)]^{1/3}. \quad (3.5.1)$$

We first show that the  $\text{Pe} = 0$  flamelet library is still a good choice when  $\text{Pe} \neq 0$ , as long as the Damköhler group  $\alpha$  is modified accordingly. Figure 3.9 shows scatter plots of some high Da solutions for the Childress–Soward flow with  $\delta = 0.5$ . The  $(Z(x, y), Y(x, y))$  data points from the numerical simulations are normalized to  $(\alpha(x, y) Z(x, y), \alpha(x, y) Y(x, y))$  with the new value of  $\alpha$ . Then, we plot the

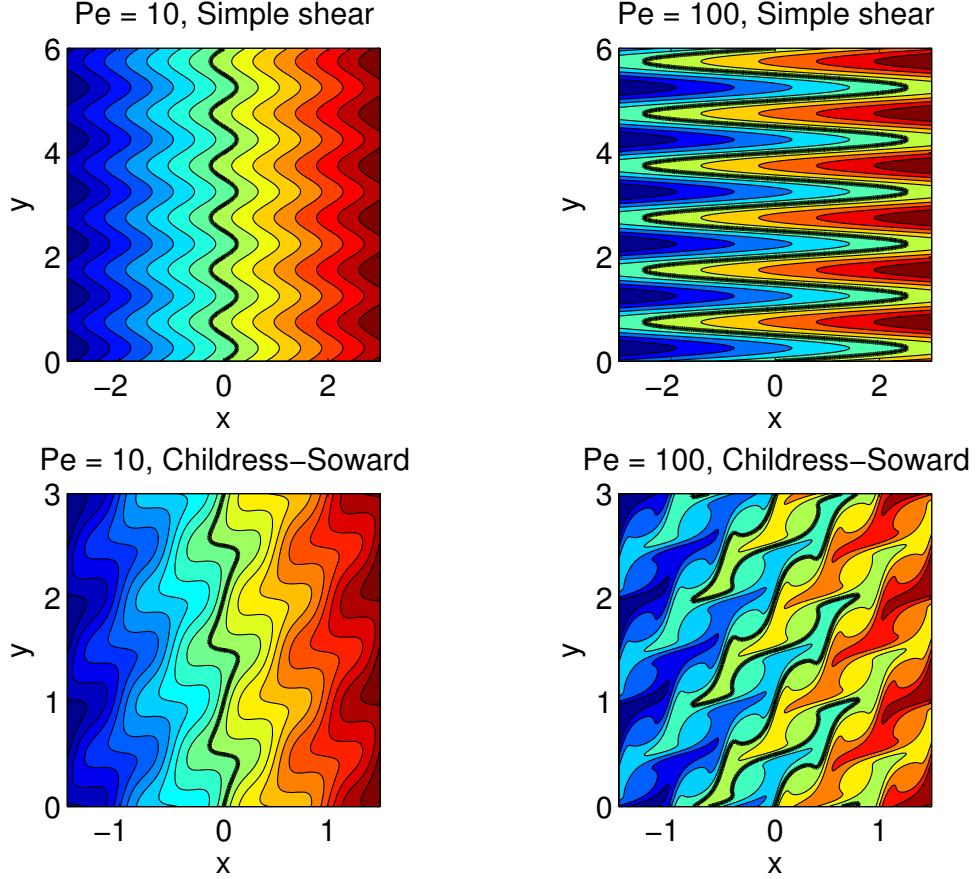


FIGURE 3.8. Passive scalar  $Z$  for various choices of  $\mathbf{v}$  and  $\text{Pe}$ . Stoichiometric level  $Z = 0$  highlighted in black.

normalized departures from equilibrium of those points and add the data from the  $\text{Pe} = 0$  flamelet library (shown in white). The agreement with the flamelet library is better as  $\text{Da}$  increases, while higher values of  $\text{Pe}$  leads to a larger scatter.

In practical applications, the exact value of the local dissipation is not always available. Instead, we might only have access to its mean value  $\langle \chi_{ld} \rangle$ , where  $\langle \cdot \rangle$  denotes space-averaging. In this paper, we will study two flamelet models, whose expressions are given by (3.4.16), with

$$\alpha = \begin{cases} [\text{Da}\chi_{ld}^{-1} \exp(-E/H)]^{1/3} & \text{(local dissipation model)} \\ [\text{Da}\langle\chi_{ld}\rangle^{-1} \exp(-E/H_0)]^{1/3} & \text{(mean dissipation model)} \end{cases} \quad (3.5.2)$$

and  $H_0$ , the value of  $H$  on the stoichiometric level  $Z = 0$ . As in the  $E = 0$  case, the mean dissipation model uses a single value of  $\alpha$  on  $\Omega$  [BM1, V].

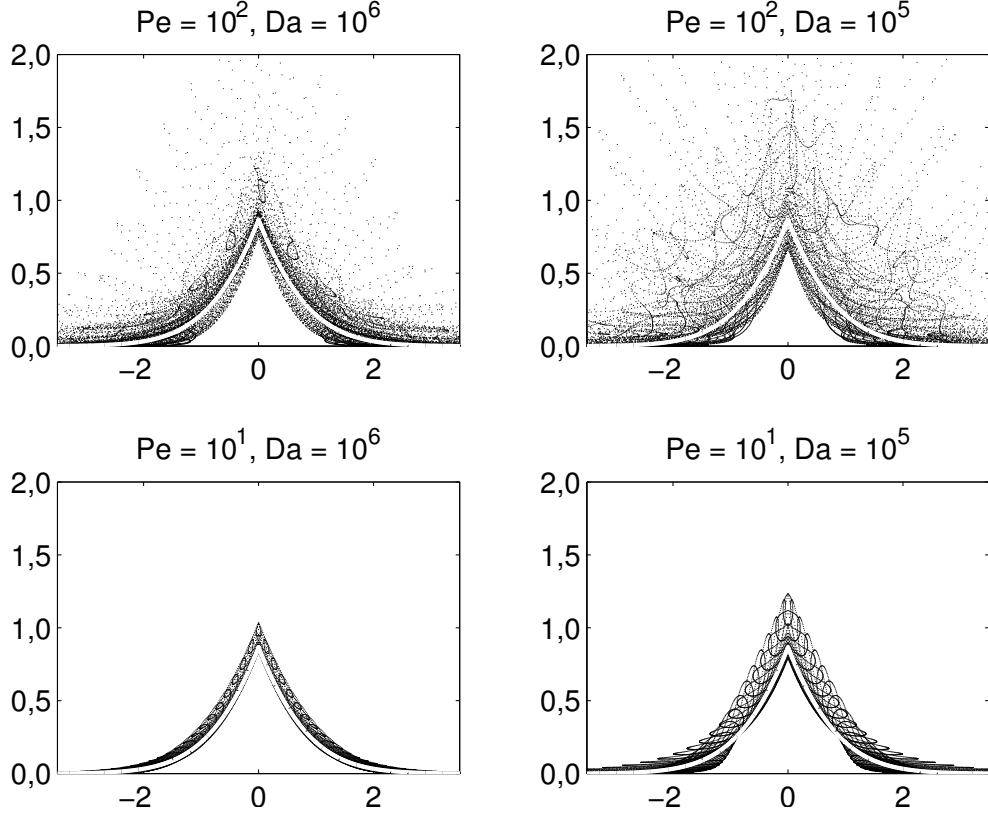


FIGURE 3.9. Childress–Soward flow,  $\delta = 0,5$ —data points  $(\alpha Z, \alpha (Y - (Z + |Z|)))$  of near-equilibrium solutions for high Da and various Pe. The flamelet library’s data points are shown in white.

Independently of the model used, the flamelet approach just described can be summarized as follows:

- (1) Compute, once and for all, the flamelet library using (3.4.13). This yields the function  $\widehat{Y}(\widehat{Z})$ , that is, a way of modeling the reactive scalar  $Y$  as a function of the passive scalars  $Z$  and  $H$ .
- (2) Compute the passive scalars  $Z$  and  $H$  using (3.3.4)–(3.3.5). These equations are independent of Da and can be solved on a grid as coarse as the flow field allows.
- (3) Compute the dissipation  $\chi$  used in the model.
- (4) Use (3.4.16) and (3.5.2) to get an approximate solution  $Y_{fl}$  to the solution  $Y$  of (3.3.6).

- (5) Integrate  $Y_{fl}(Z, H, \chi)$  following (3.4.11). To do so, we need PDF  $(Z, H, \chi)$ , the joint probability density function of both passive scalars and the dissipation.

At the end of the process, we obtain a coarse-grid solution taking small-scale features into account. For all choices of the Damköhler group  $\alpha$  considered here, the flamelet approximation is asymptotically valid for large Da [BM1, T]. The main challenge for  $E > 0$  is that, unlike the  $E = 0$  case discussed before, we have to identify the right combustion regime before determining the best model on that stable branch of the S-shaped curve. This is addressed in the next subsection.

### 3.5.2. Modeling errors

The objective here is to compare the modeling errors in each combustion regime when using the models described before. To do so, we generate numerical solutions of the full system (3.3.1)–(3.3.3) for both stable combustion regimes, as well as the approximations based on the various models. We do so for a wide range of values for the parameters Da and Pe to extract asymptotic trends for the modeling errors.

The numerical computations for the full system (no model) are performed using centered finite differences and Newton's method. Numerical parameters are chosen to control discretization errors. Convergence is very fast if we use  $Y_{ff}$  or  $Y_{fl}$  as first approximations in their corresponding combustion regimes.

Modeling errors for all three subgrid models (mean dissipation flamelet, local dissipation flamelet, frozen flow model) are obtained by comparing the approximations to the numerical solutions from the corresponding branch of the S-shaped curve. In Figures 3.10 and 3.11, we plot the  $L^2$ -norm errors of these errors. For each plot, two intersection points mark the locations where the model hierarchy changes (based on the smallest modeling errors). Denote by  $Da_1$ , the value of Da at which the curves for the frozen flow and mean dissipation flamelet models intersect, and by  $Da_2$ , the value of Da at which the curves for both flamelet models intersect. The mean dissipation flamelet is the best near-equilibrium approximation for  $Da_E < Da < Da_2$ , while the local dissipation model performs best for

$\text{Da} > \text{Da}_2$ ; we recover a similar model hierarchy as the  $E = 0$  model hierarchy [BM1]. In all cases,  $\text{Da}_1$  is located between  $\text{Da}_E$  and  $\text{Da}_I$ . Outside that range, only one combustion regime is possible, and we obtain the lowest modeling errors for an asymptotically correct model in that regime. When multiple regimes exist, the modeling error suggests a clear cut way to choose a combustion regime and a corresponding model: we would assume that a flame is in the nearly frozen regime for  $\text{Da} < \text{Da}_1$ , and in the near-equilibrium regime for  $\text{Da} > \text{Da}_1$ ; in this regime, we would favor the mean dissipation flamelet model for  $\text{Da}_1 < \text{Da} < \text{Da}_2$ , and the local dissipation flamelet model for  $\text{Da} > \text{Da}_2$ .

For each model, we compute the asymptotic slopes  $\beta$  from Figures 3.10 and 3.11, i.e., the values of  $\beta$  such that the modeling errors  $\|Y - Y_{model}\|_{L^2}$  are of order  $O(\text{Da}^{-\beta/3})$ . To do so, a polynomial fit between  $\log(\|Y - Y_{model}\|_{L^2})$  and  $\log(\text{Da}^{-1/3})$  is done using the last 5 data points in each asymptotic regime. Figure 3.12 shows the values of  $|\beta|$  for the studied flows and models (6 curves in total). As in the  $\text{Pe} = 0$  case, we obtain  $\|Y - Y_{ff}\|_{L^2} = O(\text{Da}^1)$  for the frozen flow model, both in theory and numerically. Asymptotic predictions in [BM1] for  $E = 0$  and  $\text{Pe} \neq 0$  suggest that the local error  $|Y - Y_{fl}|$  is of order  $O(\text{Da}^{-1/3})$  for the mean dissipation model, and of order  $O(\text{Da}^{-2/3})$  for the local dissipation model. Integrating the square of these quantities over a reaction zone of order  $O(\text{Da}^{-1/3})$  leads to  $\|Y - Y_{fl}\|_{L^2} = O(\text{Da}^{-1/2})$  for the mean dissipation model, and  $\|Y - Y_{fl}\| = O(\text{Da}^{-5/6})$  for the local dissipation model. Both results are recovered numerically.

### 3.6. S-SHAPED CURVES, PREDICTION OF QUENCHING AND IGNITION

As it was the case for  $\text{Pe} = 0$ , flames in the presence of advection effects can exhibit quenching and ignition behavior, as captured in the S-shaped curves. Figures 3.13 (simple shear flow) and 3.14 (Childress–Soward flow) show the S-shaped curves for various values of  $\text{Pe}$ . Those curves are generated using the numerical solutions from the previous section. On the left side, the actual curves are shown. For both flows, as  $\text{Pe}$  increases, the maximum flame temperature and

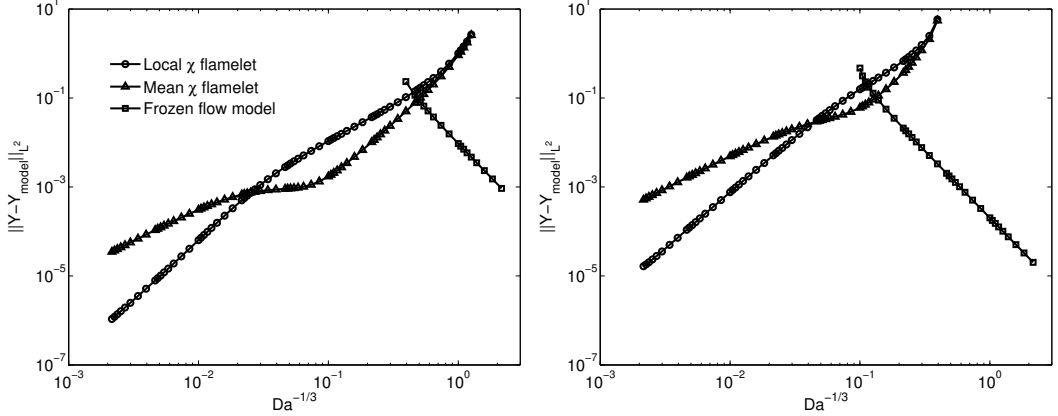


FIGURE 3.10. Simple shear flow— $L^2$ -norm errors for  $\text{Pe} = 10$  (left) and  $\text{Pe} = 100$  (right) for various  $\text{Da}$ .

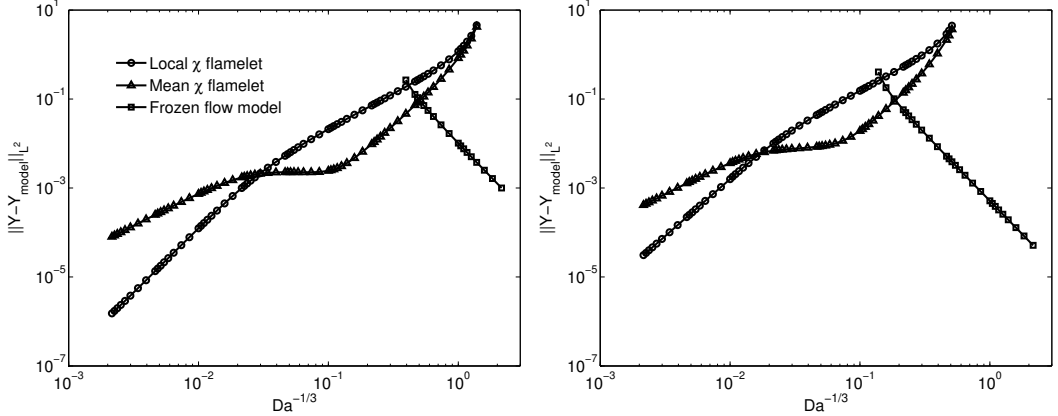


FIGURE 3.11. Childress–Soward flow,  $\delta = 0.5$ — $L^2$ -norm errors for  $\text{Pe} = 10$  (left) and  $\text{Pe} = 100$  (right) for various  $\text{Da}$ .

the values of the critical Damköhler parameters  $\text{Da}_E$  and  $\text{Da}_I$  increase. On the right side of these figures, the S-shaped curve for  $\text{Pe} = 0$  is drawn and the data points from the  $\text{Pe} > 0$  computations are normalized using the following relations:

- For the Damköhler numbers,

$$\text{Da} \longrightarrow \frac{\text{Da}}{L_G^2 \langle \chi_{ld} \rangle} \exp \left[ E \left( \left\{ T_\infty + \frac{L}{L_G} \right\}^{-1} - H_0^{-1} \right) \right]; \quad (3.6.1)$$

- For the data points on the upper branch of the S-shaped curve,

$$\max(T) \longrightarrow \left( T_\infty + \frac{L}{L_G} \right) - (H_0 - \max(T)). \quad (3.6.2)$$

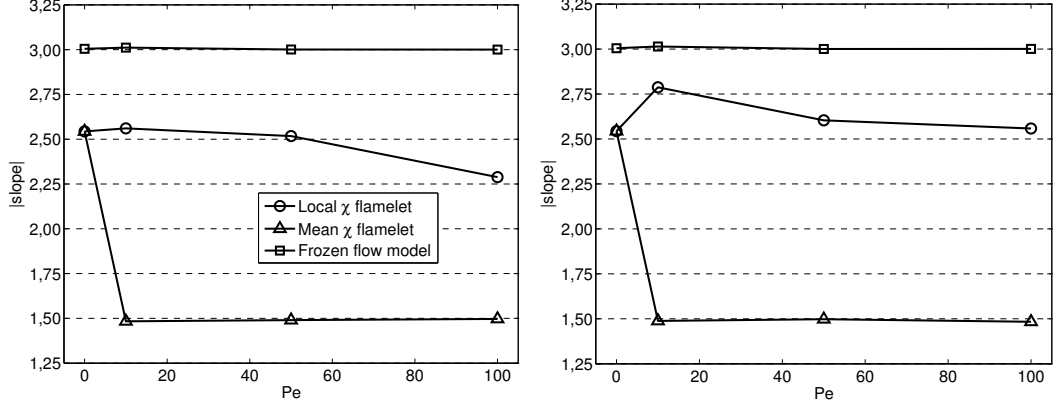


FIGURE 3.12. Absolute values of the asymptotic slopes from Figures 3.10–3.11—simple shear flow (left), Childress–Soward flow (right).

- For the data points on the lower branch of the S-shaped curve, no transformations are done on the maximum temperatures.

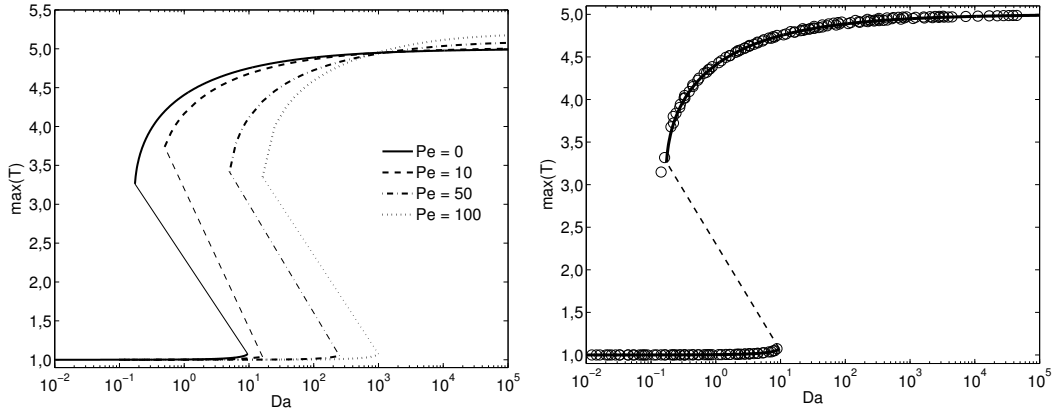


FIGURE 3.13. Simple shear flow—maximum temperature as a function of Da for various values of Pe: left, (nonnormalized) S-shaped curves; right, S-shaped curve for Pe = 0 (full line) and normalized points (circles) from the Pe > 0 data.

To obtain the first relation, we find a value of Da such that the Damköhler groups  $\alpha$ , given by (3.5.2) for the mean dissipation model, are the same at  $Pe = 0$

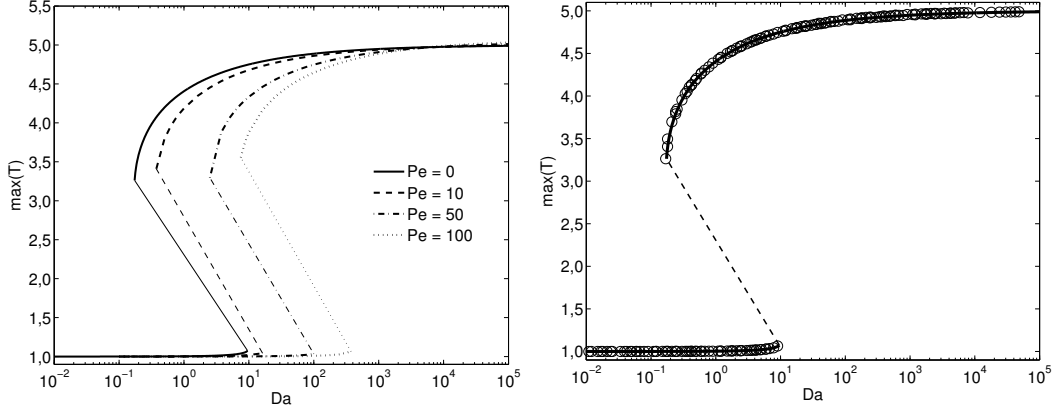


FIGURE 3.14. Childress–Soward flow,  $\delta = 0.5$ —maximum temperature as a function of  $Da$  for various values of  $Pe$ : left, (nonnormalized) S-shaped curves; right, S-shaped curve for  $Pe = 0$  (full line) and normalized points (circles) from the  $Pe > 0$  data.

and  $Pe \neq 0$ . Explicitly,

$$Da_{Pe>0} \langle \chi_{ld} \rangle^{-1} \exp \left( \frac{-E}{H_0} \right) = Da_{Pe=0} L_G^2 \exp \left( \frac{-E}{T_\infty + L/L_G} \right), \quad (3.6.3)$$

and solving for  $Da_{Pe=0}$  leads to (3.6.1). For this choice of  $Da_{Pe=0}$  and fixed values of  $E$  and  $H$ , the asymptotic expansions (3.4.6)–(3.4.7) show that  $H - T$  is a constant on the stoichiometric level  $Z = 0$ , hence (3.6.2). Independently of the flow used, the S-shaped curve for  $Pe \neq 0$  can be predicted very accurately from the S-shaped curve for  $Pe = 0$  and information about the passive scalars for  $Pe \neq 0$ . Surprisingly, the Damköhler number transformation (3.6.1) is still valid in the nearly frozen regime.

For  $Pe \neq 0$ , we use (3.6.1) to obtain predictions of the critical quenching and ignition parameters:

$$Da_E \approx Da_{E,Pe=0} \langle \chi_{ld} \rangle L_G^2 \exp \left( \frac{E}{H_0} - \frac{E}{T_\infty + L/L_G} \right), \quad (3.6.4)$$

$$Da_I \approx Da_{I,Pe=0} \langle \chi_{ld} \rangle L_G^2 \exp \left( \frac{E}{H_0} - \frac{E}{T_\infty + L/L_G} \right). \quad (3.6.5)$$

To check the accuracy of those predictions, we show the number of existing stable solutions for both flows in Figure 3.15. The circle marker indicates that both near-equilibrium and nearly frozen solutions exist for these parameters, while

the cross marker means only one of these solutions exists. Predictions for  $\text{Da}_E$  and  $\text{Da}_I$  are plotted as full lines. It turns out that (3.6.4)–(3.6.5) give very good approximations, since the full line curves mostly fall between the transitions from cross markers to circle markers and back.

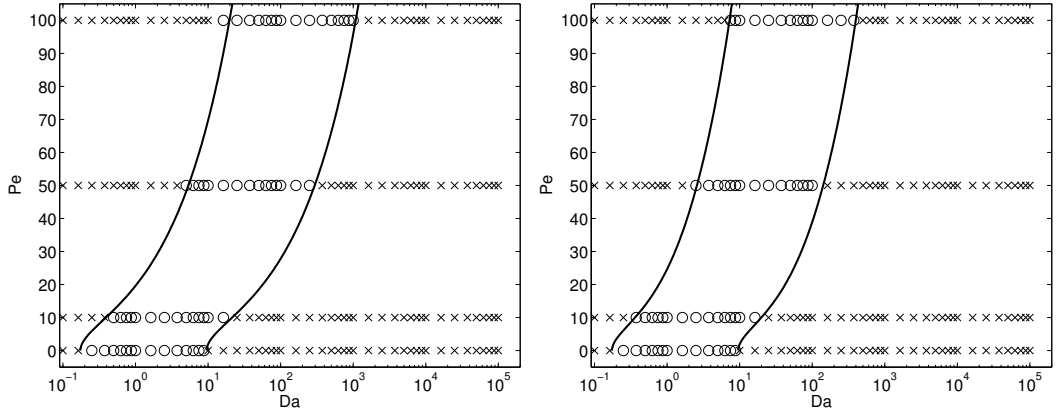


FIGURE 3.15. Existence of solutions in the near-equilibrium and nearly frozen regimes and predictions for  $\text{Da}_I$  and  $\text{Da}_E$  (full lines): left, simple shear flow; right, Childress–Soward flow,  $\delta = 0.5$ . A cross marker denotes the existence of a unique solution, a circle marker, the coexistence of two stable solutions.

### 3.7. CONCLUSION

An idealized model that allows quenching and ignition has been investigated for a wide variety of Péclet and Damköhler numbers. We have recovered the classic S-shaped curve plot of the maximum temperature against the Damköhler number, and we have shown how to obtain all S-shaped curves by using the  $\text{Pe} = 0$  curve and statistics of the passive scalars. The two stable combustion regimes, obtained via an asymptotic analysis for  $\text{Pe} = 0$ , are also observed for nonzero Péclet numbers. Flamelet models have been constructed in the near-equilibrium regime using a flamelet library; the flamelet library used in the original Bourlioux–Majda model can be reused to generate flamelets for nonzero activation energies, as long we define new Damköhler groups.

A comparison of the modeling errors for flamelet and frozen flow models has been done. As expected, the flamelet models have been shown to perform better on the upper branch of the S-shaped curve (near-equilibrium regime), similarly for the frozen flow model on the lower branch of the S-shaped curve (nearly frozen regime). By looking at the error curves for each model on their respective S-shaped curve branches, intersection points have been identified and have been used to systematically choose a combustion regime and a model where multiple stable solutions and/or models exist.

While the asymptotic trends of the modeling errors are known, obtaining quantitative estimations of those errors for  $\text{Pe} \neq 0$  is an open problem. We plan to investigate whether the dual-based a posteriori error estimator successfully used in [BET] can accurately predict which model is the best and by doing so, identify whether the flame is quenched or ignited.

### 3.8. REFERENCES

- [BET] A. BOURLIOUX, A. ERN, P. TURBIS, *A posteriori error estimation for subgrid flamelet models*, Mult. Mod. Simul., 8 (2010), pp. 481–497.
- [BM1] A. BOURLIOUX AND A. J. MAJDA, *An elementary model for the validation of flamelet approximation in nonpremixed turbulent combustion*, Comb. Theory Mod., 4 (2000), pp. 189–210.
- [BM2] A. BOURLIOUX AND A. J. MAJDA, *Elementary models with PDF intermittency for passive scalars with a mean gradient*, Phys. Fluids, 14 (2002), pp. 881–897.
- [L] A. LIÑÁN, *The asymptotic structure of counterflow diffusion flames for large activation energies*, Acta Astronautica, 1 (1974), pp. 1007–1039.
- [MK] A. J. MAJDA AND P. R. KRAMER, *Simplified models for turbulent diffusion: theory, numerical modelling, and physical phenomena*, Phys. Rep., 314 (1999), pp. 237–574.
- [MS] A. J. MADJA AND P. SOUGADINIS, *The effect of turbulence on mixing in prototype reaction diffusion systems*, Comm. Pure Appl. Math., 53 (2000), pp. 1284–1304.

- [T] P. TURBIS, *Quenching and ignition effects in an idealized nonpremixed combustion model*, Ph.D. thesis (chap. 2), Université de Montréal (2010).
- [V] O. VOLKOV, *Validation des modèles de flammelettes instationnaires en combustion turbulente non-prémélangée*, thèse de doctorat, Université de Montréal (2005).

# Chapitre 4

---

## ESTIMATION D'ERREUR A POSTERIORI POUR LES MODÈLES DE FLAMMELETTE SOUS-MAILLE EN PRÉSENCE D'EXTINCTION ET DE RÉALLUMAGE

### RÉSUMÉ

Une stratégie d'estimation d'erreur, basée sur les résidus pondérés par une solution duale, est évaluée dans le contexte des erreurs de modélisation liées à l'utilisation de modèles de flammelette sous-maille fréquemment utilisés en combustion turbulente non prétrémpée. L'approche est mise en œuvre et validée pour un problème test idéalisé formé d'un système d'équations multiéchelles d'advection-diffusion-réaction avec possibilité d'extinction et de réallumage de la flamme. Pour ce problème, deux régimes stables de combustion sont possibles : un régime presque gelé, où la réaction est gelée en première approximation, et un régime près de l'équilibre, où une flamme mince sépare deux régions à l'équilibre chimique. Une simulation numérique détaillée simulant l'échelle réactive serait trop coûteuse, donc un modèle sous-maille est utilisé afin de tenir compte des effets réactifs aux grandes échelles. Nous comparons la performance d'un modèle de «flamme gelée» à grande échelle avec celle d'une classe de modèles sous-maille basés sur l'approximation asymptotique de flammelette. Cette approximation mène aux librairies de flammelettes, des relations précalculables entre les scalaires réactifs et les scalaires passifs appropriés. Des librairies similaires peuvent être construites

pour approximer les solutions duales. La stratégie d'estimation d'erreur, utilisée afin d'identifier le bon régime de combustion et de choisir le meilleur modèle dans ce régime, est validée en comparant les estimations avec les erreurs exactes pour des cas stationnaires. Entre autres, nous obtenons les bonnes tendances asymptotiques.

# A posteriori error estimation for subgrid flamelet models with quenching and ignition

ANNE BOURLIOUX, PASCAL TURBIS

## 4.1. ABSTRACT

A dual-weighted residual error estimation strategy is applied to the modeling error associated with a class of subgrid flamelet models widely used in nonpremixed turbulent combustion. The approach is implemented and validated for an idealized test problem consisting of a system of multiscale advection-reaction-diffusion equations with possible quenching and ignition. For this problem, two stable combustion regimes can exist: a nearly frozen regime where the reaction is frozen at first approximation, and a near-equilibrium regime where a thin flame separates chemical equilibrium regions. A fully resolved numerical simulation of the reaction scale in the near-equilibrium regime would be excessively demanding, so typically a subgrid model is used instead to account for its impact at large scales. We compare the performance of a large-scale frozen flow model with a class of subgrid models based on the asymptotic flamelet approximation, which leads to the so-called flamelet libraries, i.e., precomputed tables expressing the reactive scalars in terms of the appropriate passive scalar. Similar libraries can be constructed for the dual-based estimator. The ability of the estimation strategy to identify the right combustion regime and to select the best model within that regime is validated by comparison with exact results for steady-state cases. We also recover all asymptotic scalings for the modeling errors.

## 4.2. INTRODUCTION

Turbulent combustion simulations in the fast reaction regime are challenging multiscale problems because one needs to account for a very wide range of scales, from scales associated with turbulence down to the very small scales associated with thin flames. A direct numerical simulation approach, where one attempts to resolve all of these scales, would be prohibitively expensive for most realistic simulations. Instead, in large eddy simulations, only large scales are resolved and the

effect of small scales is modeled. For the type of nonpremixed flames considered here, a widespread model is based on the so-called flamelet approach. The procedure is described in more detail in section 4.3.2; only an outline is given here. The governing equations for the chemical species mass fractions are unsteady, multidimensional, advection-diffusion-reaction equations. In the asymptotic limit of thin flames (fast reaction), it is possible to reduce those equations to a steady, one-dimensional equation, where the solution is expressed in terms of an appropriate reaction progress variable. After proper nondimensionalization, the reduced equation can be made parameter-free, and its solution can be compiled once and for all as a *flamelet library*, i.e., a precomputed table of the nondimensionalized solution for the reactive scalars in terms of the reaction progress variable [P1]. This approach has been extensively used in the simulation of turbulent flames [CR1, JLRH], including their large eddy simulations [CR2]. There are several strategies to implement the asymptotic reduction of the original equations, and this leads to a hierarchy of models. To each model corresponds a modeling error, because the reactive scalars satisfy the flamelet equations instead of the original equations. Good estimates of the modeling errors are needed to select the best model in any given situation.

The flamelet approach described above is asymptotically valid in the near-equilibrium combustion regime. In the other stable regime, the reaction is nearly frozen, possibly leading to the quenching of the flame. Models in this regime, solely based on large-scale variables, capture small flame temperature departures from the frozen reaction temperature distribution. If the combustion regime is unknown a priori, parameters in the numerical simulations should be chosen as to resolve all small scales; this ensures that a near-equilibrium flame is fully resolved. However, this procedure is prohibitively expensive. To capture the correct scaling of the flame, one must solve a two-step modeling problem: identify the correct combustion regime, then choose a good model if more than one model applies in that regime.

In this paper, we investigate a dual-weighted residual strategy to estimate the modeling errors *a posteriori*, similarly to the approach that is often used to estimate discretization errors in mesh-adaptive algorithms. With a good modeling error estimator, one could design an effective strategy to select the appropriate combustion regime and model within a hierarchy so as to satisfy some error tolerance. Taken a step further, one could then combine this control with a discretization error control, so as to balance both sources of errors (see [BE1] for an example and [BE2] for an application to combustion simulations). A requirement for a viable strategy is that this *a posteriori* error analysis must be performed at a computational cost at most of the same order as the cost of using the model in the first place. This procedure is shown to be successful in the near-equilibrium regime without quenching [BET], where the approximation of the resulting multiscale dual solution is constructed from a *dual flamelet library* to ensure a reasonable computational cost.

The strategy is evaluated in the context of an idealized model for turbulent nonpremixed flames consisting of a system of advection-reaction-diffusion equations, as described in section 4.3. We also describe the nearly frozen and near-equilibrium combustion regimes, and large-scale models based on non-turbulent asymptotic behaviour for each regime, such as the asymptotic flamelet model. The dual-weighted residual approach to modeling error estimation introduced in [BE1] is summarized and developed for our models in section 4.4. This idealized model is sufficiently simple that systematic parametric studies are feasible and numerical errors can be completely controlled. The challenge here is not only to obtain the correct dual advection-reaction-diffusion equations, but to find suitable large-scale approximations in the drastically different regimes. We implement and validate our strategy to identify the best combustion regime and model with several numerical experiments. The good performance of the regime/model selection strategy is confirmed when applied to representative test cases, starting without advection effects in section 4.5. Asymptotic behavior of solutions in each regime are known, so the advection-less case makes the error estimation strategy easier to understand and tune to find a suitable error norm for later test-cases. The last

sections validate the procedure for turbulent test-cases, where exact asymptotics are not available, firstly for a steady simple shear flow (section 4.6), and then for the Childress–Soward flow, a mix of shear and eddies (section 4.7).

### 4.3. GOVERNING EQUATIONS

The idealized turbulent nonpremixed combustion model considered herein consists of a coupled system of advection-reaction-diffusion partial differential equations (PDEs) for the reactive scalars  $Y$  (fuel mass fraction),  $Y_2$  (oxidizer mass fraction), and  $T$  (nondimensional temperature):

$$\frac{\partial Y}{\partial t} + \text{Pe } \mathbf{v} \cdot \nabla Y = \Delta Y - \text{Da } YY_2 \exp(-E/T), \quad (4.3.1)$$

$$\frac{\partial Y_2}{\partial t} + \text{Pe } \mathbf{v} \cdot \nabla Y_2 = \Delta Y_2 - \text{Da } YY_2 \exp(-E/T), \quad (4.3.2)$$

$$\frac{\partial T}{\partial t} + \text{Pe } \mathbf{v} \cdot \nabla T = \Delta T + \text{Da } YY_2 \exp(-E/T). \quad (4.3.3)$$

The flow field  $\mathbf{v}$  is chosen to be bidimensional, incompressible, and biperiodic of period  $P$ . The Péclet number  $\text{Pe}$  characterizes the importance of advection compared to diffusion, and the Damköhler number  $\text{Da}$  the importance of reaction compared to diffusion. In the limit of large values of the activation energy  $E$  and  $\text{Da}$ , the reaction zone is very thin. Both  $T$  and  $E$  are made nondimensional using the values of the heat release per unit mass of fuel ( $Q$ ) and specific heat ( $c_p$ ). As long as  $E$  is large enough, multiple combustion regimes are possible in some areas of the Pe-Da parameter space  $[\mathbf{BT}, \mathbf{T}]$ .

A convenient strategy for solving (4.3.1)–(4.3.2) stems from the observation that the passive scalars  $Z = (Y - Y_2)/2$  and  $H = T + (Y + Y_2)/2$  obey the much simpler advection-diffusion equations

$$\frac{\partial Z}{\partial t} + \text{Pe } \mathbf{v} \cdot \nabla Z = \Delta Z, \quad (4.3.4)$$

$$\frac{\partial H}{\partial t} + \text{Pe } \mathbf{v} \cdot \nabla H = \Delta H. \quad (4.3.5)$$

The resulting equations no longer contains the nonlinear reaction term; therefore analysis and numerical simulations are much simpler for the passive scalars than for the reactive scalars. One can substitute these to (4.3.2)–(4.3.3), with (4.3.1)

for the reactive scalar written as

$$\frac{\partial Y}{\partial t} + \text{Pe } \mathbf{v} \cdot \nabla Y = \Delta Y - \text{Da } Y(Y - 2Z) \exp\left(\frac{-E}{H - Y + Z}\right). \quad (4.3.6)$$

We look for a solution for the passive scalar  $Z$  as a perturbation of a mean gradient in the  $x$ -direction, i.e.,  $Z(x, y, t) = x/L_G + Z_p(x, y, t)$ , where  $L_G$  is the length scale associated with the imposed mean gradient and  $Z_p$  is a periodic, zero-mean perturbation induced by the velocity field  $\mathbf{v}$ . We compute the steady-state solutions of (4.3.6) on  $\Omega = [-L, L] \times [0, P]$ , with boundary conditions  $Y = |Z| + Z$ ,  $Y_2 = |Z| - Z$  (chemical equilibrium), and  $T = T_\infty$  on  $\{-L, L\} \times [0, P]$ ; we also enforce periodicity of all scalars in the  $y$ -direction. The boundary conditions on the passive scalar  $H$  are obtained by using its definition and the boundary conditions on the reactive scalars.

Unless otherwise mentioned, the values  $L_G = 10$ ,  $T_\infty = 1$ ,  $L = 40$  and  $E = 15$  will be used throughout the next sections. The test cases are set up so that three distinct scales exist in the problem: the large scale  $L_G$ , the intermediate scale  $P$  due to the flow field, and the very thin flame thickness. The presence of this last very small scale in the solution for the reactive scalar is a computational challenge. Equation (4.3.4) has been studied exhaustively to analyze the performance of a very wide class of turbulence models [**BM2, MK**]. The particular setup for the passive scalar allows for a direct link with homogenization theory predictions. For  $E = 0$ , the analysis was extended to the reactive case to study the performance of a hierarchy of flamelet models for both steady and unsteady cases [**BM1, V**]. For a nonzero activation energy, this system of equations was presented in [**MS**] and further analyzed in [**BT**], where a model hierarchy in the near-equilibrium regime was established.

#### 4.3.1. The stable combustion regimes

If the activation energy is large enough, multiple combustion regimes exist, leading to the well-known S-shaped curve, a plot of the maximum flame temperature as a function of Da, shown in Figure 4.1. We will focus on the two stable regimes: the nearly frozen regime, which covers the lower branch and bend of the S-shaped curve, and the near-equilibrium regime, which covers the upper branch

and bend of the S-shaped curve. The unstable middle branch cannot be computed and is crudely approximated to link the upper and lower branches.

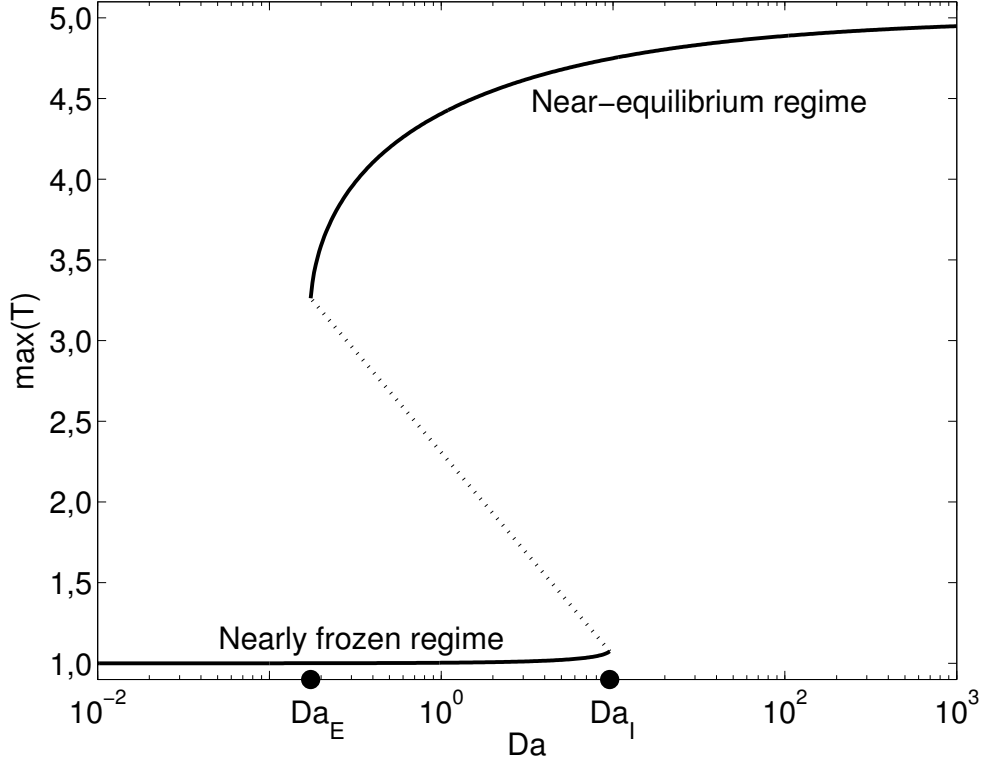


FIGURE 4.1. S-shaped curve—plot of the maximum flame temperature against  $\text{Da}$  for  $\text{Pe} = 0$ . Critical quenching and ignition parameters  $\text{Da}_E$  and  $\text{Da}_I$  are also shown.

In the nearly frozen regime, the temperature is first approximated by  $T_\infty$  everywhere in  $\Omega$ , corresponding to a frozen chemical reaction. To account for chemical effects, small departures from this temperature value are expected. The reaction term is also responsible for ignition effects. The ignition Damköhler number  $\text{Da}_I$  characterizes this switch from the existence of multiple solutions to a single near-equilibrium solution. Typical profiles for the reactive scalars in this regime are presented in Figure 4.2 for  $\text{Pe} = 0$  and  $\text{Da} = 1$ . Throughout this paper, we will use the frozen flow approximation  $T = T_\infty$  on  $\Omega$  as our model in the nearly frozen regime. Using the passive scalar definitions, this corresponds to  $Y = Y_{ff} = H - T_\infty + Z$ .

In the near-equilibrium regime, flames are made of a thin burning region, separated two equilibrium regions. The flame temperature is close to the equilibrium

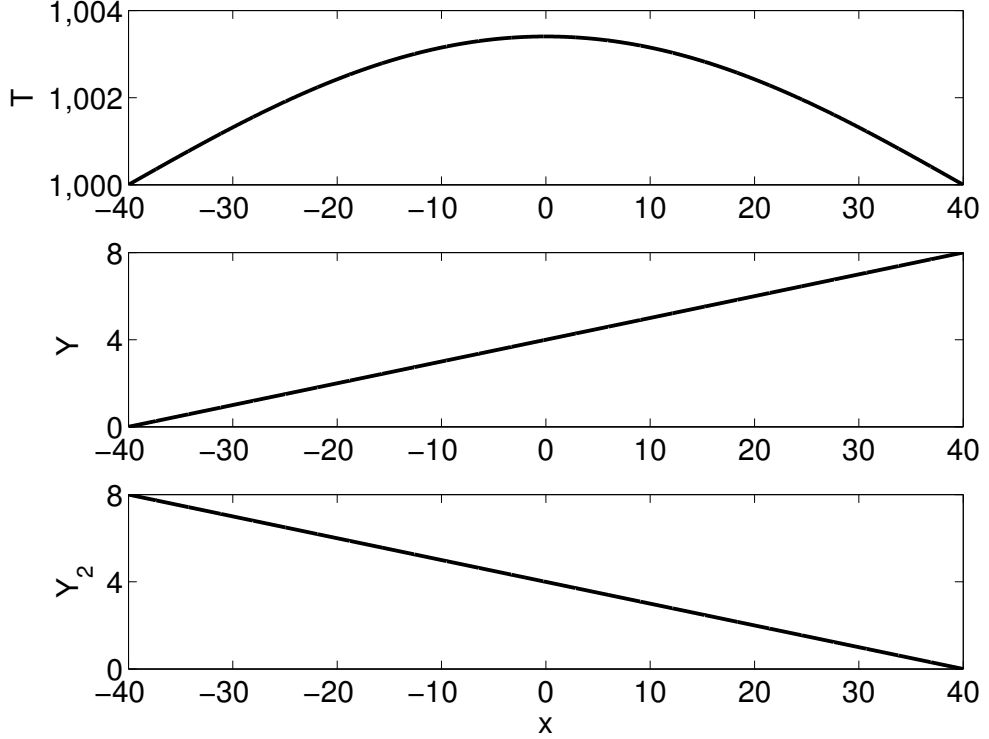


FIGURE 4.2. Typical profiles for  $T$ ,  $Y$ , and  $Y_2$  in the nearly frozen regime ( $\text{Da} = 1$ ,  $\text{Pe} = 0$ ).

value  $H$ , and small deviations are expected. The nonlinearity of the reaction term is responsible for the existence of quenching. The extinction Damköhler number  $\text{Da}_E$  characterizes the switch from the existence of multiple solutions to a single nearly frozen solution. Typical profiles for  $T$ ,  $Y$ , and  $Y_2$  in this regime are shown in Figure 4.3 for the values  $\text{Pe} = 0$  and  $\text{Da} = 100$ . Flamelet models are used to approximate the solution  $Y$  of (4.3.6) in the near-equilibrium regime, and are described in the next sections.

#### 4.3.2. The asymptotic flamelet subgrid model strategy

The flamelet subgrid modeling strategy used in the near-equilibrium regime is reviewed here. The objective is to predict the solution  $\bar{Y}$  of the equation for the reactive scalar defined as

$$\bar{Y} = \int Y(x, y) dx dy, \quad (4.3.7)$$

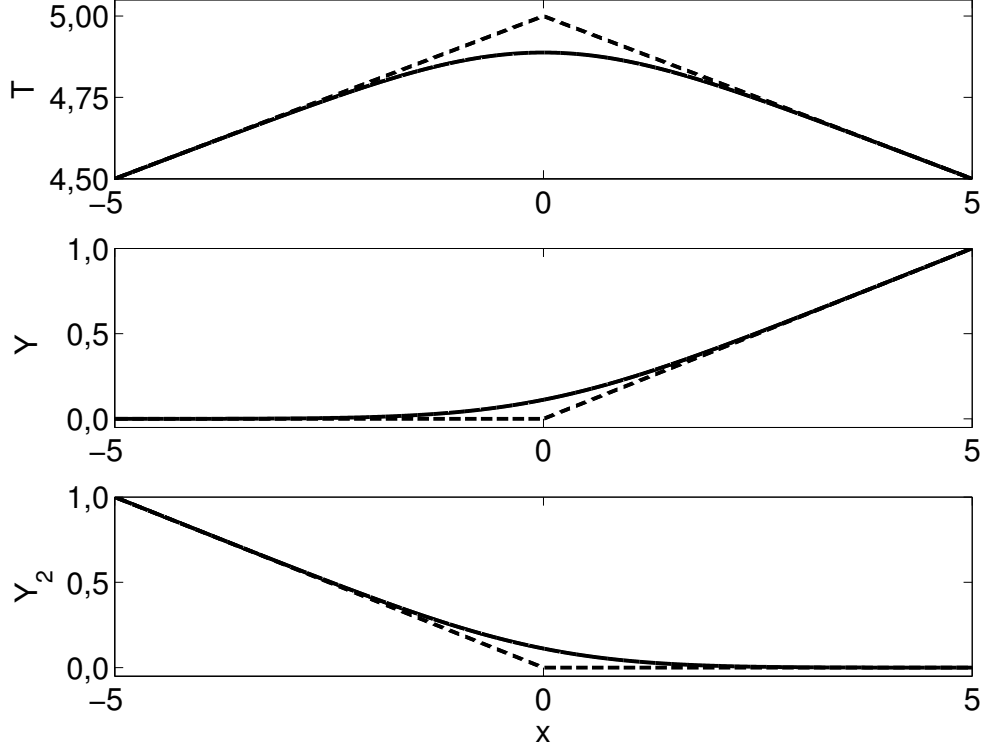


FIGURE 4.3. Typical profiles for  $T$ ,  $Y$ , and  $Y_2$  in the near-equilibrium regime ( $\text{Da} = 100$ ,  $\text{Pe} = 0$ ) around the flame location.  
 Full line: exact solutions, dashed line: equilibrium solutions.

with the integration performed over elements of the large-scale mesh. For nonreactive variables, the filtered solution can be obtained as the solution of the filtered governing equation. If the equation is nonlinear to begin with, filtering leads to terms which can no longer be expressed solely as functions of the filtered variables and subgrid models are needed to express those unclosed terms as functions of the large-scale variables only. In the case of nonlinear reaction terms, there is no known strategy to formulate such a closure model at the level of the governing equation. Instead, in the flamelet regime,  $\bar{Y}$  is approximated by

$$\bar{Y} = \int Y(Z, H) \text{ PDF}(Z, H) dZ dH. \quad (4.3.8)$$

This approximation is based on the following assumptions:

- (1) The resolved reactive scalar  $Y$  can be expressed as a function of the passive scalars  $Z$  and  $H$  (and other statistics, depending on the model).

- (2) The joint probability distribution function of  $Z$  and  $H$ ,  $\text{PDF}(Z, H)$ , is known or can be modeled.

Assumption 2 is plausible because the passive scalars satisfy much simpler equations (with no reaction term). Assumption 1 is the source of the modeling error that is investigated in this paper. Notice that the frozen flow model follows the same overall strategy, since we can write  $Y_{ff} = Y_{ff}(Z, H)$ .

#### 4.3.3. Flamelet models for $\text{Pe} = 0$

For  $\text{Pe} = 0$  and  $E = 0$ , it is easy to express  $Y$  as function of  $Z$  solely. Indeed,  $Z_p = 0$  since  $Z = x/L_G$  solves (4.3.4). With a change of variables from  $x$  to  $Z$ , we rewrite (4.3.6) as the ordinary differential equation (ODE)

$$\frac{d^2Y}{dZ^2} = \text{Da} L_G^2 Y (Y - 2Z). \quad (4.3.9)$$

Let  $\alpha = (\text{Da} L_G^2)^{1/3}$  (Damköhler group). Substitution of the normalized variables  $\widehat{Z} = \alpha Z$  and  $\widehat{Y} = \alpha Y$  in (4.3.9) leads to the parameter-free equation

$$\frac{d^2\widehat{Y}}{d\widehat{Z}^2} = \widehat{Y} (\widehat{Y} - 2\widehat{Z}). \quad (4.3.10)$$

The solution of this equation can be computed once and for all and stored in a *flamelet library*. Figure 4.4 displays the flamelet solution in terms of the normalized correction to equilibrium  $d\widehat{Y}(\widehat{Z}) = \widehat{Y} - (\widehat{Z} + |\widehat{Z}|)$ .

For  $E \neq 0$ ,  $H = T_\infty + L/L_G$  solves (4.3.5), and  $Y$  solves

$$\frac{d^2Y}{dZ^2} = \text{Da} L_G^2 Y (Y - 2Z) \exp\left(\frac{-E}{H - Y + Z}\right). \quad (4.3.11)$$

It is impossible to reduce the previous four-parameter equation (for  $L_G$ ,  $\text{Da}$ ,  $H$ , and  $E$ ) to an equation with less than three parameters. However, it was shown in [BT] that the solution of (4.3.11) can be approximated using the asymptotic relations in the near-equilibrium regime, leading to a normalized parameter-free equation and one normalization parameter.

Let  $\alpha = [\text{Da} L_G^2 \exp(-E/H)]^{1/3}$ . In the limit  $\alpha \rightarrow +\infty$ , it has been shown that the solutions of (4.3.11) converge, in  $L^2$ -norm, to the solution of (4.3.9) [BT]. Unlike the  $E = 0$  case, where the flamelet solution

$$Y_{fl} = \alpha^{-1} \widehat{Y}(\alpha Z), \quad (4.3.12)$$

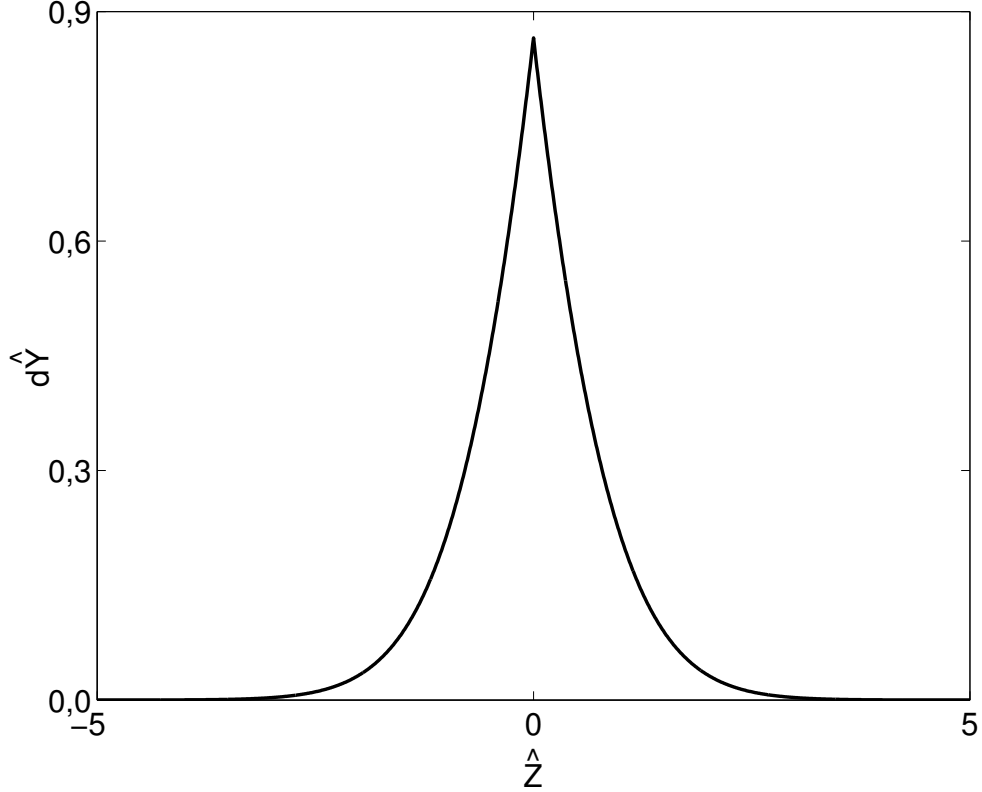


FIGURE 4.4. Flamelet library—correction term  $d\hat{Y}(\hat{Z}) = \hat{Y} - (\hat{Z} + |\hat{Z}|)$ .

is a solution of (4.3.9), modeling errors are not equal to zero when  $E \neq 0$ . However, these errors are not significant when compared to the errors obtained for  $\text{Pe} \neq 0$  in the near-equilibrium regime [BT].

#### 4.3.4. Flamelet models for $\text{Pe} \neq 0$

For  $\text{Pe} \neq 0$ , one would also like to express  $Y$  as a function of  $Z$  and  $H$  using the flamelet library previously defined. This would therefore reduce the computational cost of the problem from that of solving the bidimensional PDE (4.3.6) down to computing—once—the solution of the ODE (4.3.10) in terms of  $\hat{Z}$  and solving the much simpler passive scalar PDEs (4.3.4)–(4.3.5). Two levels of approximations are used to obtain the solution  $Y$  for  $\text{Pe} \neq 0$ . The first level of approximation consists of assuming that  $Y$  can be expressed as a flamelet from a library, obtained as the solution for  $\text{Pe} = 0$ . The second level of approximation is that this  $\text{Pe} = 0$  solution is obtained from a flamelet solution with  $E = 0$ .

Let  $\chi_{ld} = |\nabla Z|^2$  be the local dissipation. For  $\text{Pe} = 0$ ,  $\chi_{ld} = 1/L_G^2$  and one can rewrite the Damköhler group as  $\alpha = [\text{Da}/\chi_{ld} \exp(-E/H)]^{1/3}$ . In practical applications, the exact value of the local dissipation is not always available. Instead, one might have access only to its mean value  $\langle \chi_{ld} \rangle$ , where  $\langle \cdot \rangle$  denotes space-averaging. In this paper, we will study two flamelet models, whose solutions are given by (4.3.12), with

$$\alpha = \begin{cases} [\text{Da}\chi_{ld}^{-1} \exp(-E/H)]^{1/3} & \text{(local dissipation model)} \\ [\text{Da}\langle \chi_{ld} \rangle^{-1} \exp(-E/H_0)]^{1/3} & \text{(mean dissipation model)} \end{cases} \quad (4.3.13)$$

and  $H_0$ , the value of  $H$  on the stoichiometric level  $Z = 0$ . As in the  $E = 0$  case, the mean dissipation model uses a single value of  $\alpha$  on  $\Omega$  [BM1, V].

The flamelet approach just described can be summarized as follows:

- (1) Compute, once and for all, the flamelet library using (4.3.10). This yields the function  $\widehat{Y}$ , that is, a way of modeling the reactive scalar  $Y$  as a function of the passive scalars  $Z$  and  $H$ .
- (2) Compute the passive scalars  $Z$  and  $H$  using (4.3.4)–(4.3.5). These equations are independent of Da and can be solved on a grid as coarse as the flow field allows.
- (3) Compute the dissipation  $\chi$  used in the model.
- (4) Use (4.3.12)–(4.3.13) to get an approximate solution  $Y_{fl}$  to the solution  $Y$  of (4.3.6).
- (5) Integrate  $Y_{fl}(Z, H, \chi)$  following (4.3.8) to estimate statistics of  $Y$ . To do so, we need  $\text{PDF}(Z, H, \chi)$ , the joint probability density function of both passive scalars and the dissipation.

At the end of the process, we obtain a coarse-grid solution taking small-scale features into account. For all choices of the dissipation considered here, the flamelet approximation is asymptotically valid in the near-equilibrium combustion regime for large Da [BM1, T]. Out of this validity zone, modeling errors can become significant; model and regime selections become crucial. One can accomplish this

using a modeling error estimator and choosing the model (and corresponding regime of application) giving the smallest error. This approach will be investigated in the following sections of the paper.

#### 4.4. MODELING ERROR ESTIMATION

Duality arguments have been used extensively to estimate a posteriori discretization errors in numerical solutions of PDEs, for example, for finite elements [AO, BR, EJ] and finite differences [AN]. Another application is parameter identification, where an example in the context of combustion models can be found in [BBV]. A more recent application is the estimation of modeling errors [ACS, BE1, ROV], where the objective now is to efficiently assess the errors that result from the approximation of the solution of a complex equation by the solution of a simpler model equation, which can be solved at a much lesser cost.

##### 4.4.1. The dual-weighted residual estimator for nonlinear equations

In this section, we summarize the approach introduced in [BE1] for general PDEs. In the next subsections, we specialize this strategy for a specific set of PDEs and models by extending the results found in [BET] to the  $E \neq 0$  case.

The objective is to solve the following PDE, from now on referred to as the primal equation, written in weak form as

$$\text{Find } Y \in V \text{ such that } a(Y)(\varphi) + d(Y)(\varphi) = (f, \varphi) \quad \forall \varphi \in V. \quad (4.4.1)$$

The forms  $a, d : V \times V \rightarrow \mathbb{R}$  are linear in their second argument;  $V$  is an appropriate Hilbert space. Suppose that for computational efficiency reasons, one instead solves the reduced primal equation obtained by neglecting the form  $d$  in (4.4.1):

$$\text{Find } Y_m \in V \text{ such that } a(Y_m)(\varphi) = (f, \varphi) \quad \forall \varphi \in V. \quad (4.4.2)$$

The impact of using the reduced primal solution  $Y_m$  in place of the primal solution  $Y$  is evaluated in terms of a given linear output functional  $j : V \rightarrow \mathbb{R}$ . The modeling error to be estimated is  $j(Y) - j(Y_m)$ . The first step in the estimation

strategy is to consider the dual equation corresponding to  $j$ :

$$\text{Find } q \in V \text{ such that } a'(Y)(\psi, q) + d'(Y)(\psi, q) = j'(Y)(\psi) \quad \forall \psi \in V, \quad (4.4.3)$$

where  $a'(Y)(v, \varphi) = \lim_{\varepsilon \rightarrow 0} \frac{a(Y + \varepsilon v)(\varphi) - a(Y)(\varphi)}{\varepsilon}$  is the directional derivative of  $a$  at  $Y$  in the  $v$ -direction ( $d'(Y)(v, \varphi)$  and  $j'(Y)(v)$  are defined similarly). A reduced dual equation approximating (4.4.3) is obtained by ignoring the form  $d'$  and replacing  $Y$  by its approximation  $Y_m$ :

$$\text{Find } q_m \in V \text{ such that } a'(Y_m)(\psi, q_m) = j'(Y_m)(\psi) \quad \forall \psi \in V. \quad (4.4.4)$$

Braack and Ern have shown that  $j(Y) - j(Y_m) \approx -d(Y_m)(q_m)$  to first order in  $\|d\|$  [BE1].

#### 4.4.2. The dual flamelet library

We now apply the general framework to the mean dissipation flamelet model. The primal equation consists of solving (4.3.6) for  $Y$ . The reduced primal equation is obtained by differentiating (4.3.12) to obtain a PDE for the approximate solution  $Y_{fl}$ :

$$\text{Pe} \mathbf{v} \cdot \nabla Y_{fl} - \Delta Y_{fl} + \text{Da} Y_{fl} (Y_{fl} - 2Z) \exp \left( \frac{-E}{H_0} \right) \frac{\chi_{ld}}{\langle \chi_{ld} \rangle} = 0. \quad (4.4.5)$$

Thus, we obtain the forms

$$a(Y)(\varphi) = \quad (4.4.6)$$

$$\int_{\Omega} \left\{ (-\text{Pe} \mathbf{v} \cdot \nabla \varphi) Y + \nabla Y \cdot \nabla \varphi + \text{Da} Y (Y - 2Z) \exp \left( \frac{-E}{H_0} \right) \frac{\chi_{ld}}{\langle \chi_{ld} \rangle} \varphi \right\} dx dy,$$

$$d(Y)(\varphi) = \quad (4.4.7)$$

$$\int_{\Omega} \text{Da} Y (Y - 2Z) \left\{ \exp \left( \frac{-E}{H - Y + Z} \right) - \exp \left( \frac{-E}{H_0} \right) \frac{\chi_{ld}}{\langle \chi_{ld} \rangle} \right\} \varphi dx dy,$$

with the space  $V = \{f \in H^1(\Omega) \mid f(x, 0) = f(x, P) \quad \forall x \in [-L, L], f(\pm L, y) = 0 \quad \forall y \in [0, P]\}$ . Note that  $Y \notin V$ , but one can write  $Y = Y_0 + Z + |Z|$ , where  $Y_0 \in V$ ; this also applies to  $Y_{fl}$ .

Consider the output functional

$$j(Y) = \int_{\Omega} Y(x, y) dx dy. \quad (4.4.8)$$

This leads to the following expressions to be plugged into the dual and reduced dual equations (4.4.3)–(4.4.4):

$$a'(Y)(\psi, q) = \quad (4.4.9)$$

$$\int_{\Omega} \left\{ (-\text{Pe} \mathbf{v} \cdot \nabla q) \psi + \nabla \psi \cdot \nabla q + 2\text{Da} (Y - Z) \exp\left(\frac{-E}{H_0}\right) \frac{\chi_{ld}}{\langle \chi_{ld} \rangle} \varphi \right\} dx dy,$$

$$\begin{aligned} d'(Y)(\psi, q) &= \int_{\Omega} \text{Da} \left\{ \exp\left(\frac{-E}{H - Y + Z}\right) \left[ 2(Y - Z) - \frac{EY(Y - 2Z)}{(H - Y + Z)^2} \right] \right. \\ &\quad \left. + 2(Y - Z) \exp\left(\frac{-E}{H_0}\right) \frac{\chi_{ld}}{\langle \chi_{ld} \rangle} \right\} \psi dx dy, \end{aligned} \quad (4.4.10)$$

$$j'(Y)(\psi) = \int_{\Omega} \psi dx dy. \quad (4.4.11)$$

The modeling error can be approximated using

$$j(Y) - j(Y_{fl}) \approx \quad (4.4.12)$$

$$-\underbrace{\int_{\Omega} \text{Da} Y_{fl} (Y_{fl} - 2Z) \left\{ \exp\left(\frac{-E}{H - Y_{fl} + Z}\right) - \exp\left(\frac{-E}{H_0}\right) \frac{\chi_{ld}}{\langle \chi_{ld} \rangle} \right\} q_{fl} dx dy}_{\text{residual}}$$

where  $q_{fl}$  is the reduced dual solution for the flamelet model. The residual is solely a function of the passive scalars ( $Z, H$ ) and of the dissipation  $\chi_{ld}$ . If we can write  $q_{fl}$  as a function of the same variables, then

$$j(Y) - j(Y_{fl}) \approx \int_{\Omega} f(Z, H, \chi_{ld}) \text{ PDF}(Z, H, \chi_{ld}) dZ dH d\chi_{ld} \quad (4.4.13)$$

for a some function  $f$ , and the modeling error estimator would also therefore follow the general flamelet methodology.

If we assume  $q$  and  $q_{fl}$  are sufficiently differentiable, then they solve

$$-\text{Pe} \mathbf{v} \cdot \nabla q - \Delta q + \text{Da} \exp\left(\frac{-E}{H - Y + Z}\right) \left\{ 2(Y - Z) - \frac{EY(Y - 2Z)}{(H - Y + Z)^2} \right\} q = 1 \quad (4.4.14)$$

and

$$-\text{Pe} \mathbf{v} \cdot \nabla q_{fl} - \Delta q_{fl} + 2\text{Da} (Y_{fl} - Z) \exp\left(\frac{-E}{H_0}\right) \frac{\chi_{ld}}{\langle \chi_{ld} \rangle} q_{fl} = 1, \quad (4.4.15)$$

respectively, in  $\Omega$ . We will show in section 4.6 (Figure 4.11) that using the dual solution  $q$  in the error estimator, i.e., computing  $-d(Y_{fl})(q)$ , leads to excellent results. However, it is not desirable to solve (4.4.14) or even (4.4.15) numerically,

since the PDEs are multiscale problems; for large Da, the solutions have fine-scale features, and a very fine mesh is required for accuracy, making the estimation strategy an order of magnitude more expensive than the modeling strategy to which it is applied. For the modeling error estimation strategy to be useful, one must find a way to solve (4.4.15) at a cost at most that of the flamelet approximation. To approximate its solution, one goes back to the  $\text{Pe} = E = 0$  case, where (4.4.14)–(4.4.15) reduce to

$$-\frac{1}{L_G^2} \frac{d^2 q}{dZ^2} + 2 \text{Da} (Y - Z) q = 1. \quad (4.4.16)$$

Let  $\hat{q} = \text{Da}^{2/3} L_G^{-2/3} q$ . Using the previous normalizations for  $Y$  and  $Z$ , one obtains

$$-\frac{d^2 \hat{q}}{d\hat{Z}^2} + 2 (\hat{Y} - \hat{Z}) \hat{q} = 1. \quad (4.4.17)$$

As for the flamelet approximation, one can compute the solution of (4.4.17) once and for all and store it into a *dual flamelet library*; see Figure 4.5.

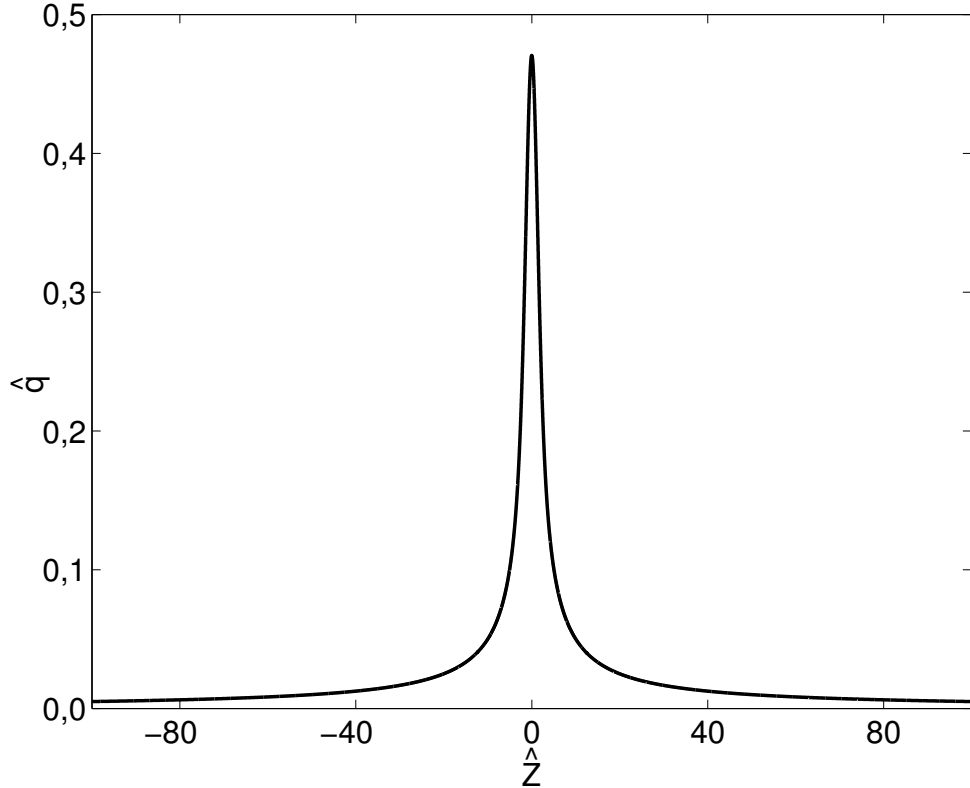


FIGURE 4.5. Dual flamelet library for  $j(Y) = \int_{\Omega} Y(x, y) dx dy$ .

As it was done previously for the flamelet approximation itself, we extend the  $q_{fl}$  normalization to the  $\text{Pe} \neq 0$  cases by defining

$$q_{fl} = \alpha_2^{-1} \hat{q}(\alpha Z), \quad (4.4.18)$$

with

$$\alpha_2 = \begin{cases} [\text{Da} \sqrt{\chi_{ld}} \exp(-E/H)]^{2/3} & \text{(local dissipation model)} \\ [\text{Da} \sqrt{\langle \chi_{ld} \rangle} \exp(-E/H_0)]^{2/3} & \text{(mean dissipation model)} \end{cases}. \quad (4.4.19)$$

For  $\text{Pe} = 0$ , Figure 4.6 shows that the dual flamelet solution  $q_{fl}$  defined above converges, in  $L^2$ -norm, to the dual solution  $q$  of (4.4.14) as  $\alpha_2 \rightarrow +\infty$ . The convergence is of order  $O(\alpha_2^{-3/2})$ , since we integrate the local error on  $q$  of order  $O(\alpha_2^{-1})$  on a reaction zone of order  $O(\alpha^{-1}) = O(\alpha_2^{-1/2})$  in size. This dual flamelet library provides a good approximation to the solutions of (4.4.14)–(4.4.15) at least if the Damköhler number is large enough, while controlling the computational cost of the error estimator. In Appendix A, we obtain the same dual library by supposing that the relation  $q_{fl} = q_{fl}(Z)$  holds, plugging this expression into (4.4.15), and making a few key approximations. In the near-equilibrium regime, the relation between  $q_{fl}$  and  $Z$  is exact for  $\text{Pe} = 0$ . However, when  $\text{Pe} \neq 0$ , the form of the advection term (the factor  $-\text{Pe}$ ) and the reactive term in (4.4.14)–(4.4.15) suggest that  $q_{fl} = q_{fl}(Z, Z_d)$ , where  $Z_d$  is a dual passive scalar solving

$$-\text{Pe} \mathbf{v} \cdot \nabla Z_d = \Delta Z_d \quad (4.4.20)$$

in the steady-state cases we are studying here. To make the error estimation strategy cost effective, we limit ourselves to the  $q_{fl} = q_{fl}(Z)$  case here. We will show below that the numerical results support this approximation.

#### 4.4.3. Estimating the modeling error in the nearly frozen regime

The passive scalars  $Z$  and  $H$  solve (4.3.4) and (4.3.5), respectively. Therefore, it is easy to show that the frozen flow model  $Y_{ff} = H - T_\infty + Z$  solves

$$\text{Pe} \mathbf{v} \cdot \nabla Y_{ff} - \Delta Y_{ff} = 0. \quad (4.4.21)$$

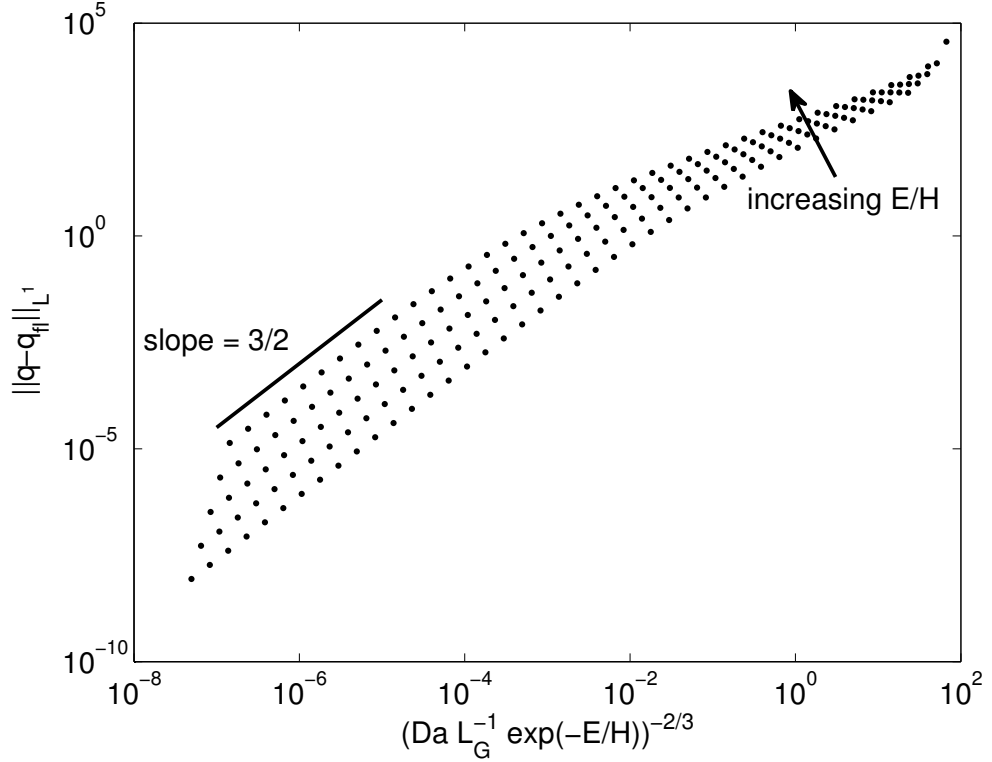


FIGURE 4.6. Convergence of the dual flamelet library solution  $q_{ff}$  to the solution  $q$  of (4.4.14) for  $\text{Pe} = 0$ .

If we repeat the same steps to find the forms  $a$  and  $d$  for this model as we did for the mean dissipation model, we find that

$$j(Y) - j(Y_{ff}) \approx - \underbrace{\int_{\Omega} \text{Da} [(H - T_{\infty})^2 - Z^2] \exp\left(\frac{-E}{T_{\infty}}\right) q_{ff} dx dy}_{\text{residual}}, \quad (4.4.22)$$

where, assuming sufficient differentiability, the reduced dual solution  $q_{ff}$  for the frozen flow model solves

$$-\text{Pe} \mathbf{v} \cdot \nabla q_{ff} - \Delta q_{ff} = 1. \quad (4.4.23)$$

The previous PDE is independent of  $\text{Da}$ , therefore the solution  $q_{ff}$  can be computed on a coarse-grid domain, similar to the one used to compute the passive scalars. Similarly to the near-equilibrium regime, the residual is a function of the passive scalars  $Z$  and  $H$ . However,  $q_{ff}$  is clearly not a function of  $Z$ , but rather a function of the dual passive scalar  $Z_d$ . We can write the modeling error estimator

in the nearly frozen regime as

$$j(Y) - j(Y_{ff}) \approx \int_{\Omega} g(Z, Z_d, H) \text{ PDF}(Z, Z_d, H) dZ dZ_d dH, \quad (4.4.24)$$

where  $g$  is the product of the residual and the reduced dual solution  $q_{ff}$ . As in the near-equilibrium regime, the flamelet methodology holds for the modeling error estimator.

#### 4.5. APPLICATION TO THE $\text{Pe} = 0$ CASE

In this section, we investigate the modeling errors for  $\text{Pe} = 0$ . There is no explicit solution for the reactive scalar  $Y$ . In the limit of infinite Da,  $Y$  converges to the equilibrium solution  $Y_{eq} = Z + |Z|$ , obtained as the solution for which the reaction rate  $\omega = \text{Da} Y(Y - 2Z)$  is a delta function centered around  $Z = 0$ ; at large but finite Da, the departure from  $Y_{eq}$  is expected to be small. It is fairly straightforward to compute it numerically with arbitrary accuracy [BM1]. We validate the error estimator by comparing the predictions with exact values for the modeling errors. The reference solution  $Y$  of (4.3.6) is obtained numerically by using Newton's method and centered finite differences. Convergence is very fast if one uses the frozen flow and flamelet models as initial guesses [BM1]. A very fine mesh is used so that discretization errors are very small compared to modeling errors.

We generate the model solutions  $Y_{ff}$  and  $Y_{fl}$  independently of the reference solution  $Y$ , then compute the exact modeling errors in the desired norm. Using  $Y_{ff}$  and  $Y_{fl}$ , we use the error estimator to obtain approximations of the exact errors for a wide range of values of the parameters. Exact and estimated errors for the output functional  $j(Y) = \int_{-L}^L Y dx = L_G \int_{-L/L_G}^{L/L_G} Y dZ$  are shown on the left side of Figure 4.7. The two models investigated here are the frozen flow model  $Y_{ff} = H - T_{\infty} + Z$  (equivalent to  $T = T_{\infty}$  everywhere) and the flamelet model. Note that both mean and local dissipation flamelet models coincide when  $\text{Pe} = 0$ . The error curves for each model are only shown for their respective S-shaped curve branches. As  $\text{Da} \rightarrow 0$ , the estimated and error curves for the frozen flow model are almost identical, and the estimator slightly underestimates the exact error as

$\text{Da}$  gets closer to  $\text{Da}_I$ . As  $\text{Da} \rightarrow +\infty$ , the agreement between error curves for the flamelet model becomes better; away from this region, the error is underestimated by less than one order of magnitude.

To quantify the asymptotic trends of the errors for each model, we compute the asymptotic slope of the error curves from Figure 4.7. As  $\text{Da} \rightarrow 0$ , the numerical trend corresponds to  $j(Y) - j(Y_{ff}) = O(\text{Da}^1)$ . This is expected from looking at equation (4.4.22), and this trend is in perfect agreement with the asymptotic analysis performed in [T] for that regime. As  $\text{Da} \rightarrow +\infty$ , the numerical trend corresponds to  $j(Y) - j(Y_{fl}) = O(\text{Da}^{-1})$  in the near-equilibrium regime. Again, this agrees with the asymptotic prediction, where the local error on  $Y$  is of order  $O(\text{Da}^{-2/3})$  [BM1, T], integrated over a reaction zone of size  $O(\text{Da}^{-1/3})$ .

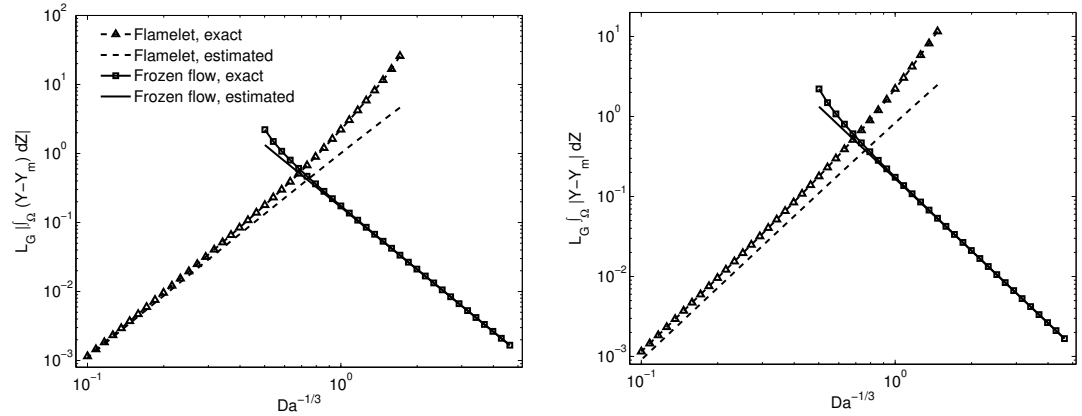


FIGURE 4.7.  $\text{Pe} = 0$  case—estimated and exact errors as functions of  $\text{Da}^{-1/3}$  for the output functionals  $j(Y) = L_G \int_Z Y dZ$  (left) and  $j(Y, Z_0) = Y(Z_0)$  (right;  $\int_Z |j(Y, Z) - j(Y_m, Z)| dZ$  is shown).

Furthermore, we can use the error estimator to predict which combustion regime is appropriate when multiple flame solutions exist. To do so, we look at the crossover value of  $\text{Da}$  for which the error curves intersect. The intersection point for the estimated error curves is located at  $\text{Da} = 2,2620$ , which is very close to 2,9320, the value of  $\text{Da}$  at which the exact error curves for both models intersect. Both points are located between  $\text{Da}_E = 1,74 \times 10^{-1}$  and  $\text{Da}_I = 9,55 \times 10^0$ . For  $\text{Da} < \text{Da}_E$  and  $\text{Da} > \text{Da}_I$ , only one regime exists. Based on the error estimator, we correctly identify that the frozen flow model is the best option in the nearly frozen

regime, and that the flamelet model is better in the near-equilibrium regime. In the  $\text{Da}_I < \text{Da} < \text{Da}_E$  region, where both stable regimes are possible, we would arbitrarily choose the nearly frozen regime for  $\text{Da} < \text{Da}^*$  and the near-equilibrium for  $\text{Da} > \text{Da}^*$ . This leads to a degenerate approximation to the S-shaped curve according to the error estimator; both the exact and approximated curves are shown in Figure 4.8.

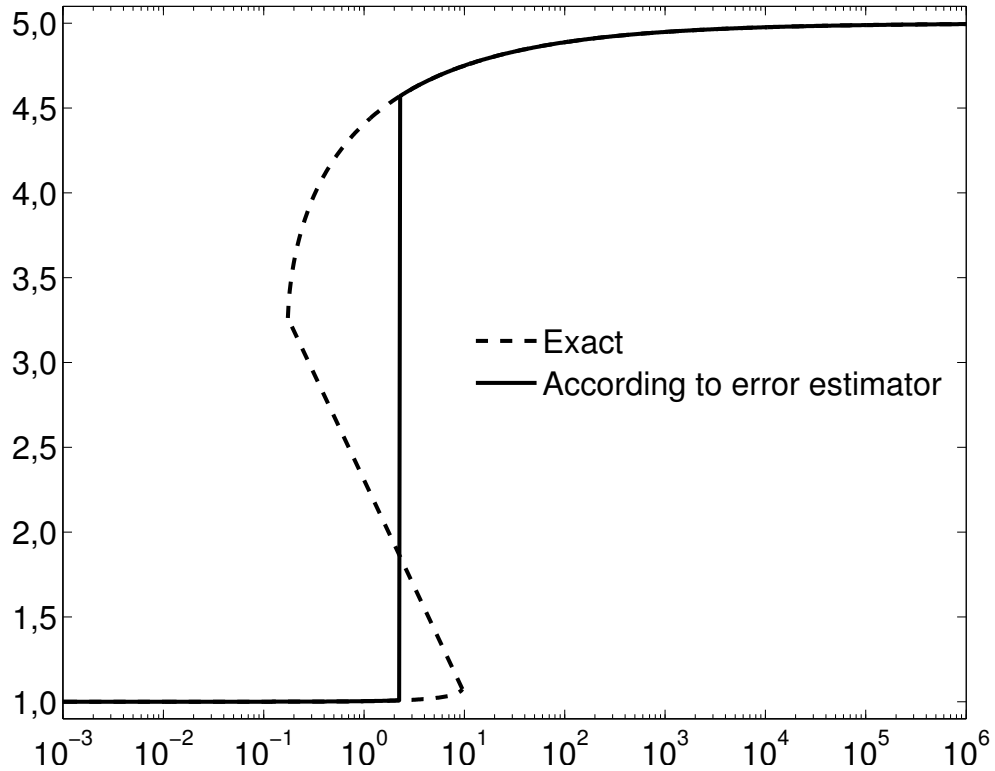


FIGURE 4.8.  $\text{Pe} = 0$  case—S-shaped curves, according to direct numerical simulation data (dashed line) and error estimator (full line).

We can also compute  $L^1$ -norm errors for  $Y$ . This procedure will be useful for  $\text{Pe} \neq 0$  when numerical cancellation appears for some choices of  $j$ . To begin, note that  $T \geq T_\infty$  is equivalent to saying that  $Y \geq Y_{ff}$  on  $\Omega$  by using the passive scalar definitions. Therefore,

$$\int_Z |Y - Y_{ff}| \, dZ = \int_Z (Y - Y_{ff}) \, dZ \quad (4.5.1)$$

and we can use

$$j(Y) = \int_x Y \, dx = L_G \int_Z Y \, dZ \quad (4.5.2)$$

as before to compute the  $L^1$ -norm error in the nearly frozen regime. To estimate the modeling error on  $Y$  for the flamelet solution, we use

$$j(Y, x_0) = Y(x_0) = Y(L_G Z_0) \quad (4.5.3)$$

as the output functional to estimate the  $L^1$ -norm error on  $Y$

$$\int_Z |Y - Y_{fl}| \, dZ = \int_Z |j(Y, Z) - j(Y_{fl}, Z)| \, dZ. \quad (4.5.4)$$

It would be impractical to compute a dual solution for each value of  $Z_0$ , as the error estimation procedure would be very costly compared to the cost of generating the flamelet in the first place. To address this concern, we propose the following methodology:

- (1) Compute, once and for all for each value of  $\widehat{Z}_0$ , the value  $\widehat{q}(\widehat{Z}_0)$ , where  $\widehat{q}$  solves

$$-\frac{d^2\widehat{q}}{d\widehat{Z}^2} + 2(\widehat{Y} - \widehat{Z})\widehat{q} = \delta(\widehat{Z} - \widehat{Z}_0). \quad (4.5.5)$$

This gives a dual flamelet library in terms of  $\widehat{Z}_0$  for the local error.

- (2) Use this new dual flamelet library in the error estimation procedure.

If we instead computed the dual solution for each value of  $\widehat{Z}_0$ , we would have to integrate the dual-weighted residual over  $\Omega$ , which does not have the same Da scaling as using the local value of  $q_{fl}$  at  $Z = \alpha\widehat{Z}_0$ , due to the extra integration step over the size of the reaction zone of order  $O(Da^{-1/3})$ . It turns out that the value of  $\alpha_2$  defined in (4.4.19) is also valid for this choice of output functional, and leads to good asymptotic behavior; more details are given in Appendix B. Equation (4.5.5) is solved using centered finite differences, replacing the delta function with the smooth test function

$$\delta(x) \approx \begin{cases} \varepsilon^{-1} \exp\left(\frac{-1}{1 - (x/\varepsilon)^2}\right) & \text{if } |x| < \varepsilon \\ 0 & \text{otherwise} \end{cases} \quad (4.5.6)$$

for a sufficiently small value of  $\varepsilon$  (in practice,  $\varepsilon$  is about twice the mesh size). Figure 4.9 shows the resulting dual flamelet library.

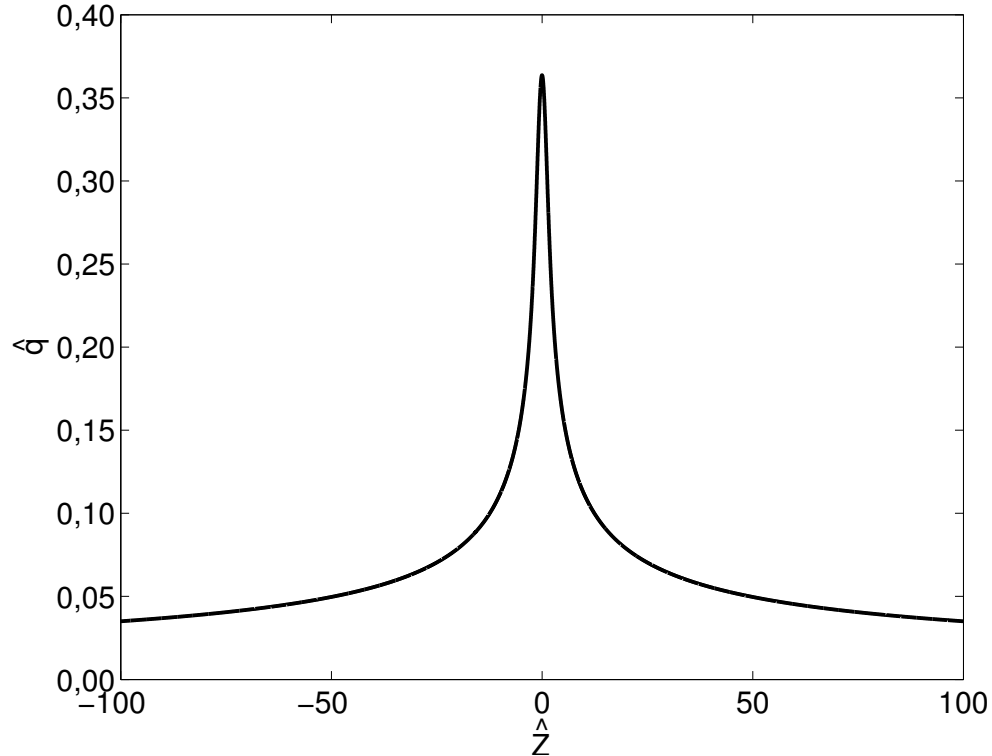


FIGURE 4.9. Dual flamelet library for  $j(Y, x_0, y_0) = Y(x_0, y_0)$ .

Exact and estimated  $L^1$ -norm errors are shown on the right side of Figure 4.7. The same comments as before can be made: both models have correct asymptotic behavior ( $O(\text{Da})$  as  $\text{Da} \rightarrow 0$  for the frozen flow model,  $O(\text{Da}^{-1})$  as  $\text{Da} \rightarrow +\infty$  for the flamelet model) and the frozen flow model curves are almost identical. A single intersection point between both models' error curves is found (at  $\text{Da} = 2,2619$  for the error estimator, at  $\text{Da} = 2,9306$  for the exact error), giving a way to choose a regime when both stable regimes are possible. The estimated error curve for the flamelet model is very close to the exact error curve as  $\text{Da} \rightarrow +\infty$ , but not exact. This is a small price to pay to obtain a cost-effective error estimating procedure to estimate  $L^1$ -norm errors using dual flamelet libraries.

#### 4.6. APPLICATION TO A STEADY SIMPLE SHEAR FLOW

We investigate next some numerical results of the application of this strategy to the estimation of the modeling error associated with the use of subgrid models when  $\text{Pe} \neq 0$ . As a first example, we consider a steady simple shear flow,  $\mathbf{v} =$

$(\sin(K_J y), 0)$ , with periodicity  $P = 2\pi/K_J$ . The steady solution of (4.3.4) is given by

$$Z(x, y) = \frac{1}{L_G} \left\{ x - \frac{\text{Pe}}{K_J^2} \sin(K_J y) \right\}. \quad (4.6.1)$$

Figure 4.10 shows the reaction rate  $\omega$ , and solutions  $Z$  and  $Y$  corresponding to  $\text{Pe} = 100$  and  $\text{Da} = 10^4$ . As before, there is no explicit formula for  $Y$ ; it is obtained numerically with very good accuracy as in the previous section. The contour corresponding to the stoichiometric level  $Z = 0$  is also shown. As seen from the figure, for this large  $\text{Da}$  example, the reaction zone is a narrow band closely aligned with the  $Z = 0$  level. The flamelet approximation is therefore very good in this case.

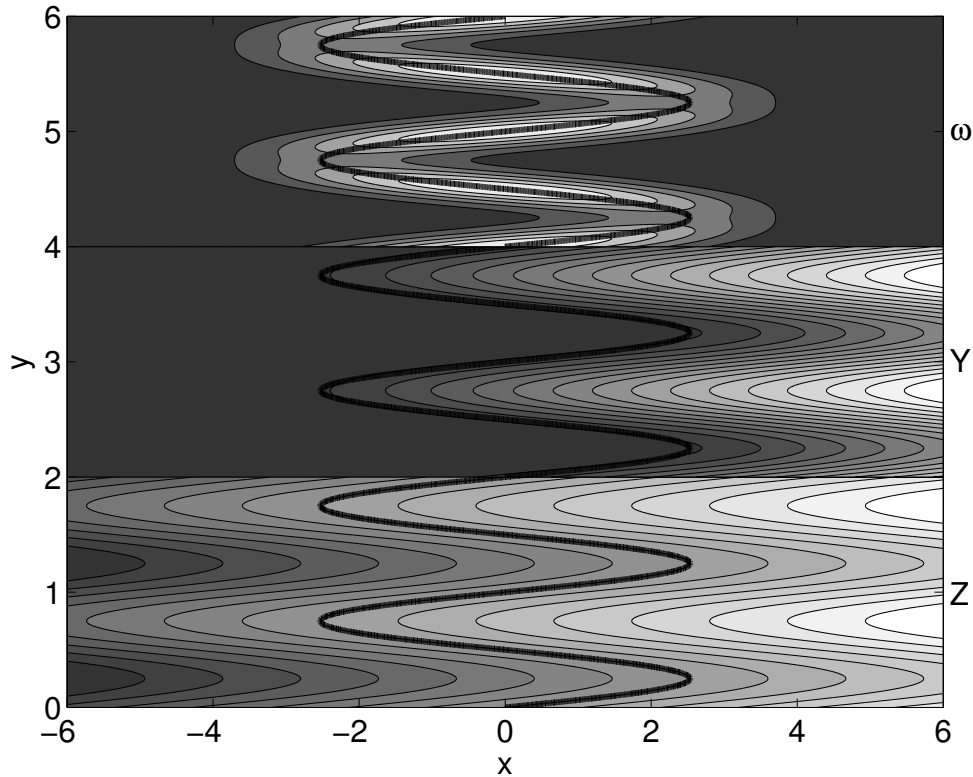


FIGURE 4.10. Simple shear— $\omega$ ,  $Y$ , and  $Z$  for  $\text{Pe} = 100$  and  $\text{Da} = 10^4$  (stoichiometric level  $Z = 0$  in black).

For the following test cases, we will focus on three models:

- (1) the local dissipation model, where  $Y_{fl}$  is given by (4.3.12) and  $\chi = \chi_{ld}$ ;
- (2) the mean dissipation model, where  $Y_{fl}$  is given by (4.3.12) and  $\chi = \langle \chi_{ld} \rangle$ ;

- (3) the frozen flow model, where  $Y_{ff}$  is given by  $Y_{ff} = H - T_\infty + Z$ .

The first numerical experiment compares two error estimation strategies:

- (1) Strategy 1: Estimating the modeling error using  $-d(Y_{fl})(q_{fl})$ , where

$$q_{fl} = \alpha_2^{-1} \hat{q}(\alpha Z), \quad (4.6.2)$$

and  $\hat{q}(\hat{Z})$  is the appropriate dual flamelet library. This strategy will be shown to be very cost effective and reliable for all test cases.

- (2) Strategy 2: Solving (4.4.14) directly and estimating the modeling error using  $-d(Y_{fl})(q)$ . As shown later, this strategy leads to excellent performance of the estimator (it is exact for linear equations). This is a purely theoretical exercise, since it is too expensive computationally for practical purposes.

Figure 4.11 shows the errors for  $j(Y) = \int_\Omega Y dx dy$  for the local dissipation model. Three curves are shown: exact error, estimated error  $-d(Y_{fl})(q_{fl})$  (strategy 1, dual flamelet library), and estimated error  $-d(Y_{fl})(q)$  (strategy 2, dual solution). For both values of Pe, the curves for the second strategy follow the exact error curves very closely. This indicates that the linearization step in the procedure to determine the dual equation is not a concern. The difference between the estimation using  $q_{fl}$  and the exact values is therefore the result of the flamelet-type approximation for the dual solution. In the flamelet regime, the agreement between the estimated and exact errors is very good. Out of this zone, the estimators overestimate the errors by at most two orders of magnitude. When computing the asymptotic slopes of the error curves, we find that both the estimated and exact errors are of order  $O(Da^{-4/3})$  for large Da. This scaling can be obtained by expressing  $-d(Y_{fl}, q_{fl})$  as a function of the normalized variables and integrating in the  $(\hat{Z}, y)$ -space.

For this choice  $j(Y) = \int_\Omega Y dx dy$ , one cannot compare all flamelet models accurately; for  $E = 0$ , the modeling error estimator is identically 0 for the mean dissipation model [BET], and for  $E \neq 0$ , cancellation errors appear in some

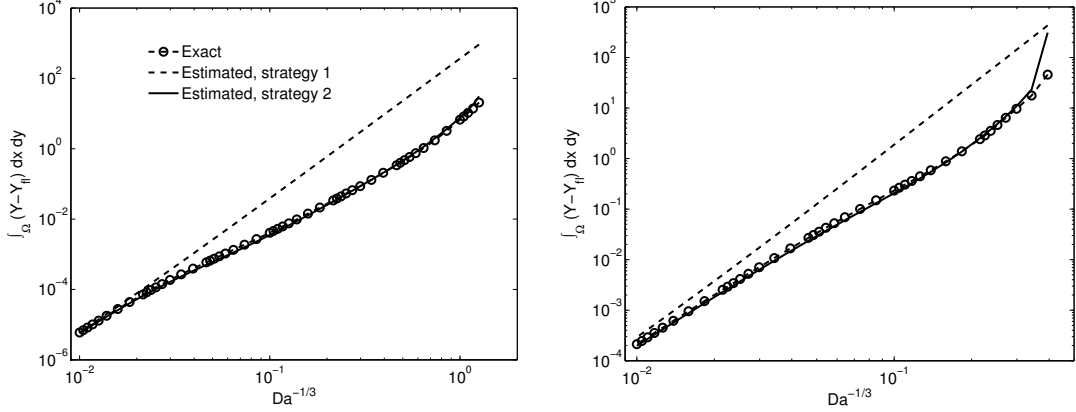


FIGURE 4.11. Shear flow—exact and estimated errors for  $j(Y) = \int_{\Omega} Y dx dy$ , plotted against  $Da^{-1/3}$ , for the local dissipation model.  
Left:  $Pe = 10$ , right:  $Pe = 100$ .

numerical computations. To compare all models effectively, we use

$$j(Y, y_0) = \int_x Y(x, y_0) dx = L_G \int_Z Y(Z, y_0) dZ \quad (4.6.3)$$

as the output functional, as done in [BET]. With this new choice of  $j$ , the dual equation (4.4.14) becomes

$$-\text{Pe} \mathbf{v} \cdot \nabla q - \Delta q + Da \exp\left(\frac{-E}{T}\right) \left\{ 2(Y - Z) - \frac{EY(Y - 2Z)}{T^2} \right\} q = \delta(y - y_0), \quad (4.6.4)$$

with  $T = H - Y + Z$ . Using our previous approximations and normalizations, we obtain the dual flamelet library

$$-\frac{d^2 \hat{q}}{d \hat{Z}^2} + 2(\hat{Y} - \hat{Z}) \hat{q} = \delta(y - y_0). \quad (4.6.5)$$

Since the mean and local dissipations are constant for a given value of  $y$  and  $(x, y) \mapsto (\hat{Z}, y)$  is a valid coordinate system, the solution of (4.6.5) can be written as the solution of the dual flamelet library (4.4.17) times  $\delta(y - y_0)$ . Thus the previous primal and dual flamelet libraries are used to estimate

$$\int_{y_0} \left| j(Y, y_0) - j(Y_{fl}, y_0) \right| dy_0 = L_G \int_y \left| \int_Z (Y(Z, y) - Y_{fl}(Z, y)) dZ \right| dy. \quad (4.6.6)$$

This new choice of  $j$  ensures that no analytical cancellations appear in the process. Similar expressions can be written for the frozen flow model.

We validate the error estimator by comparing the predictions with exact values of the modeling errors. Figure 4.12 shows the errors for  $j(Y)$  for Péclet numbers 10 and 100. Six curves are shown: the exact and estimated modeling errors for all three models. For each model, the exact error curves are only shown in their corresponding combustion regimes. In the nearly frozen regime (low Da), the estimated error curve almost overlaps the exact error curve. The estimation is also asymptotically correct as Da goes to 0, recovering the  $O(Da^1)$  asymptotic modeling error scaling, the same scaling obtained in the  $Pe = 0$  numerical experiments. In the near-equilibrium regime (large Da), both error estimations are very good and asymptotically correct (orders  $O(Da^{-2/3})$  and  $O(Da^{-4/3})$  for the mean and local dissipation models, respectively); we recover these scalings by expressing  $-d(Y_{fl}, q_{fl})$  as a function of the normalized variables and integrating in the  $(\hat{Z}, y)$ -space. For lower values of Da, the estimator overestimates the exact error by at most two orders of magnitude. The modeling error estimator predicts which model is better with good accuracy. For  $Pe = 10$ , there is qualitative agreement between exact and estimated curves' crossover values of Da ( $6,86 \times 10^0$  and  $7,21 \times 10^4$  for the estimated error curves,  $6,32 \times 10^0$  and  $6,35 \times 10^4$  for the exact error curves). For  $Pe = 100$ , the crossover value of the near-equilibrium models' curves is slightly overestimated ( $4,35 \times 10^2$  and  $2,20 \times 10^4$  for the estimated error curves,  $2,99 \times 10^2$  and  $7,80 \times 10^3$  for the exact error curves).

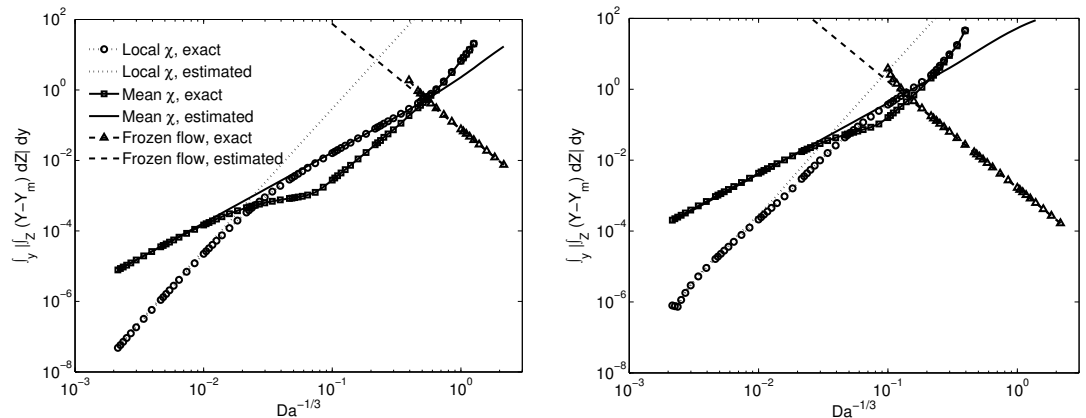


FIGURE 4.12. Shear flow—estimated (see (4.6.6)) and exact errors as functions of  $Da^{-1/3}$  for  $Pe = 10$  (left) and  $Pe = 100$  (right).

When more than one regime or model exists, one can use the estimator to efficiently predict which combustion regime and model is appropriate for a given set of parameters. According to the estimator, the solution is in the nearly frozen regime for low Da, and in the near-equilibrium regime otherwise; the transition happens between the ignition and extinction Damköhler numbers. In the near-equilibrium regime, the mean dissipation model is preferable for moderately large Da, while the local dissipation model performs better at large Da.

#### 4.7. APPLICATION TO THE CHILDRESS–SOWARD FLOW

We investigate the modeling error estimator's performance for the flow given by

$$\mathbf{v} = \left( -\frac{\partial F}{\partial y}, \frac{\partial F}{\partial x} \right), \quad (4.7.1)$$

where

$$F(x, y) = K (\sin(K_J x) \sin(K_J y) + \delta \cos(K_J x) \cos(K_J y)). \quad (4.7.2)$$

For the Childress–Soward flow, the constant  $K$  is chosen so that the mean kinetic energy is 1. The behavior of the flow changes drastically with  $\delta$ ;  $\delta = 0$  corresponds to a tilted shear flow, while  $\delta = 1$  is a small-scale array of eddies. The case  $\delta = 0,5$  is of particular interest to complex flows, as it is a mix of shear and eddies [BM1]. Numerical results for the passive scalar  $Z$ , the reactive scalar  $Y$ , and the reaction rate  $\omega$  are shown in Figure 4.13 for  $\delta = 0,5$ , alongside the stoichiometric level  $Z = 0$ . The change of variables from  $(x, y)$  to  $(Z, y)$  is no longer bijective, as was the case for the simple shear flow, and the dissipation is no longer a function of  $y$  only.

As it was the case for  $E = 0$  in the near-equilibrium regime, cancellation errors appear in the numerical computations for the choice  $j(Y) = \int_{\Omega} Y(x, y) dx dy$  [BET]. To compare all approximations effectively, we compute the  $L^1$ -norm errors using the dual flamelet library defined in section 4.5. Figure 4.14 shows the  $L^1$ -norm errors for  $Y$  for Péclet numbers 10 and 100, the equivalent of Figure 4.12 for the new output functional and flow. The same comments can be made for the error estimations: they are very good in the combustion regimes where the

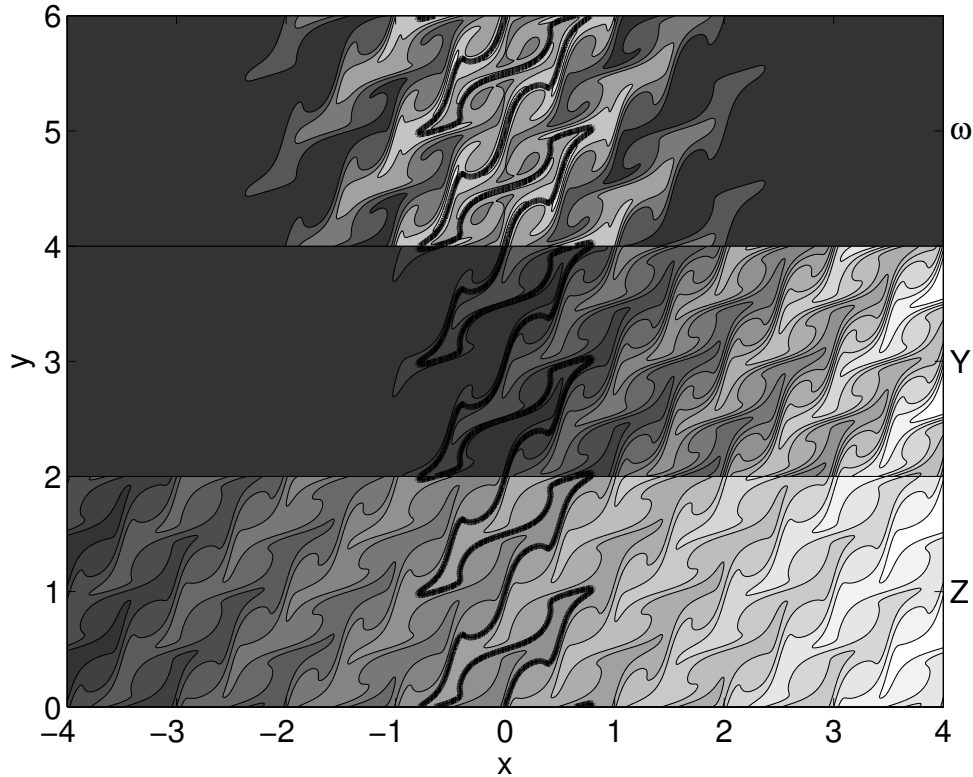


FIGURE 4.13. Childress–Soward flow—solutions  $\omega$ ,  $Y$ , and  $Z$  for  $\text{Pe} = 100$ ,  $\text{Da} = 10^4$ , and  $\delta = 0.5$  (stoichiometric level  $Z = 0$  in black).

models perform better, asymptotically correct, and not far off from the exact error away from the asymptotic behavior zones. Asymptotically, the modeling error is of order  $O(\text{Da}^1)$  for the frozen flow approximation, of order  $O(\text{Da}^{-2/3})$  for the mean dissipation model, and of order  $O(\text{Da}^{-1})$  for the local dissipation model. The same arguments used to obtain the scalings in the  $\text{Pe} = 0$  case are valid (the local error on  $Y$  is of order  $O(\text{Da}^{-1/3})$  for the mean dissipation model). Values of  $\text{Da}$  for which the best model changes according to the error curves are predicted with good accuracy. For  $\text{Pe} = 10$ , the exact error curves crossover at  $\text{Da} = 5.82 \times 10^0$  and  $\text{Da} = 4.12 \times 10^4$ , while the estimated error curves crossover at  $\text{Da} = 7.84 \times 10^0$  and  $\text{Da} = 1.27 \times 10^5$ ; for  $\text{Pe} = 100$ , the exact error curves crossover at  $\text{Da} = 1.14 \times 10^2$  and  $\text{Da} = 2.10 \times 10^5$ , while the estimated error curves crossover at  $\text{Da} = 1.88 \times 10^2$  and  $\text{Da} = 5.35 \times 10^5$ .

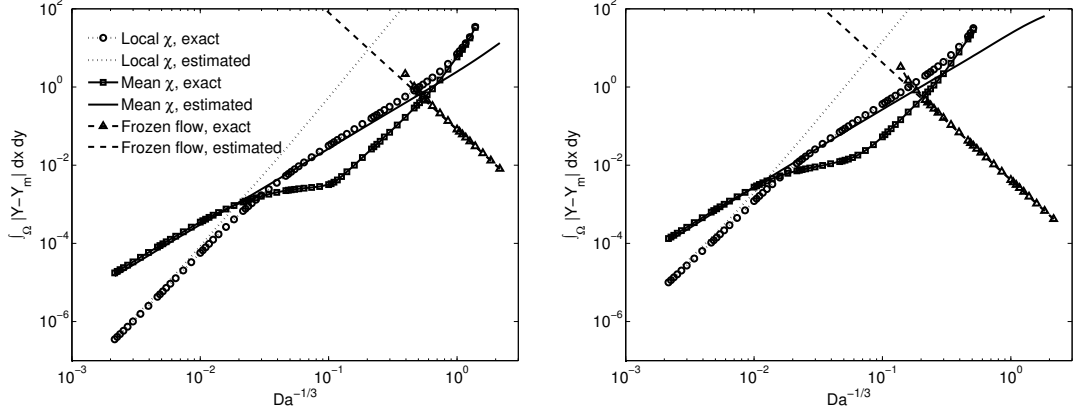


FIGURE 4.14. Childress–Soward flow—estimated and exact  $L^1$ -norm errors as functions of  $Da^{-1/3}$  for  $Pe = 10$  (left) and  $Pe = 100$  (right).

We can efficiently predict which combustion regime and model are appropriate for a given set of parameters: frozen flow model (nearly frozen regime) for low  $Da$ , local dissipation model (near-equilibrium regime) for large  $Da$ , and mean dissipation model (near-equilibrium regime) for intermediate values of  $Da$ .

#### 4.8. CONCLUSION

A dual-weighted residual strategy has been successfully implemented to assess the performance of subgrid models frequently used in large-scale simulations in nonpremixed combustion with quenching and ignition. The modeling error estimations are asymptotically correct for all models in their respective combustion regimes. The error estimator also gives a way of choosing between nearly frozen and near-equilibrium flames, and correctly identifies a posteriori the best model for each combustion regime. The estimation strategy can be made as computationally efficient as the modeling strategy itself, because precomputed libraries using large-scale passive scalars can be used. The error estimator can be computed using flamelet libraries (primal and dual) and the joint probability density function (PDF) of the passive scalars and their statistics.

For the local dissipation model, the required joint PDF to estimate the modeling error involves both passive scalars ( $Z, H$ ), the dissipation  $\chi_{ld}$ , as well as

a "dual" passive scalar  $Z_d$ . In typical large-eddy simulations, one relies on presumed PDF models; the number of variables involved would make this challenging. One alternative strategy we are exploring is to rely on the so-called heterogeneous multiscale methods (HMMs). In the HMM framework, explicit micro-sampling of the passive scalars at their smallest length scale is performed at selective locations and times as a substitute for a presumed PDF formulation. This work is in progress.

Another extension of the work presented here is to combine the flamelet modeling error estimation with estimations of other sources of errors in a typical large-scale simulation in turbulent combustion, such as other modeling errors (reduced chemistry, simplified diffusion models, other subgrid models for the passive scalar and the velocity field, etc.) as well as discretization errors. Yet another extension is to study unsteady test cases. When  $E = 0$ , corresponding to a single combustion regime, there exists several models based on steady flamelets [V]. We showed that the error estimator is able to select the best model for a given setup [BET]. When  $E > 0$  and multiple regimes are possible, an interesting question is whether the type of modeling error estimator used in this paper will be able to detect combustion regime changes, so that the appropriate modeling strategy for the reactive scalars can automatically be adjusted as the simulation runs.

#### 4.9. REFERENCES

- [ACS] R. L. ACTIS, B. A. SZABO, C. SCHWAB, *Hierachic models for laminated plates and shells*, Comput. Meth. Appl. Mech. Eng., 172 (1999), pp. 79–107.
- [AN] A. K. ALEKSEEV, I. M. NAVON, *On a posteriori pointwise error estimation using adjoint temperature and Lagrange remainder*, Comput. Methods Appl. Mech. Eng., 194 (2000), pp. 2211–2228.
- [AO] M. AINSWORTH, J. T. ODEN, *A posteriori error estimation in finite element analysis*, First ed., John Wiley & Sons, New York, 2001.

- [BBV] R. BECKER, M. BRAACK, B. VEXLER, *Parameter identification for chemical models in combustion problems*, Appl. Numer. Math., 54 (2005), pp. 519–536.
- [BE1] M. BRAACK AND A. ERN, *A posteriori control of modeling errors and discretization errors*, SIAM J. Mult. Mod. Simul., 1 (2003), pp. 221–238.
- [BE2] M. BRAACK, A. ERN, *Coupling multimodeling with local mesh refinement for the numerical computation of laminar flames*, Comb. Theory Mod., 8 (2004), pp. 771–788.
- [BET] A. BOURLIOUX, A. ERN, P. TURBIS, *A posteriori error estimation for subgrid flamelet models*, Mult. Mod. Simul., 8 (2010), pp. 481–497.
- [BM1] A. BOURLIOUX AND A. J. MAJDA, *An elementary model for the validation of flamelet approximation in nonpremixed turbulent combustion*, Comb. Theory Mod., 4 (2000), pp. 189–210.
- [BM2] A. BOURLIOUX AND A. J. MAJDA, *Elementary models with PDF intermittency for passive scalars with a mean gradient*, Phys. Fluids, 14 (2002), pp. 881–897.
- [BR] R. BECKER, R. RANNACHER, *An optimal control approach to a posteriori error estimation in finite element methods*, Acta Numer., 10 (2001), pp. 1–102.
- [BT] A. BOURLIOUX, P. TURBIS, *An elementary model for the validation of flamelet approximations in nonpremixed combustion with quenching and ignition*, Ph.D. thesis (chap. 3), Université de Montréal (2010).
- [CR1] A. W. COOK AND J. J. RILEY, *A subgrid model for equilibrium chemistry in turbulent flows*, Phys. Fluids, 6 (1994), pp. 2868–2870.
- [CR2] A. W. COOK AND J. J. RILEY, *Subgrid-scale modeling for turbulent reacting flows*, Combust. Flame, 112 (1998), pp. 593–606.
- [EJ] K. ERIKSSON, C. JOHNSON, *An adaptive finite element method for linear elliptic problems*, Math. Comp., 50 (1988), pp. 361–383.
- [JLRH] J. JIMENEZ, A. LIÑÁN, M. ROGERS, F. HIGUERA, *A priori testing of sub-grid models for chemically reacting nonpremixed turbulent shear flows*, J. Fluid Mech., 349 (1998), pp. 149–171.

- [MK] A. J. MAJDA AND P. R. KRAMER, *Simplified models for turbulent diffusion: theory, numerical modelling, and physical phenomena*, Phys. Rep., 314 (1999), pp. 237–574.
- [MS] A. J. MADJA AND P. SOUGADINIS, *The effect of turbulence on mixing in prototype reaction diffusion systems*, Comm. Pure Appl. Math., 53 (2000), pp. 1284–1304.
- [P] N. PETERS, *Laminar diffusion flamelet models in non-premixed models in turbulent combustion*, Prog. Energy Combust. Sci., 10 (1984), pp. 319–339.
- [ROV] A. ROMKES, J. T. ODEN, K. VEMAGANTI, *Multi-scale goal-oriented adaptive modeling of random heterogeneous materials*, Mechanics of Materials, 38 (2006), pp. 859–872.
- [T] P. TURBIS, *Modèles de flammelette en combustion turbulente avec extinction et réallumage : étude asymptotique et numérique, estimation d'erreur a posteriori et modélisation adaptative*, thèse de doctorat, Université de Montréal (2010).
- [V] O. VOLKOV, *Validation des modèles de flammelettes instationnaires en combustion turbulente non-prémélangée*, thèse de doctorat, Université de Montréal (2005).

## APPENDIX A

If we assume that  $q_{fl} = q_{fl}(Z)$  for the mean dissipation model, (4.4.15) becomes

$$\begin{aligned} 1 &= -Pe \mathbf{v} \cdot \nabla q_{fl} - \Delta q_{fl} + 2Da(Y_{fl} - Z) \exp\left(\frac{-E}{H_0}\right) \frac{\chi_{ld}}{\langle \chi_{ld} \rangle} q_{fl} \\ &= -\frac{d^2 q_{fl}}{dZ^2} \chi_{ld} - 2 \frac{dq_{fl}}{dZ} \Delta Z + 2Da(Y_{fl} - Z) \exp\left(\frac{-E}{H_0}\right) \frac{\chi_{ld}}{\langle \chi_{ld} \rangle} q_{fl} \end{aligned} \quad (4.9.1)$$

We have

$$\int_{\Omega} \Delta Z dx dy = \int_{\partial\Omega} \nabla Z \cdot \mathbf{n} dl = \int_{\partial\Omega} \left( \frac{1}{L_G} \mathbf{e}_x + \nabla Z_p \right) \cdot \mathbf{n} dl = 0 \quad (4.9.2)$$

since  $Z_p$  is biperiodic. Therefore we choose to neglect the advection term in  $-2\frac{dq_{fl}}{dZ}\Delta Z$ . With the usual normalizations for  $Y_{fl}$  and  $Z$ , we define

$$\hat{q} = \left[ \frac{\text{Da}}{\langle \chi_{ld} \rangle} \exp(-E/H_0) \right]^{2/3} \chi_{ld} \quad (4.9.3)$$

to obtain

$$-\frac{d^2\hat{q}}{d\hat{Z}^2} + 2(\hat{Y} - \hat{Z})\hat{q} = 1. \quad (4.9.4)$$

To obtain an unique normalization value for  $q_{fl}$  on  $\Omega$ , we replace  $\chi_{ld}$  by its mean value  $\langle \chi_{ld} \rangle$  and obtain the normalizing factor  $\alpha_2$  given by (4.4.19).

## APPENDIX B

To estimate the modeling error on the output functional  $j(Y, x_0) = Y(x_0)$  in the  $\text{Pe} = 0$  case, we would have to solve

$$-\frac{d^2q_{fl}}{dx^2} + 2\text{Da}(Y_{fl} - Z)\exp\left(\frac{-E}{H}\right)q_{fl} = \delta(x - x_0) \quad (4.9.5)$$

and then compute

$$-\int_x \text{Da} Y_{fl} (Y_{fl} - 2Z) \left\{ \exp\left(\frac{-E}{H - Y_{fl} + Z}\right) - \exp\left(\frac{-E}{H}\right) \right\} q_{fl} dx \quad (4.9.6)$$

to estimate  $Y(x_0) - Y_{fl}(x_0)$ . Instead, we propose to approximate the local modeling error on  $Y$  by

$$Y - Y_{fl} \approx \text{Da} Y_{fl} (Y_{fl} - 2Z) \left\{ \exp\left(\frac{-E}{H - Y_{fl} + Z}\right) - \exp\left(\frac{-E}{H}\right) \right\} q_{fl}, \quad (4.9.7)$$

where  $q_{fl}$  is obtained from  $\hat{q}$ , the solution of

$$-\frac{d^2\hat{q}}{d\hat{Z}^2} + 2(\hat{Y} - \hat{Z})\hat{q} = \delta(\hat{Z} - \hat{Z}_0). \quad (4.9.8)$$

At this point, the normalization on  $q_{fl}$  is still unknown. To normalize (4.9.5), we define

$$\hat{q} = [\text{Da} L_G^{-1} \exp(-E/H)]^{1/3} q_{fl}, \quad (4.9.9)$$

$$\hat{Y} = [\text{Da} L_G^2 \exp(-E/H)]^{1/3} Y_{fl}, \quad (4.9.10)$$

$$\hat{Z} = [\text{Da} L_G^2 \exp(-E/H)]^{1/3} Z = [\text{Da} L_G^{-1} \exp(-E/H)]^{1/3} x. \quad (4.9.11)$$

Using these normalizations, we transform (4.9.5) into

$$-\frac{d^2\hat{q}}{d\hat{Z}^2} + 2(\hat{Y} - \hat{Z})\hat{q} = \delta(\hat{Z} - \hat{Z}_0) \quad (4.9.12)$$

Since  $dx = [DaL_G \exp(-E/H)]^{-1/3} d\hat{Z}$ , the integration in (4.9.6) leads to another normalizing factor. If we want to use (4.9.7) to approximate (4.9.6), we must then redefine  $\hat{q}$  as

$$\begin{aligned}\hat{q} &= \left[ (DaL_G^{-1} \exp(-E/H))^{1/3} \right] \left[ (DaL_G \exp(-E/H))^{-1/3} \right]^{-1} q_{fl} \\ &= (DaL_G \exp(-E/H))^{2/3} q_{fl}\end{aligned} \quad (4.9.13)$$

to compensate for this integration factor. Therefore, the normalization  $q_{fl} = \alpha_2^{-1}\hat{q}(\alpha Z)$  defined in (4.4.19) is correct. The same type of argument is valid for estimations in multidimensional cases.

# CONCLUSION

---

Dans cette thèse, un estimateur d'erreur a posteriori a été utilisé en vue de la modélisation adaptative en combustion turbulente non prémixée. Pour y arriver, il a été montré qu'une librairie duale de flammelettes peut être construite pour approximer la solution duale utilisée dans l'estimation d'erreurs basée sur les résidus pondérés. Cette librairie permet de limiter le coût numérique relié à l'utilisation de l'estimateur à celui de la construction de la flammelette elle-même. Les erreurs de modélisation estimées dans le régime près de l'équilibre sont asymptotiquement exactes. L'estimateur donne également une hiérarchie des modèles de flammelette similaire à celle obtenue par les simulations numériques détaillées.

Une extension du modèle Bourlioux-Majda en combustion turbulente non prémixée a été construite pour inclure les phénomènes d'extinction et de ré-allumage. Trois régimes de combustion sont identifiés : le régime presque gelé (stable), le régime en combustion partielle (instable) et le régime près de l'équilibre (stable). En traçant le profil de la température maximale en fonction du nombre de Damköhler, nous obtenons la courbe en «S» classique. L'analyse asymptotique sans effets d'advection mène à une caractérisation et une estimation des valeurs des nombres de Damköhler d'extinction ( $Da_E$ ) et de réallumage ( $Da_I$ ). Lorsque des effets advectifs sont ajoutés, ces nombres, ainsi que le reste de la courbe en «S», peuvent être obtenus en fonction de la courbe en «S» sans advection et des statistiques sur les scalaires passifs avec advection.

Une nouvelle hiérarchie de modèles a été construite pour une flamme ayant plus d'un régime stable de combustion possible. Les erreurs de modélisation des différentes approximations donnent une façon systématique de choisir le régime et

le modèle appropriés. Ces choix peuvent être répétés avec un estimateur d'erreur. Comme pour le système d'équations idéalisé avec un terme de réaction plus simple (chapitre 1), une librairie duale de flammes permet de mettre en œuvre un estimateur d'erreurs de modélisation peu coûteux au point de vue numérique et asymptotiquement correct. Il permet également d'identifier le régime de combustion stable approprié, ainsi que le meilleur modèle dans ce régime.

La prochaine étape sera d'étendre l'analyse à des flammes instationnaires en présence d'extinction et de réallumage. Dans un premier lieu, il faudra déterminer la hiérarchie des modèles sur chaque branche stable de la courbe en «S», en particulier pour les modèles instationnaires basés sur les flammes stationnaires. Des cycles de réallumage et d'extinction sont possibles, rendant la modélisation plus difficile. Il sera intéressant de vérifier si l'estimateur d'erreur de Braack et Ern (avec une librairie duale de flammes) permet d'une part de déceler un changement de régime de combustion instantanément, et d'autre part d'ordonner la performance des modèles disponibles.

## BIBLIOGRAPHIE

---

- [ACS] R. L. ACTIS, B. A. SZABO, C. SCHWAB, *Hierarchic models for laminated plates and shells*, Comput. Meth. Appl. Mech. Eng., 172 (1999), pp. 79–107.
- [AN] A. K. ALEKSEEV, I. M. NAVON, *On a posteriori pointwise error estimation using adjoint temperature and Lagrange remainder*, Comput. Methods Appl. Mech. Eng., 194 (2000), pp. 2211–2228.
- [AO] M. AINSWORTH, J. T. ODEN, *A posteriori error estimation in finite element analysis*, First ed., John Wiley & Sons, New York, 2001.
- [BBV] R. BECKER, M. BRAACK, B. VEXLER, *Parameter identification for chemical models in combustion problems*, Appl. Numer. Math., 54 (2005), pp. 519–536.
- [BE1] M. BRAACK, A. ERN, *A posteriori control of modeling errors and discretization errors*, Mult. Mod. Simul., 1 (2003), pp. 221–238.
- [BE2] M. BRAACK, A. ERN, *Coupling multimodeling with local mesh refinement for the numerical computation of laminar flames*, Comb. Theory Mod., 8 (2004), pp. 771–788.
- [BET] A. BOURLIOUX, A. ERN, P. TURBIS, *A posteriori error estimation for subgrid flamelet models*, Mult. Mod. Simul., 8 (2010), pp. 481–497.
- [BM1] A. BOURLIOUX, A. J. MAJDA, *An elementary model for the validation of flamelet approximation in nonpremixed turbulent combustion*, Comb. Theory Mod., 4 (2000), pp. 189–210.
- [BM2] A. BOURLIOUX, A. J. MAJDA, *Elementary models with PDF intermittency for passive scalars with a mean gradient*, Phys. Fluids, 14 (2002), pp. 881–897.
- [BR] R. BECKER, R. RANNACHER, *An optimal control approach to a posteriori error estimation in finite element methods*, Acta Numer., 10 (2001), pp. 1–102.

- [BT] A. BOURLIOUX, P. TURBIS, *An elementary model for the validation of flamelet approximations in nonpremixed combustion with quenching and ignition*, Ph.D. thesis (chap. 3), Université de Montréal (2010).
- [CEP] B. CUENOT, F. N. EGOLFOPOULOS, T. POINSOT, *An unsteady laminar flamelet model for non-premixed combustion*, Comb. Theory Mod., 4 (2000), pp. 77–97.
- [CKP] C. M. CHA, G. KOSÁLY, H. PITTSCH, *Modeling extinction and reignition in turbulent nonpremixed combustion using a doubly-conditional moment closure approach*, Phys. Fluids, 13 (2001), pp. 3824–3834.
- [CR1] A. W. COOK, J. J. RILEY, *A subgrid model for equilibrium chemistry in turbulent flows*, Phys. Fluids, 6 (1994), pp. 2868–2870.
- [CR2] A. W. COOK, J. J. RILEY, *Subgrid-scale modeling for turbulent reacting flows*, Combust. Flame, 112 (1998), pp. 593–606.
- [EE] W. E, B. ENGQUIST, *The heterogeneous multiscale methods*, Comm. Math. Sci., 1 (2003), pp. 87–132.
- [EJ] K. ERIKSSON, C. JOHNSON, *An adaptive finite element method for linear elliptic problems*, Math. Comp., 50 (1988), pp. 361–383.
- [GSCP] L. Y. M. GICQUEL, G. STAFFELBACH, B. CUENOT, T. POINSOT, *Large eddy simulations of turbulent reacting flows in real burners: the status and challenges*, conférence invitée, dans SciDAC 2008 Conference, Seattle, USA, pp. 12–29.
- [HRP] V. HIREMATH, Z. REN, S. B. POPE, *A greedy algorithm for species selection in dimension reduction of combustion chemistry*, Comb. Theory Mod., 14 (2010), pp. 619–652.
- [ICP] M. IHME, C. M. CHA, H. PITTSCH, *Prediction of local extinction and reignition effects in non-premixed turbulent combustion using a flamelet/progress variable approach*, Proc. Combust. Inst., 30 (2005), pp. 793–800.
- [JLRH] J. JIMENEZ, A. LIÑÁN, M. ROGERS, F. HIGUERA, *A priori testing of subgrid models for chemically reacting nonpremixed turbulent shear flows*, J. Fluid Mech., 349 (1998), pp. 149–171.
- [KP1] K. A. KEMENOV, S. B. POPE, *Molecular diffusion effects in LES of a piloted methane-air flame*, Combust. Flame, 158 (2011), pp. 240–254.

- [KP2] S. H. KIM, H. PITSCHE, *Conditional filtering method for large-eddy simulation of turbulent nonpremixed combustion*, Phys. Fluids, 17 (2005), article 105103.
- [L] A. LIÑÁN, *The asymptotic structure of counterflow diffusion flames for large activation energies*, Acta Astronautica, 1 (1974), pp. 1007–1039.
- [LB] C. LEBRIS, *Systèmes multiéchelles : modélisation et simulation*, Mathématiques et Applications, 47 (2005), Springer.
- [MK] A. J. MAJDA, P. R. KRAMER, *Simplified models for turbulent diffusion: theory, numerical modelling, and physical phenomena*, Phys. Rep., 314 (1999), pp. 237–574.
- [MS] A. J. MADJA, P. SOUGADINIS, *The effect of turbulence on mixing in prototype reaction diffusion systems*, Comm. Pure Applied Math., 53 (2000), pp. 1284–1304.
- [P1] N. PETERS, *Laminar diffusion flamelet models in non-premixed models in turbulent combustion*, Prog. Energy Combust. Sci., 10 (1984), pp. 319–339.
- [P2] H. PITSCHE, *Large-eddy simulation of turbulent combustion*, Annu. Rev. Fluid Mech., 38 (2006), pp. 453–482.
- [PCF] H. PITSCHE, C. M. CHA, S. FEDOTOV, *Flamelet modeling of non-premixed turbulent combustion with local extinction and re-ignition*, Comb. Theory Mod., 7 (2003), pp. 317–332.
- [PDBI] H. PITSCHE, O. DESJARDINS, G. BALARAC, M. IHME, *Large-eddy simulation of turbulent reacting flows*, Prog. Aerospace Sci., 44 (2008), pp. 466–478.
- [PR] S. B. POPE, Z. REN, *Efficient implementation of chemistry in computational combustion*, Flow Turb. Combust., 82 (2009), pp. 437–453.
- [ROV] A. ROMKES, J. T. ODEN, K. VEMAGANTI, *Multi-scale goal-oriented adaptive modeling of random heterogeneous materials*, Mechanics of Materials, 38 (2006), pp. 859–872.
- [T] P. TURBIS, *Quenching and ignition effects in an idealized nonpremixed combustion model*, Ph.D. thesis (chap. 2), Université de Montréal (2010).
- [V] O. VOLKOV, *Validation des modèles de flammelettes instationnaires en combustion turbulente non-prémélangée*, thèse de doctorat, Université de Montréal (2005).

- [WP] H. WANG, S. B. POPE, *Large eddy simulation/probability density function modeling of a turbulent CH<sub>4</sub>/H<sub>2</sub>/N<sub>2</sub> jet flame*, Proc. Combust. Inst. (2010), doi :10.1016/j.proci.2010.08.004.
- [WS+] P. WOLF, G. STAFFELBACH, L. Y. M. GICQUEL, T. POINSOT, V. MOUREAU, C. BÉRAT, *Massively parallel LES of azimuthal thermo-acoustic instabilities in annular gas turbines*, 2e colloque INCA, CORIA, Rouen, France, 2008.

## **Annexe A**

---

### **AUTORISATIONS ÉCRITES DES COAUTEURS ET DE L'ÉDITEUR POUR LA DIFFUSION**